SYNAPTIC MECHANISMS OF OPRM1 A118G SINGLE NUCLEOTIDE POLYMORPHISM IN HUMAN NEURONS

By

APOORVA HALIKERE, BA

A dissertation submitted to the

School of Graduate Studies

Rutgers, The State University of New Jersey

In partial fulfillment of the requirements

For the degree of

Doctor of Philosophy

Graduate Program in Neuroscience

Written under the direction of

Dr. Zhiping Pang

And approved by

_____

_____

_____

_____

New Brunswick, New Jersey

May 2018

ABSTRACT OF THE DISSERTATION

Synaptic Mechanisms of OPRM1 A118G

Single Nucleotide Polymorphism

in Human Neurons

By APOORVA HALIKERE

Dissertation Director:

Dr. Zhiping Pang

Association of the non-synonymous single nucleotide polymorphism (SNP) rs1799971 in OPRM1 to drug dependence and alcohol abuse suggests it may have a functional consequence in altering receptor signaling in the brain. The A118G SNP causes a switch of asparagine (N) at position 40 of the mu-opioid receptor (MOR) to aspartate (D). To dissect the underlying neural and synaptic basis of the N40D MOR variant, we generated human GABAergic induced neuronal (iN) cells from induced pluripotent stem (iPS) cells of donors homozygous for either the major (N40) or minor (D40) alleles of the MOR. We found that the subject-derived iN cells exhibit mature neuronal properties such as action potential firing and neuronal excitability and express functional MORs. Interestingly, upon MOR activation by the agonist DAMGO, D40 MOR iN cells exhibit consistently stronger suppression of spontaneous inhibitory postsynaptic currents (sIPSCs) than N40 MOR iN cells across multiple subjects. To mitigate the

complexity of diverse genetic backgrounds of the subject iN cells derived from multiple human subjects, we employed CRISPR/Cas9 genome-editing to generate two pairs of isogenic human pluripotent stem cell lines. Remarkably, the synaptic regulation of MOR activation in the isogenic lines recapitulate those of neurons generated from different individuals, i.e. stronger suppression in D40 MOR carrying human neuronal cells by MOR activation. We further determined that the increased sensitivity of D40 iN cells to DAMGO was caused by a more robust inhibition of excitability and synaptic release by DAMGO in D40 MOR expressing neurons. Additionally, we found that the N40D SNP influences the development of long-term tolerance at the MOR. Specifically, D40 iN cells are unable to develop adaptive changes in synaptic function unlike N40 iN cells following long-term mu opioid receptor activation by DAMGO. This study utilizes patient-specific iPS cells as well as a gene edited isogenic neurons to advance our understanding of the fundamental synaptic alterations associated with OPRM1 A118G in a human neuronal context.

Acknowledgements

There have been several key individuals who have walked alongside me to whom I owe my deepest appreciation. First and foremost, I would like to express my sincere gratitude to my mentor, Dr. Zhiping Pang, for his undying support, encouragement and enthusiasm in developing my skills as a scientist. From day one in his laboratory, Dr. Pang has been receptive to my specific scientific interests, learning styles, and both short term and long term goals. He has provided constructive feedback on my scientific progress, provided moral support and given me the freedom I needed to grow and move forward. Not only has Dr. Pang has actively encouraged both my scientific and professional development, but he has challenged me to achieve goals that I would never have thought possible during the beginning of my scientific career.

I would like to give a special thanks to the additional members of my thesis committee, Drs. Ron Hart, John Pintar, and Julie Blendy for their guidance in my scientific growth. Thank you to Dr. Hart who has mentored me since before my start of graduate school, to Dr. Blendy who has trekked to the lab several times to support my research progress, and to Dr. Pintar for his efforts in strengthening the Neuroscience Graduate Program. I would also like to thank Dr. Janet Alder for all her support to the Neuroscience graduate students.

I would also like to give a special thanks to Dr. Arnold Rabson who has an incredible spirit of enthusiasm for the scientific advancement of the Child Health Institute, for his tremendous support to my growth and endeavors in obtaining research funding. I would also like to give a thanks to the administrative staff upholding the workings of CHI, the Neuroscience Graduate Program, and the Graduate School of Biomedical Sciences particularly Ms. Kathey Semler, Ms. Christine Mahedy, Ms. Joan Mordes, Ms. Perry Dominguez and Ms. Tina Cicollela. I would also like to give a special thanks to my

colleagues at the Guangzhou Institute of Biomedicine and Health for giving me an opportunity to study and hosting me for 2 months.

I also give my genuine thanks to the Pang Lab family members who have been monumental in shaping my graduate school experience. Each member of the lab has influenced my path in science and provided a robust intellectual environment to learn. I want to give a special thanks to Vincent Mirabella for not just his scientific support, but also for his moral support and friendship during my tenure in the lab.

Also, I cannot express the invaluable love and support that I have received from my family and friends. I would like to extend my gratitude to my parents and brother for their unconditional love and support during my journey and for being such big champions of my career and academic development. To my mother who has supported me far and beyond and to my father who has endlessly encouraged my intellectual growth for whom I have great admiration. To my closest friends who have been my biggest cheerleaders since childhood. And thank you to my love, Neel, for being my closest confidant and supporter. My deepest love and gratitude goes to each one of you for all you have done.

I would also like to acknowledge National Science Foundation (NSF) for their financial support for one year of my graduate studies. Also, I would like to acknowledge the National Institute for Alcohol Abuse and Alcoholism (NIAAA) as I am thankful to be the recipient of the Ruth L. Kirschtstein National Research Service Award (NRSA) Individual Predoctoral Fellowship, which has supported my studies and research efforts.

Last but not least, I would like to acknowledge Dr. Eileen Oni with whom I have co-authored a study early in my graduate career. *Scientific Reports* is an open access journal that applies a Creative Commons license allowing re-use of this published work.

Oni E*, **Halikere A***, Li G, Toro-Ramos AJ, Swerdel MR, Verpeut JL, Moore JC, Bello NT, Bierut LJ, Goate A, Tischfield JA, Pang ZP, Hart RP. Increased nicotine response in iPSC-derived human neurons carrying the CHRNA5 N398 allele. *Scientific Reports*. 2016 Oct 4;6:34341. PMID: 27698409. ***These authors contributed equally to this work.**

Table of Contents

List of Figures

Chapter 1: Introduction

Synaptic transmission is a tightly regulated process that controls the flow of information in the brain. The pattern of synaptic connectivity and the spatial and temporal flow of information through a brain circuit not only determines its function but also guides regulated and adaptive human behaviors. Thus, pathological changes in regulated synaptic transmission impacts the synchronized flow of information through neural circuits and is the neural correlate of mental illnesses (6). Distinct dysfunctions of specific neural circuitry underlie the unique symptoms of neuropsychiatric diseases, including addiction.

Although the brain circuitry mediating addiction in humans is multifaceted and complex, it is indisputable that reward and addictive behavior associated with alcohol and other drugs of abuse are mediated by synaptic plasticity within the mesolimbic dopamine system, which consists of the ventral tegmental area (VTA) and the nucleus accumbens (NAc) and other associated limbic structures (6). Neural adaptations that develop over several minutes to even days and months following initial exposure to drugs are involved in the synaptic plasticity of the mesolimbic dopamine system (6). These brain regions serve as the critical substrates for mediating the neural adaptations that underlie addiction behavior in humans.

Substance abuse and drug addiction pose a great threat to human health. Evidence for a genetic predisposition to addiction has been provided by many family, twin and adoption studies (7). Overall, studies have predicted that the heritability of alcohol use disorders ranges from 40-60% while the heritability of smoking initiation and nicotine dependence is 50% and 59%, respectively (7). These genetic causes of addiction are not the rare and highly penetrant mutations that are traditionally thought to manifest in mental illness, but instead represent single nucleotide polymorphisms

(SNPs), which are the simplest example of DNA variation in individuals that can occur throughout the genome. There are many SNPs found in the human genome that are associated with vulnerability to reward related behaviors such as substance use disorders.

In humans, a commonly investigated SNP (rs1799971) occurs in exon 1 of OPRM1, the gene encoding the mu opioid receptor (MOR), in which an adenine to a guanine (A118G) substitution replaces an asparagine (N) to an aspartate (D) at a putative N-glycosylation site (N40D) at the N-terminus of the receptor (7). Despite the enormity of research that has been done investigating the functional role of this SNP in human disease and drug addiction, a consensus has yet to be reached about the cellular, molecular, and synaptic consequences of MOR N40D function. The focus of this dissertation is to unravel the neural and synaptic basis of N40D function. In contrast to previous studies in animal models or overexpression systems, this study exemplifies the use of human induced neuronal (iN) cells derived directly from patient-specific induced pluripotent stem (iPS) cells as well as gene targeted isogenic stem cell lines to advance our understanding of the fundamental cellular and synaptic alterations associated with MOR N40D in human neuronal context.

1.1 Neural Substrates of Addiction

1.1.1 The Reward Pathway and Addiction

Drug addiction is a chronically relapsing brain disorder characterized by a loss of control over drug intake. The reinforcing effects of drugs during intoxication set the stage for later neuronal adaptations that result in addiction. There are complex neural adaptations that develop with different time courses ranging from hours to even months and can induce changes at the behavioral, circuit and synaptic levels (8).

Drugs of abuse such as alcohol, nicotine, cocaine, amphetamine, morphine etc. are all structurally and chemically diverse and all have different molecular targets in the human brain, each eliciting a specific set of behavioral and physiological effects upon acute administration (4). Although they exhibit different mechanisms of action and pharmacological consequences, all addictive drugs are acutely rewarding, which thus promotes repeated drug exposures and leads eventually to loss of control over drug use, which we refer to as addiction (9). Due to these common functional effects upon acute and chronic exposure, it is not surprising that drugs of abuse converge on a common neurocircuit within the midbrain, the mesolimbic dopamine pathway which includes the dopaminergic (DA) neuronal projections from the ventral tegmental area (VTA) to the nucleus accumbens (NAc) (9-14) (**Figure 1**). On the basis of these common acute actions of addictive drugs, it is thought that chronic functional changes in the VTA-NAc pathway are also elicited in response to drug abuse as well (4).

In the VTA, MORs are expressed on GABAergic interneurons (15). MOR agonists, whether they be endogenously released β-endorphin or an exogenously administered agonist such as morphine of fentanyl, enhance dopaminergic neuronal activation by lessening the tonic inhibition of the GABAergic interneurons that project to the NAc (16, 17). Additionally, MORs are also present pre-synaptically on GABAergic and glutamatergic nerve terminals where they decrease neurotransmitter release (18, 19). By modulating the activity of GABAergic interneurons and the release of GABA and glutamate, MORs can influence dopaminergic input to the NAc and thus mediate the reinforcing and rewarding effects addictive drugs (16, 17, 20). Thus, pathological alterations in synaptic plasticity mechanisms mediated by MOR signaling are key to the initiation and progression of diseases such as addiction.

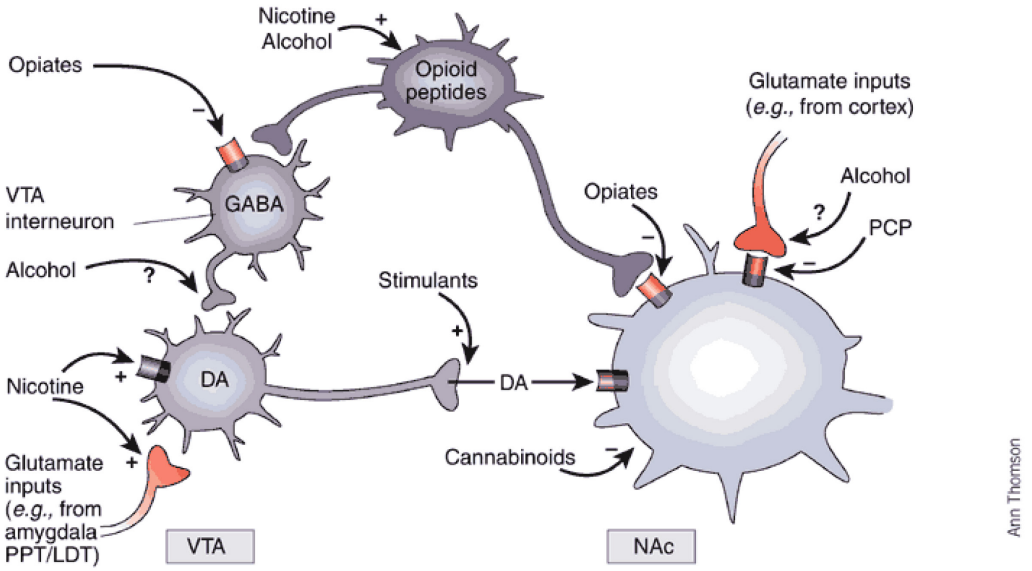

Figure 1: Converging Actions of Drugs of Abuse on the VTA-NAc Circuit
Drugs of abuse converge on the mesolimbic dopamine pathway to produce similar functional effects upon acute administration. Stimulants, opiates as well as endogenous ligands act to increase dopaminergic neurotransmission in the NAc, which is enhanced by the activation of MORs. *Taken from Nestler, Nature Neuroscience (2005)* (4).

1.1.2 Cellular and Circuit Mechanisms of Addiction

Although different drugs of abuse have different molecular targets in the brain and different pharmacological effects, they function to cause very fast increases of dopamine in the NAc shell subregion, which is the mechanism by which the brain signals reward (21). In fact, VTA Dopamine neurons project to the NAc, where dopamine binds to D1R, D2R, and D3R which are primarily expressed in the medium spiny neurons (MSNs) (22). The large dopamine increases triggered by DA cell firing are necessary to stimulate D1 receptors (D1R) in the NAc and also cause longer lasting stimulation of D2R as well (23). Drug intake must cause dopamine increases that need to be fast and large enough to stimulate low-affinity D1R in addition to D2R, which leads to the activation of the direct pathway and inhibition of the indirect pathway (23). Only the large increases in dopamine that are triggered over a short time span of less than 10 min are

associated with reward whereas dopamine increases over a longer time span of 1 hour were not associated with reward (23). This would explain that routes of drug administration that achieve higher drug levels in the brain more quickly such as smoking or injection are more rewarding than routes that result in slower mechanisms such as oral administration (23).

The firing of D1R and D2R MSNs are dependent on each other; thus, enhanced DA signaling stimulates one population but inhibits the other. Enhanced DA signaling from drug exposure can alter the balance between striatal signaling through the direct (D1R mediated) and the indirect (D2R mediated) pathways (6). An imbalance between signaling in these pathways is potentially the neurophysiological mechanism underlying behavioral changes observed in addiction. D1R mediated signaling enhances sensitivity to drug reward and thus an enhanced D1R mediated signaling could contribute to compulsive drug taking (6). Moreover, addiction is thought to be associated with hypodopaminergic signaling within the brain, which is substantiated by neuroimaging studies in humans. In fact, PET studies have enabled the quantification of drug induced dopamine increases in humans where investigators have found that dopamine increases triggered by stimulant drugs are significantly lower in cocaine abusers compared to control subjects (23). Similarly, blunted dopamine responses to a drug challenge were also observed in alcoholics.

Dopamine increases in the nucleus accumbens are not the only neural mechanisms to contribute to addiction behaviors. In fact, drug addiction progresses from a shift from controlled drug taking behavior mediated by the NAc (which drives reward) to compulsive drug taking behavior mediated by the dorsal striatum (which drives habit formation) (23, 24). Moreover, chronic and repeated exposures of addictive drugs have been associated with downregulation of the D2R in the NAc, which leads to reduced dopamine inhibition of the indirect pathway (25). Reduced indirect pathway activity leads

to decreased thalamo-cortical stimulation and thus decreased activity in the prefrontal cortex (PFC), including the anterior cingulate (ACC) and orbitofrontal (OFC) cortical regions (25). Because the PFC plays a key role in the regulation of limbic reward regions and higher order executive functions such as self-control, it is not surprising that this ultimately affects behavioral choices and decreased ability to avoid specific drugs of abuse (26). In fact, increased PFC activity is thought to lead to a syndrome of impaired response inhibition and salience attribution (iRISA) in addiction, which is characterized by increased salience to the drug and decreased interest to non-drug related rewards (26, 27).

The use of imaging tools has aided in the understanding of associated brain circuits that are disrupted in addiction and how these dysfunctions can lead to decreased motivation for non-drug rewards, decreased executive control, and increased motivation to engage in drug abuse behaviors (23). In spite of the circuit level understanding of addiction and reward behaviors, a lack of understanding in the specific synaptic and cellular level alterations of key brain circuits has impeded the development of targeted therapeutics to treat addiction behaviors.

1.1.3 Single Nucleotide Polymorphisms (SNPs): Biological Markers of Disease

The inheritance of a psychiatric disorder such as addiction is determined by multiple factors including genetic predisposition (7). However, this is not attributable to mutations in a single gene, but instead to a combination of effects from gene variants in multiple different genes. In contrast to the rare and highly penetrant mutations that are sufficient to cause disease, single nucleotide polymorphisms (SNPs) are the simplest example of DNA variation among individuals that can occur throughout the genome at a frequency of about 1 every 300 nucleotides, and account for approximately 90% of human genetic variation (28). SNPs that occur within the coding region of a gene can be

silent SNPs in which the variant allele encodes for the identical amino acid as the original or it can be non-synonymous in which the variant allele changes the encoded amino acid thus having potential consequences on protein configuration (29). Non-synonymous SNPs as well as those in regulatory DNA regions are thought to have the greatest effect on phenotype (29). Other SNPs affect gene regulation and gene expression while most SNPs are neutral and have no effect on phenotype (29, 30). Over 10 million SNPs have been identified in the human genome and these non-synonymous amino acid substitutions are thought to manifest as the diverse phenotypic variations among individuals (31). There is, however, an ongoing stream of research involved in identifying the biologically relevant SNPs that are associated with vulnerability to various psychiatric diseases, including substance use disorders.

Genome-wide association studies (GWAS) can identify common SNPs within the human population that are correlated with risk for complex human brain disorders (32). For example, the Collaborative Genetic Study of Nicotine Dependence (COGEND) has identified several SNPs associated with risk for addiction behaviors, particularly rs16969968, which encodes a change of amino acid at position 398 from aspartic acid (D) to asparagine (N) in the α5 subunit (33, 34). A number of studies in overexpression systems and mouse models of CHRNA5 D398N have investigated the functional consequences of this SNP (34-37). However, the utility of mouse models is limited given the evolutionary distance between the mouse and the human and overexpression systems do not mimic the endogenous cholinergic signaling occurring in a human brain, making these studies have little relevance toward understanding the mechanisms of human disease. Thus, to clarify and build upon previous work, we have used human subject-derived iPS cell lines to generate human neurons in which we have conducted detailed mechanistic analyses to understand the cellular and synaptic consequences of CHRNA5 D398N (**Appendix**).

Another commonly occurring disease-associated SNP is rs1799971 (OPRM1 A118G), which produces a non-synonymous amino acid substitution in the human MOR, replacing an Asparagine at residue 40 (MOR N40) with Aspartate (MOR D40) and is associated with AUDs in specific ethnic groups (38-43). Of the many non-synonymous amino acid substitutions in the coding region of the human MOR, the N40D SNP is of particular importance because it has the highest overall allelic frequency of all OPRM1 coding region variants, as much as 10-12% in Caucasian populations and up to 50% in certain Asian and Indian populations (44). Despite its high prevalence and physiologic relevance, its role in the modulation of synaptic plasticity in the brain is largely unknown.

In order to fill in the gaps of previous work, it is necessary to understand and dissect the functional consequences of such disease associated SNPs in a human model system. The focus of this dissertation is to dissect the functional role of ORPM1 A118G and prove the utility of subject-derived stem cell model systems in understanding the mechanisms underlying psychiatric disease.

1.2 Mu Opioid Receptor Signaling and Function

1.2.1 Neurophysiology of MORs

The MOR, encoded by the genetic locus OPRM1, is widely distributed throughout the central nervous system. It is highly expressed in the thalamus, ventral tegmental area (VTA), dorsal and ventral striatum, periaqueductal gray (PAG), locus coeruleus, and the dorsal horn of the spinal cord (45). Thus, it modulates a diverse range of physiological functions including nociception and analgesia, reward and euphoria, immune functions, stress responsivity, and respiration (44, 46, 47). The MOR has a few endogenous ligands as it binds with high affinity to β-endorphin and enkephalin but with lower affinity to dynorphin (46). Along with endogenously released ligands, the MOR

binds with high affinity to exogenous opioid drugs including morphine, heroin, methadone, fentanyl, etc (48). It has been repeatedly shown that endogenous opioids and MOR signaling play a role in the reinforcing effects of alcohol and other drugs of abuse. Levels of endorphins are increased following alcohol consumption in the hypothalamus, VTA and ventral striatum (48-51).

1.2.2 Structural Basis of MOR Function

MORs are class A G protein-coupled receptors (GPCRs) which possess seven transmembrane domains linked by three intracellular loops (ICL1-3) and three extracellular loops (ECL1-3), a 66 amino acid extracellular N terminus and a 70 amino acid intracellular C terminal tail within the transmembrane region (52). Opioid peptides approach the receptor from the extracellular space and activate the receptor by interacting with the binding pocket formed by transmembrane (TM) domains TM3, TM5, TM6 and TM7 and some residues in extracellular loop 2 (52, 53). The transmembrane domains are largely made up of hydrophobic amino-acids and organized in an alpha helix (3). The G protein interacts with ICL2 and ICL3 as well as the C terminal tail (3). The C terminal tail has putative phosphorylation sites at Serine, Threonine and Tyrosine for G protein receptor kinases (GRKs) involved in phosphorylation and the regulatory events after ligand binding (54). Moreover, ECL2 creates a wide opening allowing unobstructed access to the binding pocket, which is much more exposed to the extracellular surface compared to that of other GPCRs (52).

1.2.3 Mu Opioid Receptor Signaling

1.2.3.1 MOR signaling and desensitization

The mechanisms mediating MOR function during acute agonist exposure are critical to their role in modulating neurotransmission. MORs are coupled to pertussis toxin-sensitive heterotrimeric $G_{i/o}$ proteins (**Figure 2**) (3, 54, 55). The classical and most immediate response to MOR activation by an endogenous agonist such as β-endorphin or exogenous agonist such as morphine or fentanyl is the regulation of ion channel function, occurring within 0.1 seconds of agonist binding (54, 56). Specifically, the Gα and Gβγ subunits dissociate from one another and activate G-protein coupled inwardly rectifying K^+ (GIRK) channels and inhibit P/Q-type, N-type, and L-type voltage-dependent Ca^{2+} channels, respectively (3, 54). These processes collectively result in neuronal hyperpolarization and inhibit neural excitability. When the G protein signal saturates within milliseconds after agonist exposure, G protein receptor kinases (GRK) phosphorylate the Ser^{375} and Thr^{370} residues of the C terminal tail of the MOR which facilitates β-arrestin binding, promoting endocytosis (54).

1.2.3.2 Biased Agonism

MOR activation and regulation is strongly agonist dependent, meaning distinct MOR ligands preferentially activate different cell signaling pathways to result in different physiologic outcomes (57). Molecularly, this is due to the fact that different agonists do can stabilize different active conformations of the MOR, which thus engage a different subset of intracellular signaling molecules (58). The ability of distinct GPCR-agonist complexes to differentially activate intracellular signaling molecules provides new opportunities for the development of drugs that activate a desired intracellular pathway to mediated a desired physiological effect while minimizing side effects that are elicited by activation of undesired signaling pathways. For example, functional selectivity at the

MOR is used in drug discovery to improve the pharmacological profiles of opioid analgesics that can induce adverse effects such as respiratory depression (59).

Molecular investigations have also revealed differences in MOR signaling. For example, endogenous opioid peptides such as β endorphin as well as the synthetic MOR agonist DAMGO ([D-Ala^2, N-MePhe^4, Gly-ol]-enkephalin) induce robust MOR endocytosis whereas the exogenous agonist morphine fails to promote endocytosis in vitro (60, 61). This was observed both in vivo as well as in a variety of cultured neurons (61, 62). While morphine has traditionally been thought to not induced internalization, cultured striatal neurons and cultured nucleus accumbens neurons have proved otherwise in that morphine has promoted MOR internalization (63). While these are important observations, it is important to quantify signaling bias in such a way that reveals the unique signaling profile that is induced by the ligand and would allow the signaling bias profiles of ligands in different cell types to be compared. This involves comparing the drug potency and efficacy in cell-based signaling assays to the performance of a reference agonist that fully activates the system. This involves the use of a relative transduction ratio which estimates a 'transduction coefficient' log (τ/K_A) which is comprised of the functional equilibrium dissociation constant K_A as well as τ which accounts for the intrinsic efficacy of an agonist along with the receptor density (64). These values can be compared across two signaling pathways for an agonist to obtain a relative transduction ratio $\Delta\Delta\log(\tau/K_A)$ that measures agonist bias (64).

The distinct effects displayed by morphine in MOR desensitization and internalization suggest that ligands that display bias toward G-protein mediated pathways and against β arrestin recruitment may have improved therapeutic profiles as analgesics because they would provide pain relief with fewer adverse effects such as addiction or respiratory depression (65, 66). This is demonstrated in a recent study exploring how structural variations of MOR ligands as well as prescription opiates can

stabilize alternative receptor conformations to induce a distinct pattern of intracellular signaling cascades (59). Authors found that SR compounds potently activate GTPγS binding but have differential βarrestin2 signaling profiles at the MOR and analyzed the bias factor parameters of MOR agonists across multiple functional assays to find that agonists that displayed G protein signaling bias promote greater antinociception with less respiratory suppression (59). Further studies that investigate a more diverse array of signaling profiles along with multiple chemical and structural variations of agonists and how they may promote other behavioral and therapeutic advantages will lead to an increased understanding of functional selectivity at the MOR as well as the development of safer opioid therapies. MOR regulation and signaling is not only species and cell type dependent, but also dependent on the expression levels and the subcellular localization of GRKs and β-arrestin proteins (67-70). Thus, it is necessary to study ligand efficacy and signaling of MOR agonists in a cell-type specific and human-specific system.

1.2.4 MOR Mediated Mechanisms of Tolerance

Although MORs have distinct effects on ion channel modulation, they also exhibit more prolonged and robust effects on other signal transduction processes, particularly receptor desensitization, internalization, and downregulation which cause short-term and long-term opioid tolerance (54). Tolerance can be conceived as a type of homeostasis, by which MOR expressing neurons adapt to prolonged opioid receptor activation by rapid receptor desensitization to normalize overall neural activity. Agonist-dependent phosphorylation of MORs changes the receptor conformation and increases its affinity to β-arrestin, which causes uncoupling of G protein and leads to the recruitment of endocytic machinery leading to receptor internalization (54). Receptor internalization, which reaches a steady state within 30 minutes, ensures that MORs are uncoupled from

downstream signaling pathways (**Figure 2**) (54). This has been observed in MOR transfected cells, neuroblastoma cells as well as mature cultured neurons (60, 62, 71, 72). MOR phosphorylation and uncoupling and subsequent receptor internalization have long been considered to directly contribute to development of opioid tolerance by reducing the number of functional receptors at the cell surface. However, internalized receptors are predominantly dephosphorylated and recycled back to the cell surface in a re-sensitized state (54). This agonist induced internalization plays an important role in reducing the development of opioid tolerance after chronic agonist treatment (71, 73, 74).

While desensitization and short-term tolerance are both associated with a loss of functional cell-surface MORs, mechanisms responsible for long-term tolerance also involve reduced receptor reserve. Downregulation of opioid receptors after chronic opioid treatment is a long-term adaptive process that likely occurs from the degradation of internalized receptors or from decreased receptor synthesis (54). Long-term opioid exposure related downregulation of MORs has been demonstrated *in vitro* whereas results have varied *in vivo*, likely due to the fact that mechanisms of long-term tolerance vary by species and brain regions.

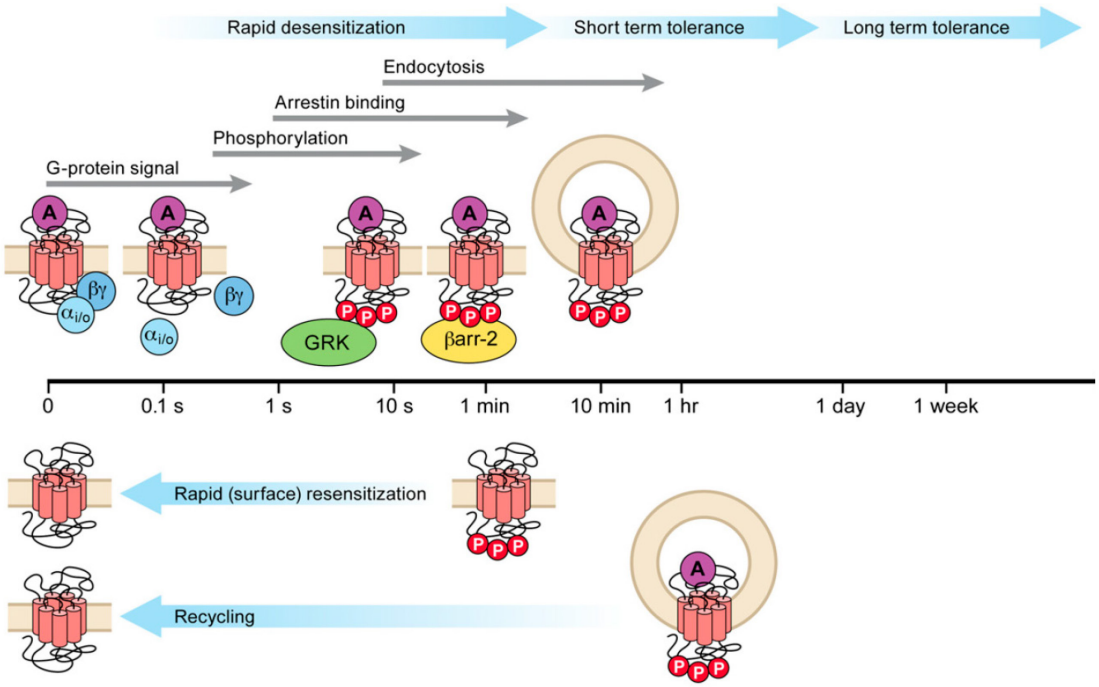

Figure 2: General scheme of MOR activation following agonist binding. Acute activation and rapid desensitization includes activation of the G-protein signal, phosphorylation of C terminus, binding of β-endorphin, and endocytosis. Short-term tolerance occurs on a time scale of 1 day, long-term tolerance requires 1 week or longer. Time scales for each process are shown (log scale). *Taken from Williams et al (2013) (4).*

1.3 Functional Genetic Variation at the MOR

1.3.1 Disease Associated MOR SNPs

Large-scale sequencing of human OPRM1 gene has revealed non-synonymous amino acid substitutions that occur within the coding region of the receptor (75). These non-synonymous amino acid substitutions are found not only on the N-terminus but through the transmembrane domains and intracellular loops (ICLs) of the receptor (**Figure 3**). Not only do MOR genetic variants change the amino acid sequence of the receptor, but they have been implicated in altering receptor stability, expression and downstream signal transduction (3). This is due to the fact that GPCR signaling is complex, as described in section 1.3. Thus, it is unlikely that simple changes in receptor conformation from SNPs can lead to predictable changes in MOR signal transduction.

Thus, due to their role in mediating reward, it is not surprising that genetic variants of MORs are linked to addiction and other reward related behaviors.

With respect to mu opioid receptors, the commonly prescribed opioids such as morphine and buprenorphine have relatively low efficacy and event small differences in receptor expression and signaling efficacy due to MOR SNPs could have more significant impact on an individual's response to these drugs (3). Also, clinically used opioids are structurally and chemically diverse and likely to be induce different pharmacokinetic responses with even minor changes in MOR structure (76) . Thus, even single amino acid substitutions resulting from SNPs have the potential to alter MOR signaling globally or in a ligand dependent manner in multiple ways. First, SNPs have the ability to affect the ligand's ability to bind the receptor in the situation that the SNP alters the stability of the MOR or the composition of the binding pocket. Second, SNPs potentially may alter the ligand-receptor complex and thus stabilize a slightly different active conformation of the MOR. Third, SNPs have the ability to alter the receptor's ability to couple to G proteins and associated signaling and regulatory proteins. Thus, the effects of non-synonymous SNPs on MOR function and an individual's clinical response can be mediated through various mechanisms. Thus, given that the MOR modulates a diverse range of physiological functions including nociception and analgesia, reward and euphoria, stress responsivity, etc, it is not surprising that MOR SNPs have been implicated in variability of clinical outcomes to opioid mediated pain relief and the prevalence of drug abuse.

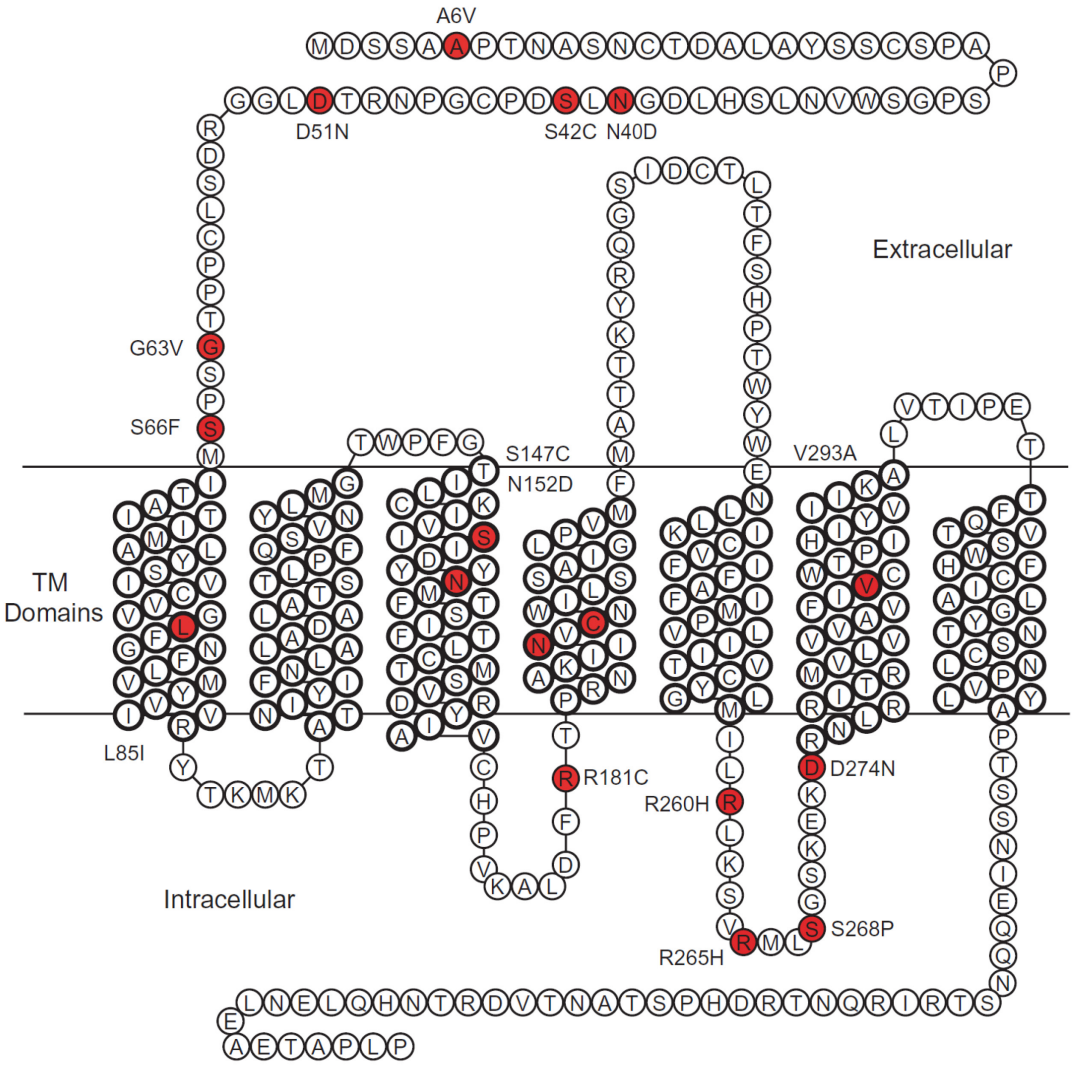

Figure 3: Naturally occurring, non-synonymous OPRM1 gene variants in the human population.
Amino acid substitutions and their position in the MOR protein are indicated in red.
Taken from: Knapman and Conner (2014) (3)

1.3.2 Functional Characterization of MOR N40D

Due to their role in mediating reward, it is not surprising that genetic variants of MORs are linked to addiction and other reward related behaviors. Particularly, the A118G single nucleotide polymorphism (SNP) in OPRM1, rs1799971, is a non-synonymous gene variant which replaces an asparagine (N) to an aspartate (D) at N-terminal position 40 (N40D), and is associated with drug dependence phenotypes in

humans (77). For example, the MOR N40D gene variant has been linked in various clinical studies to alcohol dependence (38-40, 42, 43, 78-82), nicotine reward (83), and smoking relapse (83-85), suggesting it has a physiologic function in the modulation of MOR signaling in reward. Additionally, of the many non-synonymous amino acid substitutions in the coding region of the human MOR, the N40D SNP is of particular importance because it has the highest overall allelic frequency of all OPRM1 coding region variants, specifically 10-12% in Caucasian populations and up to 50% in certain Asian and Indian populations (44). Due to its association at varying levels with multiple drugs of abuse, understanding the functional consequences of the MOR N40D SNP as opposed to other SNPs within OPRM1 will help clarify mechanisms of addiction that are shared across different addictive substances.

1.3.2.1 Human Epidemiologic Studies: Understanding Substance Abuse

Epidemiological studies investigating the possible association of the G118 allele to alcohol dependence have been inconsistent. For example, several case-control studies have reported associations between the G118 allele of OPRM1 and alcohol dependence (79, 80, 82, 86) whereas other studies reported a lack of association between the SNP and alcohol dependence (81, 87). Others have even reported the opposite result that the A118 allele confers risk for alcohol dependence (39, 88, 89). Two subsequent meta-analyses were conducted aiming to combine the results from multiple studies to increase power. One concluded that an association does not exist between G118 and alcohol dependency (90) whereas another reported an association in Asian populations but none in Caucasians (1, 91). It is possible that the lack of association of epidemiological studies and the diversity of results may result from small sample sizes involved in the studies, the ethnic heterogeneity of the study populations or the lack of

appropriate population-based controls (92). Moreover, gene-environment interactions as well as the clinical heterogeneity of alcohol use disorders necessitates larger population based studies in which individuals are selected from homogenous populations of similar ethnicity and behaviorally similar in terms of their DSM-V diagnosis of alcohol dependence and alcohol abuse in order to be able to make appropriate comparisons (93). Thus, epidemiological studies are not best suited to understand the role of human genetic variation in neuropsychiatric disease development.

1.3.2.2 Animal models of MOR N40D

Modeling human neuropsychiatric disorders, particularly the role of MOR N40D in addiction related behaviors, has been modeled in animals using various approaches. Although there are two mouse models for the MOR N40D genetic variant, studies using either of these two mouse lines have provided ambiguous results about the functional consequences of the SNP (91, 94-96). Because of the high sequence similarity between the mouse and human MORs nucleotide sequence (86.9%) as well as at the amino acid level (92.3%), one knock-in mouse model was developed using bacterial artificial chromosome engineering that carried A112G, which is the mouse equivalent of the human A118G SNP at OPRM1, by introducing an asparagine (N) to aspartate (D) substitution in the context of a murine N terminal receptor protein sequence (96). The A112G mouse exhibits decreased transcription and translation of the D40 MOR due to decreased mRNA levels in the hypothalamus, periaqueductal grey (PAG), ventral tegmental area (VTA), nucleus accumbens (NAc), cortex, but not in the hippocampus (**Figure 4B**) (96). Moreover, these mice exhibit a blunted antinociceptive response and diminished locomoter activity to acute morphine treatment (96). These results mimic that

of human post mortem samples (97) as well as human patients who require higher morphine doses achieve adequate analgesia (98).

There is also evidence that the loss of a potential glycosylation site at the N40D position at the N-terminus of the receptor may contribute to lower receptor expression levels and even alter the molecular weight of MORs in mice carrying the G118 alleles (55 kDa) compared to mice carrying the A118 alleles (62 kDa) (99). This difference in molecular weight between A118 and G118 receptors was abolished upon de-glycosylation using PNGase F, suggesting the difference in initial molecular weights is due to loss of N-terminal glycosylation at position 40 in the N-terminus (**Figure 4A**) (99).

To evaluate whether changes in receptor function were responsible for these behavioral alterations, experiments using voltage sensitive dye imaging (VSDi) techniques in the hippocampus along with EEG recordings to study oscillatory activity in the hippocampus found that the augmented excitatory response elicited by opiate administration in A112 animals was reduced in G112 animals (96). Given that MOR protein levels are similar in the hippocampus of A112 and G112 mice, these data suggest that the A112G SNP in MOR reduces receptor functionality. The OPRM1 A112G SNP was also implicated in influencing complex human behaviors as the G112 mice were found to exhibited increase home-cage dominance and increased nonaggressive social interactions and increased resilience to social defeat compared to A112 mice. Overall, this A112G mouse model suggests that the SNP elicits a “loss-of-function” phenotype on the basis of cellular and behavioral differences from A112G.

A complementary approach was used to generate a second humanized mouse in which conflicting phenotypic evidences were found (1). This OPRM1 A118G humanized line was generated by replacing the mouse OPRM1 exon 1 with human exon 1 sequence on a C57BL/6 background carrying either homozygous alleles for A118 or

G118 of OPRM1 (1). The G118 mice exhibited increased Dopamine response to alcohol compared to A118 mice as measured by in vivo microdialysis (**Figure 4C**) (1). Moreover, an OPRM1 SNP that is functionally equivalent to the human A118G polymorphism has been identified in rhesus macaques as the C77G SNP, which confers a homologous amino acid change from an asparagine (N) to aspartate (D) at the N terminus of the MOR (100, 101). Multiple groups have reported that male macaques carrying the OPRM1 G77 allele exhibit not only increased alcohol consumption but also drank to intoxication more frequently than C77 male macaques (100, 101). These studies together suggest that the G allele confers an increased rewarding experience to alcohol, suggesting a “gain-of-function” phenotype.

These animal models suggest that the OPRM1 A118G SNP causes not only molecular and cellular alterations in MOR expression and function, but also have revealed that this SNP has important implications in complex human behaviors including stress resiliency as well as social affiliation and social defeat behaviors. Despite the utility of animal models in understanding the molecular and functional consequences of OPRM1 A118G, the results are quite conflicting. This suggests that identifying genetic sources of variability to more complex behavioral traits such as alcohol preference and attributing these traits to specific molecular and cellular changes in specified brain regions is very challenging. These results suggest that the sources of variability are due to species-specific mechanisms of MOR function that must be elucidated using a human specific model system.

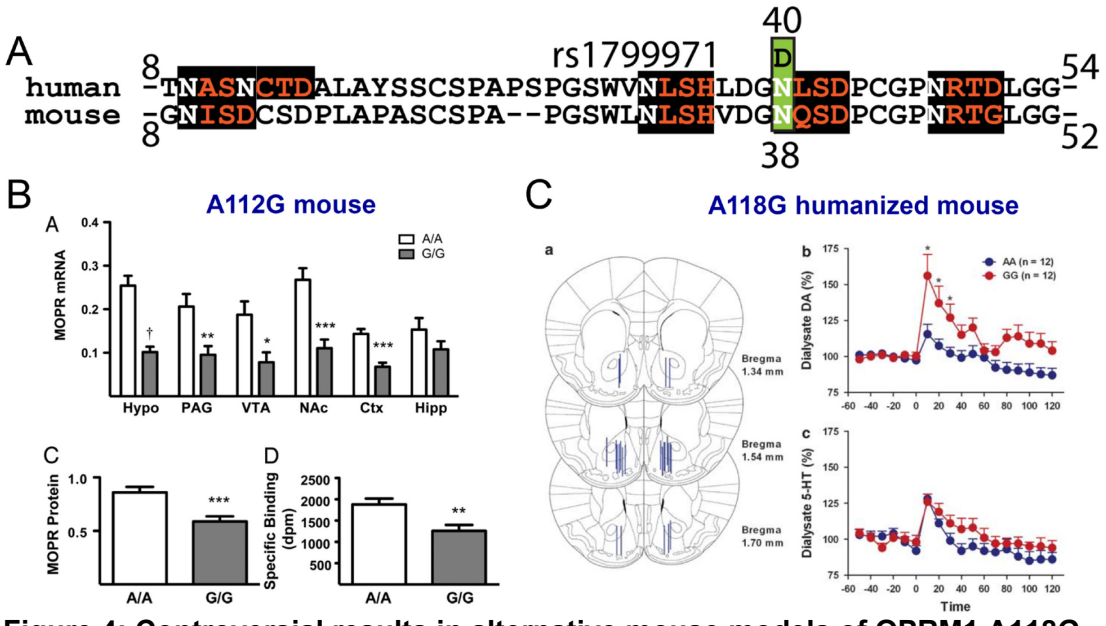

Figure 4: Controversial results in alternative mouse models of OPRM1 A118G. **(A)** Alignment of human and mouse MOR N-termini reveals 5 putative glycosylation sites in the human whereas mouse exhibits only 4, revealing potential mechanism for controversial results. **(B)** A112G mouse model exhibits a "loss of function" phenotype. **(C)** A118G humanized mouse model exhibits a "gain of function" phenotype. *Taken from Berrettini (2013) and Ramchandani et al. (2011)* (1, 2).

1.3.2.3 Heterologous expression systems

Given the heterogeneous results of animal models, this SNP has been the subject of countless molecular investigations as to its functional consequences by understanding differences in gene expression, protein expression and receptor signaling mechanisms. The majority of these functional studies understanding MOR N40D use heterologously expressed receptors in immortalized cell lines such as HEK 293, CHO-K1, or rat SCG cells. These studies have provided a wealth of information on the consequences of N40D on receptor expression, localization and pharmacology although the results of these studies have been highly contradictory (3). For instance, the N40 allele of the MOR was originally thought to cause a threefold increase in binding affinity for endogenously released ligand β-endorphin in a *Xenopus* oocyte expression system (102). However, this result was refuted in subsequent investigations in which the N40D

SNP was found to have no impact on not only binding affinity (1), but also rate of desensitization, internalization or re-sensitization for β-endorphin, morphine and morphine-6-glucuronide in HEK293 cells (103). Ramchandani et al (2010) found similar [^{3}H]-DAMGO and β-endorphin binding in CHO cells as well as in trigeminal ganglion neurons from humanized mouse line (1). Befort et al (2001) similarly identified unchanged binding affinities for a variety of structurally diverse opioids (β-endorphin, met-enkephalin, dynorphin A, morphine, diprenorphine, DAMGO, CTOP) in wild type and mutant receptors in COS cells (104).

Findings that G112 expressing mice may have lower MOR expression compared to A118 expressing mice was supported by experiments done in heterologous expression systems as well. Zhang et al (2005) and Huang et al (2012) found that not only do D40 MOR exhibit lower expression levels compared to N40 MORs but also have a shorter half-life (12 hours) compared to N40 MORs (28 hours) in CHO cells (97, 99). Similar enzymatic de-glycosylaton of MOR decreased receptor expression in HEK-293 cells by 90%, further corroborating the loss of glycosylation as a potential mechanism for the functional consequences of MOR N40D (105).

Further investigations into differential G-protein mediated ion channel regulation and downstream signal transduction following MOR activation due to MOR N40D have similarly yielded conflicting results. Margas et al (2007) first reported increased DAMGO and morphine potency for Ca_V channel inhibition at D40 expressing rat SCG cells (106) while Mahmoud et al (2011) report decreased morphine potency in mouse trigeminal ganglion cells expressing “humanized” D40 MORs (107). Similar conflicts were observed for DAMGO for Ca_V inhibition by subsequent studies repeated in HEK 293 cells and sympathetic neurons. The effect of MOR N40D on adenylate cyclase (AC) inhibition and cyclic adenosine monophosphate (cAMP) production were further examined in several studies and refuted, further underscoring the idea that there is unlikely to be one true

functional consequence for MOR N40D function. For example, Beyer et al (2004) found no differences in the effect of morphine, morphine-6-glucuronide (M-6-G) or β-endorphin to inhibit forskolin stimulated cAMP accumulation (103), and Fortin et al (2010) found no differences in DAMGO, endomorphin 1 or leu-enkephalin's ability to modify cAMP mediated gene transcription in HEK293 cells expressing either D40 or N40 MORs . In contrast, Kroslak et al (2007) has reported a decreased potency for cAMP inhibition for morphine, methadone, and DAMGO in D40 cells (105).

These contradictory results suggest that the consequences of the N40D substitution on the signaling profile of the MOR are not well understood. While there are no straightforward explanations for the observed differences, it is possible that the variability arises from the fact that each study uses different expression systems for analysis. More importantly, the physiological relevance of differences in binding affinities, signaling, and desensitization rates exhibited by MOR variants in these engineered expression systems is difficult to predict, making it impractical to make direct comparisons between signaling profiles in different heterologous systems. Each engineered cell line or transgenic mouse line may exhibit differences in the availability of G proteins, effector molecules and regulatory proteins, which may be causing the variability in results. Moreover, MORs are expressed in a variety of different cell types within the brain, making it likely there are cell-type specific signaling mechanisms that are involved in the manifestation of disease pathology in a human. It is thus necessary that we use a species-specific model system to capture the signaling and functional heterogeneity of MOR signaling.

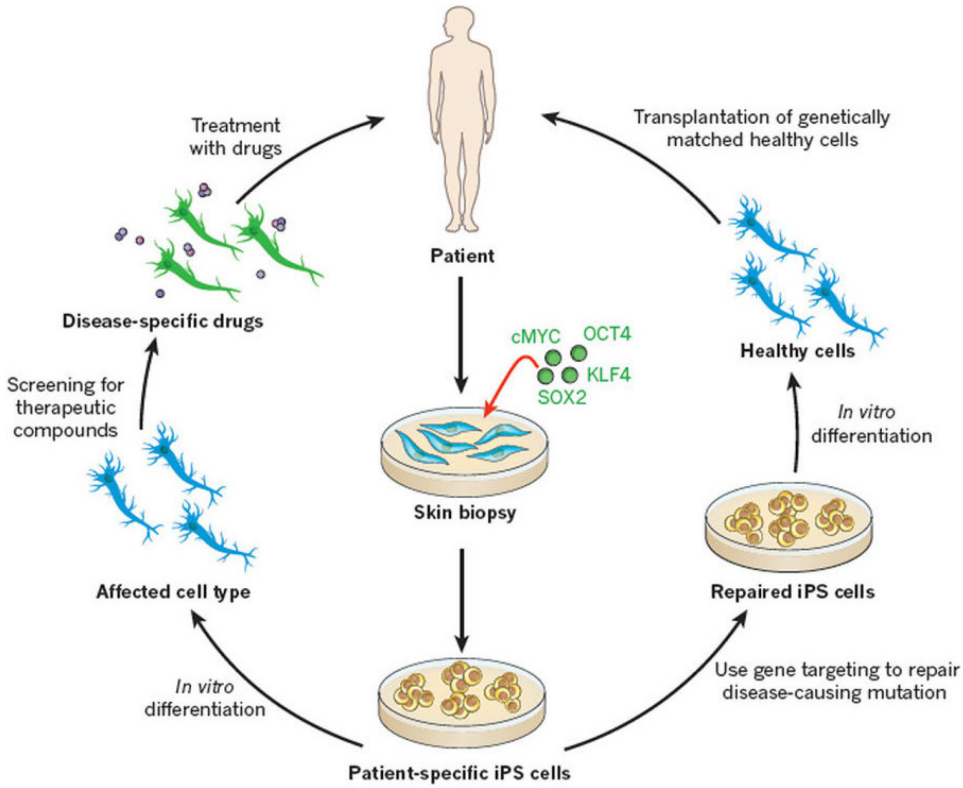

Figure 5: iPS Cells to Model and Treat Human Disease.
Patient-specific iPS cells from ectopic expression of OCT4, c-Myc, KLF4 and Sox2 in cells isolated from a skin biopsy can be used in one of two ways. **(1)** In the situation where the disease causing mutation is known, genome engineering can be used to repair the DNA sequence in iPS cells, which can then be differentiated into the affected neuronal subtype for transplantation into the patient (right side). **(2)** Patient-specific iPS cells can also be differentiated into the affected neuronal subtype to model the neuropsychiatric disease in vitro (left side). Taken from *Daisy A. Robinton & George Q. Daley, Nature (2012)* (5).

1.4 Using Human Induced Neuronal (iN) Cells to Model MOR N40D Function

1.4.1 Hypothesis & Approach

The MOR N40D SNP is thought to cause molecular and cellular changes in neuronal function. While the studies using heterologous expression systems and transgenic mice carrying the OPRM1 A112G SNP have provided an abundance of information about the functional consequences of MOR N40D, they give very limited and even *contradictory* evidence about the molecular and cellular consequences of the N40D

SNP in human neuronal context. Human neural tissue, on the other hand, is often limited to either aborted fetal tissue or postmortem tissue. Fetal tissue is limited and may not be suitable to study addiction, as alcohol and substance abuse are adult disorders. Obtaining patient biopsies or post mortem brain samples can be highly invasive, extremely rare and yield little material for functional analyses on synaptic transmission defects. Therefore, it has been impossible to study cellular and molecular consequences of MOR N40D and its role in synaptic function in a *human* system.

Understanding of the molecular and cellular underpinnings of neuropsychiatric disease, particularly MOR N40D, will require the use of technology that yields a robust source of human neuronal subtypes affected in a given mental illness and is able to capture the role of genetic variants in disease etiology. To satisfy this need, we used subject-specific induced pluripotent stem (iPS) cells to model disease etiology, which is a technology developed by Takahashi and Yamanaka in 2006 involving the reprogramming of adult fibroblasts to a pluripotent state by overexpression of defined transcription factors, Oct3/4, Sox2, c-Myc, and Klf4 (108). Since then, iPS cells from other terminally differentiated cells such as peripheral blood mononuclear cells, hair follicles, keratinocytes, urine cells, and a number of other somatic cell types have been developed (109-113). Research into the development of novel methodology to improve reprogramming techniques through the use of integration free viruses, small molecules and even the development of a fully automated robotic cell reprogramming system have eased their use in disease modeling.

The iPS cell technology thus yields access to patient-specific cells for two specific purposes (**Figure 5**): **(1)** In the situation where the function of the disease-causing mutation is in question, genome engineering can be used to repair the DNA sequence, differentiate the cells into the affected neuronal subtypes, and be used to study gene function or be engrafted back into the patient's brain. **(2)** Alternatively,

directed differentiation of the patient-specific iPS cells into the defined neuronal subtypes can be used for functional readouts, thus offering a novel platform for modeling the genetic contribution to neuropsychiatric disorders (114).

Therefore, to address MOR N40D function in a human-specific neuronal context, we take advantage of both these strategies presented in **Figure 5.** We have used the induced neuronal (iN) cell technique using ectopic expression of neuronal transcription factors (TFs), to dissect the underlying neural and synaptic basis of the N40D MOR variant (115, 116). We specifically generated human GABAergic iN cells (**Figure 6**) from iPS cells of donors with well-characterized drug abuse behaviors that are homozygous for either the major (N40) or minor (D40) alleles of the MOR. Using this approach, I will test the *hypothesis that the N40D SNP in the MOR impairs MOR trafficking and expression, ultimately perturbing opioid sensitivity to synaptic function.*

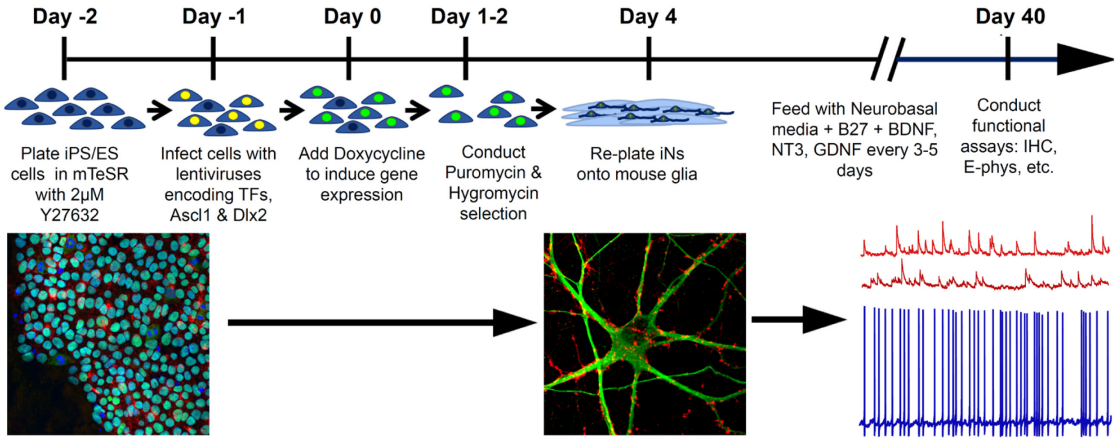

Figure 6: Generating human GABAergic iN cells from human pluripotent stem cells.
We transduce human iPS cells or ES cells using lentiviruses expressing lineage specific transcription factors (TFs), specifically Ascl1 and Dlx2, which effectively convert the stem cells into subtype-specific human neurons that are synaptically active 2-5 weeks following lentiviral mediated gene expression. Protocol to generate GABAergic iN cells taken from *Yang et al. Nature Methods (2017)*.

1.4.2 Project Overview

The goal of this project is to dissect the neural and synaptic consequences of the MOR N40D SNP in human iN cells generated from human pluripotent stem cells carrying OPRM1 A118G in the human MOR. This A118G SNP produces a non-synonymous amino acid substitution in the MOR, replacing Asparagine 40 (MOR N40) with Aspartate (MOR D40) and has been implicated in altering receptor signaling and contributing to drug abuse behaviors in certain ethnic groups (38, 39, 42, 87, 88, 93, 117). However, the neural synaptic mechanisms that mediate these alterations have not yet been determined, likely due to species-specific and context-specific mechanisms of MOR function. This makes it increasingly necessary to dissect the cellular and molecular mechanisms underlying MOR function in the N40D SNP in the context of *human* neurons. Thus, we use human iPS cell lines carrying either homozygous MOR N40 or MOR D40 alleles from multiple subjects with well-characterized alcohol abuse, nicotine dependence behaviors, and known ethnicity (European descent) to generate GABAergic human neurons to study MOR mediated synaptic alterations that have implications in understanding drug abuse behavior in humans. To mitigate the complexity of diverse genetic backgrounds of the subject iN cells derived from multiple human subjects, we also have employed CRISPR/Cas9 genome-editing to generate two pairs of isogenic human pluripotent stem cell lines for further phenotypic validation. To achieve my objective and test my hypothesis, I will address the following two **Specific Aims**:

1.4.2.1 Characterize the functional impact of the N40D SNP on neuronal function and acute MOR signaling in human neuronal cells

To characterize the functional impact of N40D on MOR signaling, I have: **(A)** Conducted biochemical and morphological analyses to uncover whether N40D affects

neuronal maturation and differentiation of human iN cells. **(B)** Used electrophysiology to elucidate the synaptic consequences of the N40D SNP on MOR activation and synaptic inhibition by MOR specific agonist, DAMGO. **(C)** Recapitulated synaptic phenotype of human subject derived iN cells in two sets of CRISPR/Cas9 genome-edited isogenic cell line derived neurons.

1.4.2.2 Understand the role of the N40D SNP on the development of long term tolerance at the MOR

To study the role of N40D SNP on MOR trafficking and the development of long term tolerance, I have: **(A)** Elucidated the synaptic effect of chronic DAMGO exposure on MOR function in human patient derived neurons. **(B)** Recapitulated the synaptic consequences of long term MOR activation in two sets of isogenic human iN cells.

Chapter 2: CRISPR/Cas9 Genome Editing for Disease Modeling

2.1 Introduction

The advent of human iPS cell technology has provided unanticipated opportunities to generate unlimited sources of human neural tissue to model human neuropsychiatric diseases in a culture dish. Reprogramming somatic cells from human patients into pluripotent stem cells followed by directed differentiation into disease-relevant neuronal types has created opportunities for mechanistic studies into the development of neuropsychiatric diseases as well as for the discovery of new disease therapies (118). However, there are in fact a number of caveats to studying genetic disorders in patient derived cells.

Individual iPS cell lines derived from human somatic cells exhibit high biological variability, hampering their suitability as models of psychiatric disease (119). First, genetic background variation between individuals from which cells are obtained can severely hamper the elucidation of clear phenotypic differences between control and diseased subjects (120, 121). Many GWAS studies have identified disease-associated loci for alcohol abuse disorders and drug addiction (30, 122). However, determining the individual contribution of these genetic variants is very difficult due to modest individual effects and epistatic effects from genetic background (123).

Moreover, a number of studies have reported that iPS cells retain epigenetic memory of the somatic cell from which they were reprogrammed which is retained through their duration in culture (124-130). This retention of epigenetic memory is thought to affect the differentiation capability of different iPS cell lines and thought to cause preferential lineage-specification, promoting differentiation into some neuronal cell types as opposed to others (124). Compounding these difficulties includes the reprogramming methods that utilize viral vectors that may integrate into the iPS cell

genome or the use of oncogenic transcription factors that might introduce mutations into the genome (119). Obtaining clear disease associated phenotypes for risk associated genetic variants would thus require the analysis of large collections of patient-derived iPS cell lines, which is logistically challenging and extremely labor intensive.

Thus, the most rigorous possible comparisons to determine phenotypic alterations are those that are done between cell lines that differ *only* with respect to the disease associated mutations. These cell lines would involve using wild-type and mutant cell lines that are derived from the same parental lines and would mitigate the confounding factors of background genetic variation or retention of epigenetic memory that might influence phenotypes between lines. To generate isogenic cell lines, recent advances in genome editing technologies has made it feasible to engineer disease relevant genetic variations into human stem cells, which will help control for these sources of variability (131, 132). Thus, we have adopted the use of CRISPR/Cas9 (Clustered, regularly interspaced short palindromic repeats/Cas9) genome engineering to generate a pair of isogenic cell lines from the well characterized H1 ES cell line for phenotypic analyses. This will help mitigate the major sources of genetic and phenotypic variation in iPS cells and allow for the elucidation of more well-defined phenotypes.

2.2 Materials and Methods

2.2.1 H1 ES Cell Culture and Maintenance

H1 embryonic stem (ES) cells used for genome editing are an NIH approved cell line. H1 ES cells were cultured feeder-free on Matrigel ® Matrix (Corning Life Sciences)-coated 6-well plates or 10 cm dishes in mTeSR medium (STEMCELL Technologies) at 37°C and 5% CO_2. The mTeSR media was refreshed daily, and the H1 ES cells were passaged once a week by dissociation into single cells and plated for maintenance into

6-well plates or for transfection into 10 cm dishes for genome editing. To passage, mTeSR medium was removed, and the wells were washed with Minimal Essential Media (MEM, Gibco), 1 mL for 6-well plate, and 5 mL for 10 cm dish. The MEM was then aspirated, and replaced with 1 mL of Accutase™ (STEMCELL Technologies), 1 mL for 6-well plate and 5 mL for 10 cm dish, and incubated at 37°C for 5 minutes to allow cells to dissociate from the dish. The dissociated stem cells were subsequently collected into a 15 mL conical tube, remnant cells were collected in MEM and added to the conical tube. H1 ES cells were then collected into a pellet at 1000 RPM for 5 minutes, using a tabletop centrifuge. Supernatant was removed and cells were resuspended in 1 mL of mTeSR media containing 5 μM ROCK inhibitor (Stemolecule™ Y27632, Stemgent). A sample of this resuspension was diluted 1:10 and used for counting on a hemocytometer. Using estimation of cell density, 150,000 cells were plated into a 6-well plate for maintenance and 200,000 cells were plated into a 10 cm dish for genome-editing.

2.2.2 Designing Guide RNA for Cas9 Nuclease Cleavage

To convert H1ES cells carrying homozygous major alleles (AA) to homozygous minor alleles (GG), a single guide RNA (sgRNA) sequence was designed from an Optimized CRISPR Design Tool from Feng Zhang's lab at MIT (http://crispr.mit.edu/) to target OPRM1 at exon1 near A118. A total of 4 potential 20 nucleotide (nt) sgRNAs were screened in HEK 293T cells for cutting efficiency and one was selected for OPRM1 genome editing. The target site in the H1ES cells included the major allele sequence; thus, the sgRNAs were designed to incorporate the major allele, and a G was added to the 5' end to increase on-target efficiency (gTCGGACCGCATGGGTCGGACAGG). See Section 2.3.1 for more details on Guide RNA Design and selection.

2.2.3 Cloning sgRNA into PX459 Expression Vector

To clone the 4 sgRNAs into a mammalian expression vector, we designed two oligos for each sgRNA containing the 20nt sgRNA sequence along with its reverse sequence. The forward sequence was flanked by CACC at the 5' end while the reverse sequence was flanked by CAAA at the 3' end. Example shown below:

5' CACC gTCGGACCGCATGGGTCGGAC 3'

3' cAGCCTGGCGTACCCAGCCTG CAAA 5'

These oligo pairs were annealed by mixing 40 µl H2O, 5 µl of 10µM forward primer, and 5µl of 10µM reverse primer in a parafilmed Eppendorf tube. This oligo mixture was heated to a 95°C temperature setting in a heatblock for 10 minutes, and allowed to cool and anneal overnight.

These annealed oligos were then cloned into the PX459 Expression Vector (pSpCas9(BB)-2A-Puro) downstream of a U6 promoter (Addgene Plasmid #62988). To do so, the 8 µg of the PX459 backbone was first digested with the 2 µl of BbsI restriction enzyme (NEB Catalog# R3539S) in a 50 µl volume as directed by manufacturer's instructions. The digestion is then purified using the QIAquick PCR Purification Kit (Qiagen) according to the manufacturer's instructions and the digested plasmid is eluted into 30µl EB Buffer. The annealed sgRNA is then cloned into PX459 by mixing 5 µl of the annealed sgRNA oligo, 0.75 µl of PX459 digested backbone, 3 µl T4 DNA Ligase, 3 µl of T4 DNA Ligase Buffer, and totaled to 20 µl ligation volume using 6.75 µl of deionized and filtered H_2O. Simultaneously, a control ligation is performed using the same setup described but eliminating the 5 µl of annealed oligo. Both ligation tubes are incubated at room temperature for 1 hour.

Half of each ligation product is then transformed into DH10B competent cells by adding 10µl of the ligation product into 100 µl of DH10B competent cells and incubating

on ice for 10 minutes. The competent cells are subsequently heat shocked for 90 seconds in a 42°C water bath and allowed to recover on ice for 5 minutes. The cells are then brought to a sterile area upon which 1000 µl of LB broth is added to the heat shocked bacteria for recovery, and allowed to shake at 650 RPM for 1 hour at 37°C. The bacteria are then centrifuged at 400RPM for 2 minutes and the resulting pellet is resuspended in 200µl of fresh LB buffer. One-tenth (20 µl) of the control ligation as well as the experiment ligation are each plated onto ampicillin agar plates and spread using a sterilized metal spreader. The plates are incubated at 37°C overnight and are examined after 16 hours for colonies. The control ligation had 2-3 colonies whereas the experimental ligation had >200 colonies. Given this optimal ratio, 10 colonies on the experimental plate were picked and each was innocolated overnight in 4 mL of LB buffer with 100µg/µl ampicillin at 37°C. The following day, each inoculation is centrifuged at 8000 RPM for 5 minutes at room temperature, and DNA is extracted using the QIA Miniprep kit by Qiagen according to the manufacturer's instructions, and each miniprep was eluted in 30 µl of EB buffer. Each of these 10 clones were sent to Macrogen USA for Sanger sequencing to confirm successful insertion of the sgRNA sequence into the PX459 backbone. After Sanger Sequencing, one correctly ligated clone was selected and amplified by transformation and amplification using Qiagen Maxiprep. The identical procedure was used to clone each of these sgRNAs into a PX458 backbone, which is similar to the PX459 except that it carries a GFP expression cassette instead of Puromycin resistance for visualization of transfection efficiency.

2.2.4 Human HEK 293T Cell Culture and Maintenance

Human Embryonic Kidney (HEK) 293T cells were cultured for maintenance on 10 cm plates in 10 mL of Dulbecco's Modified Eagle Medium (DMEM, Gibco) with 10%

Fetal Bovine Serum (FBS, VWR) and 1% Penicillin-Streptomycin (P/S, Gibco). HEK 293T cells were passaged 1:6 for maintenance every 2-3 days. To passage the HEK 293T cells, the culture media was removed and the cells were washed with 5 mL of sterile Phosphate Buffered Saline (PBS, Gibco), dissociated using 5 mL of Trypsin-EDTA (Gibco) for 5 minutes at 37°C. The dissociated cells are collected into a 15 mL conical tube with an additional 5 mL of DMEM with 5% FBS and 1% P/S to inactivate the Trypsin. The cells are centrifuged at 1000 RPM for 5 minutes, and the pelleted cells are resuspended in fresh DMEM with 5% FBS and 1% P/S and plated at 1:6 in new 10 cm dishes for maintenance.

2.2.5 Validate Cutting of sgRNAs in HEK 293T Cells

To validate the 4 potential sgRNAs, we transfected each cloned sgRNA using Lipofectamine 3000 Reagent (ThermoFisher Scientific, L300015), isolated DNA, and sequenced to observe degree of insertions and deletions (indels) (**Figure 7**). To begin on Day 0, HEK 293T cells were passaged and plated at 1:4 density in individual wells of a 6-well plate. On Day 1, 0.25 µg of each newly cloned PX459 sgRNA plasmid was transfected into one well of HEK 293T cells using Lipofectamine 3000 Reagent. One well additional well was transfected with 0.25 µg of a PX458 plasmid carrying GFP to be able to visualize the successful transfection, and one well was left untransfected as a negative control. For each transfection, two tubes were prepared. For the first tube, 0.25 µg of plasmid was added, along with 6 µl of P3000 reagent, and the tube was agitated on a vortex. In the second tube, 125 µl of OPTI MEM was added along with 6 µl of Lipo 3000 reagent. Tube 1 was subsequently added to Tube 2 and further agitated again on a vortex, the mixture was incubated at room temperature for 5 minutes and added to the well containing HEK 293 T cells cultured in 2mL of DMEM with 5% FBS and 1% P/S. On

Day 2, cells were treated with 1 µg/mL Puromycin. On Day 3, HEK293T cells were dissociated, pelleted, and digested in Proteinase K for subsequent DNA extraction and screening.

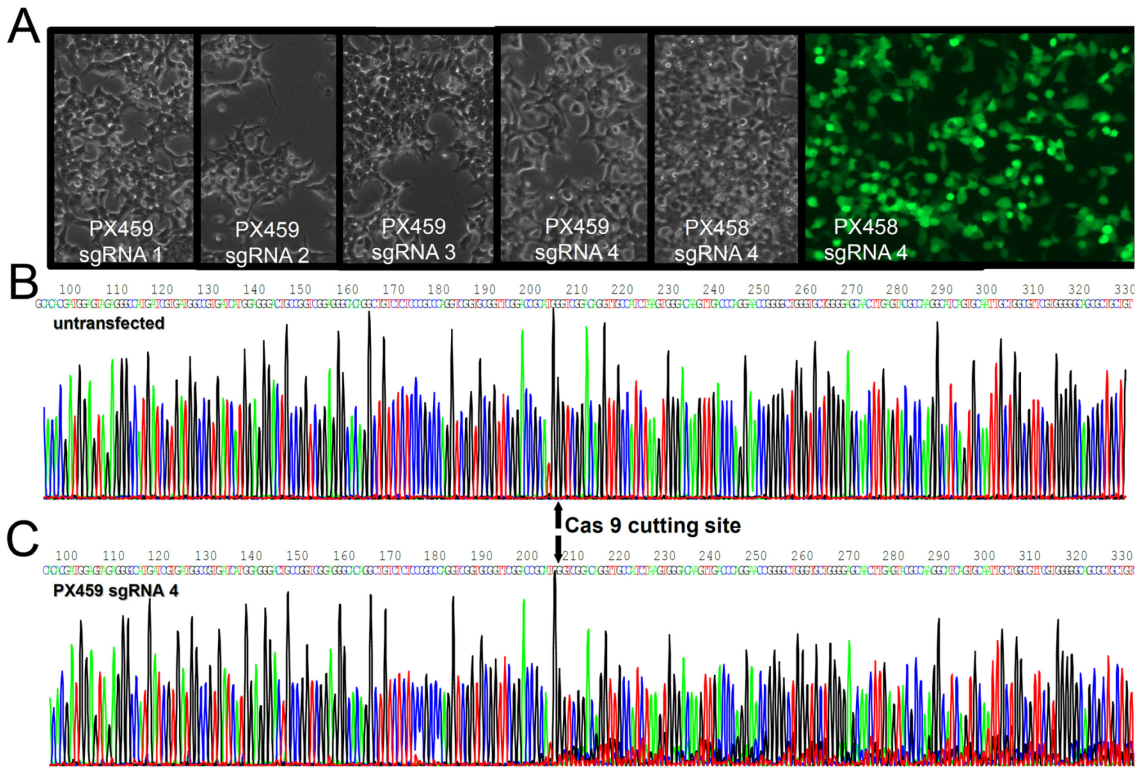

Figure 7: Validation of Candidate sgRNAs for OPRM1 Exon1 in HEK293T Cells. **(A)** Phase contrast images of sgRNA transfected HEK293T cells and one PX458 transfected condition as a control for transfection efficiency. **(B)** Sequencing of PCR amplified products of OPRM1 Exon 1 from untransfected and sgRNA4 transfected HEK293T cells with Cas9 cutting site indicated. Indels observed beyond Cas9 cutting site in HEK 293T cells transfected with sgRNA4, illustrating successful cutting.

2.2.6 Lipofectamine Transfection of Human Pluripotent Stem Cells

Lipofectamine 3000 Reagent (ThermoFisher Scientific) was used to transfect 4.5 µg of the PX459 vector carrying sgRNA4 and Cas9 along with 4.5 µg of the ssODN as per manufacturer's instructions into 200,000 H1 ES cells. These were plated sparsely onto a Matrigel ® Matrix coated 10cm dish. We transfected either with 1 µM SCR7 or without SCR7, which is an inhibitory of non-homologous end joioing. We also transfected

1 plate with PX458 carrying sgRNA4 as a positive control for transfection efficiency. Four independent transfections were conducted in this manner.

2.2.7 Clonal Isolation

After transfection and plating, we conducted 48 hours of Puromycin selection and refreshed media on Day 3 to mTeSR without Y compound or Puromycin antibiotic. We allowed colonies to grow from individual cells while refreshing mTeSR media daily. When individual colonies were approximately 500 μM in diameter, we used an EVOS digital inverted microscope to manually pick colonies using a P200 pipette-man in a 100 μl volume of mTeSR. These were transferred to a 1.5 mL Eppendorf tube, agitated to break the colony into smaller colonies, and immediately transferred into individual wells of a Matrigel ® Matrix-coated 24-well plate. Individual clones were allowed to grow for 7-8 days upon which they were individually Accutase-passaged into 6-well plates and a fraction of cells was taken for Phenol Chloroform DNA Purification, PCR and Restriction Enzyme screening, and subsequent sequencing.

2.2.8 Phenol Chloroform DNA Purification

DNA was purified from all iPS cell clones, H1 ES cell clones, and HEK 293T cells using Phenol Chloroform DNA Purification. A cell sample was centrifuged in a 1.5 mL Eppendorf tube at 1000 RPM for 5 minutes to form a tight cell pellet, which then is resuspended in 400 μl of SNET Buffer (1M Tris (pH 8.0), 0.5M EDTA (pH 8.0), 5M NaCl, H_2O) and supplemented with 10μl of Proteinase K each, and digested at 55°C in the table top shaker overnight. The following day, 400 μl of phenol chloroform is added to the digested cells and centrifuged at 13,000 RPM for 10 minutes. The aqueous layer is carefully removed from the sample into a new tube to which 400 μl of isopropanol is

added to precipitate the DNA and this mixture is then centrifuged at 13,000 RPM for another 10 minutes. The supernatant is discarded and the pellet is washed with 70% ethanol solution and centrifuged at 13,000 RPM for another 10 minutes. The supernatant is discarded and the DNA pellet is allowed to dry overnight at room temperature. When dried, the DNA sample is then dissolved in 50µl of deionized H_2O at 37°C for 5-10 minutes. The DNA concentration is then determined using a spectrophotometer.

2.2.9 PCR Amplification of OPRM1 Exon1 and Enzyme Digestion

For PCR based screening, a PrimeStar PCR assay was used to amplify a 1211 bp region of Exon 1 carrying the A118G locus. The PCR reaction included 5µl of 5x PrimeStar Buffer, 2µl of dNTP, 0.25µl Primestar Enzyme, 0.25µl of Forward Primer AH 16114, 0.25µl of Reverse Primer AH16115, 1µl (100ng) of genomic DNA isolated from Phenol Chloroform DNA purification, and deionized H_2O totaling to a 25µl reaction. PCR protocol was: [98°C (10 sec), 59°C (5 sec), 72°C (1min)]x35 cycles, 72°C (7min), 4°C. The 25 µl PCR sample was digested with 1 µl BamHI restriction enzyme, 2.5µl of 10x Cutsmart Buffer and 1.5 µl of deionized H_2O to total a 30µl digestion. The digestion is run on a 2% agarose gel to visualize PCR amplification and restriction enzyme cutting, to yield two DNA fragments of 502 bp and 709 bp.

2.2.10 Subcloning

Clone 9, 9.2, 9.2.17, and 9.2.18 were subcloned, each at various stages by plating 20,000 cells of each line into a Matrigel ® Matrix-coated 10 cm dish in mTeSR medium with 2 µM Y-compound. Individual cells were allowed to develop into colonies and when the colonies were approximately 500µM in diameter, they were picked, transferred into 24-well plates, and expanded as described in Section 2.2.7.

2.3 Experimental Design

2.3.1 Target Selection for sgRNA

The specificity of cutting for the Cas9 nuclease is determined by the 20-nt guide sequence within the sgRNA (133, 134). To target OPRM1 in H1 ES cells, we designed and screened 4 candidate sgRNAs that target OPRM1 Exon 1 near the A118G locus, and identified one sgRNA which we used for successful gene editing. Our sgRNA sequences were designed from an Optimized CRISPR Design Tool from Feng Zhang's lab at MIT (http://crispr.mit.edu/). A 500 nt sequence carrying the A118G locus of OPRM1 Exon 1 was submitted for CRISPR design and analysis on the Optimized CRISPR Design Tool, which lists >20 potential sgRNAs for analysis that are each scored based on the inverse likelihood of off-target binding. The target site in the H1ES cells included the major allele sequence; thus, the 20 nucleotide (nt) gRNA which we selected was designed to incorporate the major allele (TCGGACCGCATGGGTCGGACAGG). There are two main criteria we used in the selection of a 20-nt guide sequence for OPRM1 gene editing:

(1) The gRNA target sequence must be immediately upstream of a Protospacer Adjacent Motif (PAM), which is a sequence absolutely necessary for target binding (134). This sequence is dependent on the species of Cas9 and in our case for *Streptococcus pyogenes* Cas9, is 5' NGG 3'. The PAM sequence should immediately follow the target DNA locus, but should not be part of the 20-nt guide sequence within the sgRNA. The 20-nt gRNA sequence base pairs with the opposite strand to mediate Cas9 cleavage at ~3 base pairs upstream (5') of the PAM.

(2) The sgRNA sequence is unique compared to the rest of the genome in order to minimize off-target Cas9 cleavage. Using the CRISPR Design Tool, we

selected 4 sgRNAs for screening and ultimately chose one gRNA sequence with a quality score of 94, which is a score based on the inverse likelihood of off-target binding. For this sgRNA chosen, CRISPR Design Tool lists predicts 16 potential off-target sites, 9 of which are in genes, which is much better than some other lower scored gRNA which had >100 predicted off-target cutting sites.

While these two criteria were used in the selection of candidate sgRNAs to be potentially used in CRISPR/Cas9 mediated knock-in of G118 into H1 ES cells, we carefully examined the literature to dissect the specific criteria necessary for efficient knock-in of G118. In theory, all sgRNAs should be usable for genome editing; however, there is evidence for different sgRNAs targeting NGGPAM sites to produce DSBs with quite varying efficiencies (135, 136). In order to identify specific sequence features that increase the ability of Cas9 to bind DNA and improve DSB efficiency and ultimately increase efficiency of knock-in, we considered the additional criteria:

(1) The Cas9 mediated DSB site is of close proximity to the A118G locus on Exon 1. We specifically chose sgRNA#4 because it produces a DSB in OPRM1 Exon 1 that is 7 bp from the A118G locus. Previous work has illustrated that single-base correction rates drop by 75% at 100 bp away from the DSB site and drop to ~10% at 300bp away from the DSB site (137).

(2) The sgRNA must have minimal off-target cutting efficiency. The effect of mismatching bases between the sgRNA and its target DNA is dependent on both position and quantity of those mismatches. For example, the 8-14 bases on the 3’ end of the sgRNA sequence is less tolerant of mismatches as opposed to the 5’ bases (134, 138). Additionally, it has been shown that greater than three mismatches between the sgRNA sequence and target DNA sequence is not tolerated for sgRNA binding and Cas9 cutting (134).

Thus, of the 16 predicted off-target cutting sites in our selected guide RNA, all carried 4 mismatches except one off-target site which carried 3 mismatches. Moreover, most of these off-target cutting sites were found in intronic regions, which are unlikely to have significant changes in gene function.

2.3.2 Design of Repair Template

Predefined genetic modifications can be made using repair templates of various forms. Traditionally, double-stranded DNA plasmid donors were used to make larger genomic alterations and these plasmid donors would contain homology arms of 200-800 base pairs flanking the site of genomic modification (139). However, for smaller genomic alterations of <50bp, a single stranded oligodeoxynucleotide (ssODN) can be used, which has multiple advantages. Primarily, it requires no cloning and can be designed and synthesized in just a few days as opposed to plasmid donors which require multiple weeks to construct. Also, ssODNs can yield much higher integration efficiencies compared to plasmid donors if the DNA modification of interest is <50 bp (140-142). Recently, ssODN donors have been used to successfully edit DNA in a variety of experimental conditions including cultured cells (134, 142, 143) or embryos (144-146).

We thus, designed a 140 nt ssODN with homology arms flanking the A118G mutation site carrying four mutations: A to G at position 118 to generate G118 knock-in, C to T at position 121 of exon 1 to mutate PAM sequence, C to G at position 126 and C to T at position 129 of exon 1 to generate a BamHI restriction enzyme site for screening (**Figure 8**). Aside from the A to G mutation at position 118, all remaining mutations engineered into the ssODN confer synonymous changes in amino acid sequence. These specific DNA modifications were engineered for a few precise reasons:

(1) The mutation in the PAM sequence is designed to prevent Cas9 from digesting the template DNA strand upon transfection into cells, and would prevent re-cutting of DNA upon successful HDR. The Cas9 protein requires a PAM adjacent to the sgRNA homology region to achieve efficient DNA binding and create a DSB. Thus, we disrupted the PAM sequence with a silent mutation in the ssODN.

(2) Moreover, we specifically engineered these mutations 3' to the A118G locus as previous studies found that in a majority of cases, unexpected sequence modifications and indels were located 5' to the side of the desired insert (147). We tried to design these homology arms to be relatively symmetric in length around the desired insert (G118 of OPRM1 Exon 1). However, due to the mutations in the PAM sequence and generation of the BamHI restriction enzyme site, our ssODN was asymmetric. Specifically, the homology arm 5' to the A118G locus is 64 nt in length whereas the 3' homology arm is longer and is 75 nt in length. However, this was not of much concern due to the fact that HDR templates with asymmetric homology arms was either shown to yield insertion rates that were similar to those seen with symmetric homology arms (CiT) or even enhance HDR rates in cultured cells (148).

(3) BamHI restricton enzyme site was designed using two silent mutations to facilitate screening. Of the various potential restriction enzyme sites that could be engineered in Exon 1 from silent mutations, we specifically chose BamHI due to its proximity to the G118 locus. Moreover, inserting the BamHI restriction enzyme site would coincidentally mutate other nucleotides with the sgRNA sequence, which would further prevent re-cutting of DNA upon successful HDR.

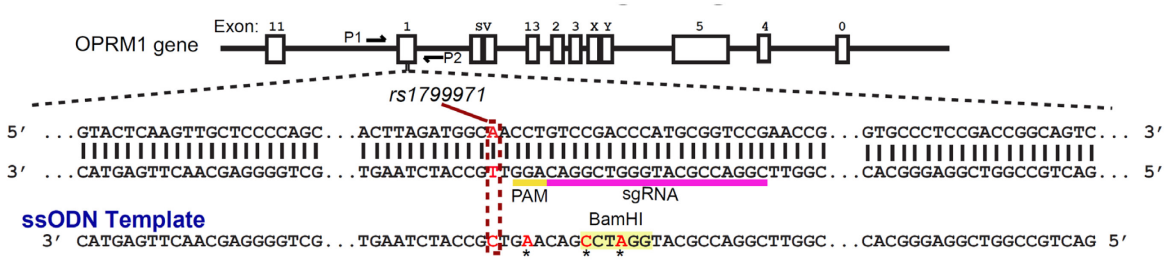

Figure 8: Structure of OPRM1 gene on chromosome 6 and schematic overview of CRISPR Cas9 gene targeting strategy to knock-in homozygous G118 alleles into human H1 embryonic stem (H1ES) cells.
In the 140 base pair template strand, we inserted a T to C mutation to incorporate OPRM1 GG118, G to A for PAM mutation, G to C and G to A mutation to incorporate BamHI restriction enzyme site.

2.4 Experimental Results

2.4.1 Screening of Candidate Clones by Enzyme Digestion

Upon successful transfection and isolation of H1ES cell clones, we conducted DNA isolation, and PCR and enzyme digestion for 120 clones as described in Sections 2.2.7-2.2.9. Of the 120 clones screened from 4 independent transfections of the parental H1ES cell line, 8 of 60 clones transfected with 1 μM SCR7 (16.7%) and 11 of 60 clones transfected without SCR7 (13.3%) exhibited partial digestion by BamHI (**Figure 9**). Upon screening of all 19 of these clones by sequencing, we identified that 6 clones did not incorporate G118, but only incorporated the BamHI restriction enzyme site and the PAM mutation. We thus eliminated those 6 clones and chose clone 9 for further analysis.

The partial digestion of several clones from PCR and BamHI restriction enzyme digestion and subsequent sequencing results suggests two possibilities: **(1)** The clone exhibits a heterozygous knock-in of G118 with one untargeted allele; **(2)** The clone exhibits a homozygous knock-in of G118 but is mixed with unedited cells. It is thus necessary to confirm the exact genotype of the cells following genome editing, as this is especially important for the downstream utility of these cells in disease modeling.

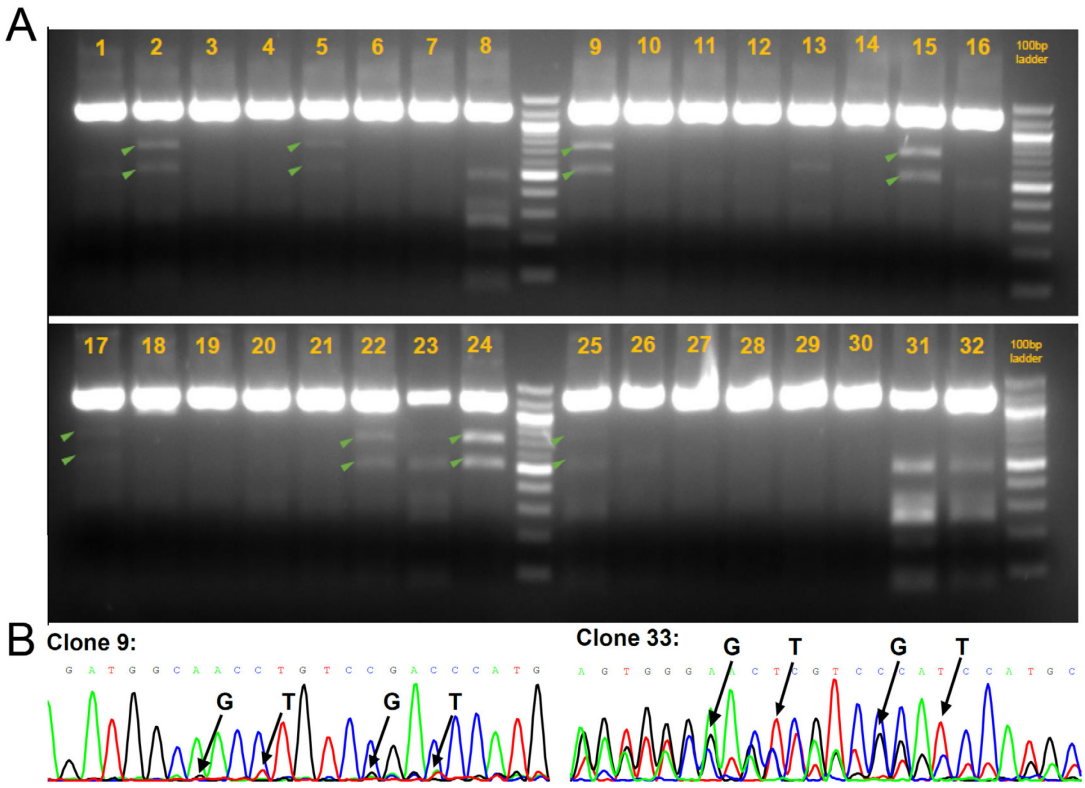

Figure 9: Screening of 120 Clones Using PCR and Enzyme Digestion. **(A)** Agarose Gel Electrophoresis (2% agarose) of PCR amplified products of OPRM1 Exon 1 digested with BamHI (Shown are 32 of 120 clones screened. **(B)** Sample of sequencing results from Clone 9 and 33 which exhibited partial BamHI digestion.

2.4.2 Subcloning

To correctly identify the exact genotype of these targeted cells, we selected clones 9, 33, 103, and 107 for subcloning and sequencing. Subcloning was conducted as described in Section 2.2.9 and a total of 36 subclones were picked for each clone, expanded, and screened by PCR and enzyme digestion (**Figure 10**). Subclones isolated from clones 9, 33, and 107 all exhibited primarily partial digestion, confirming that each clone was a mixture of unedited cells and heterozygous cells.

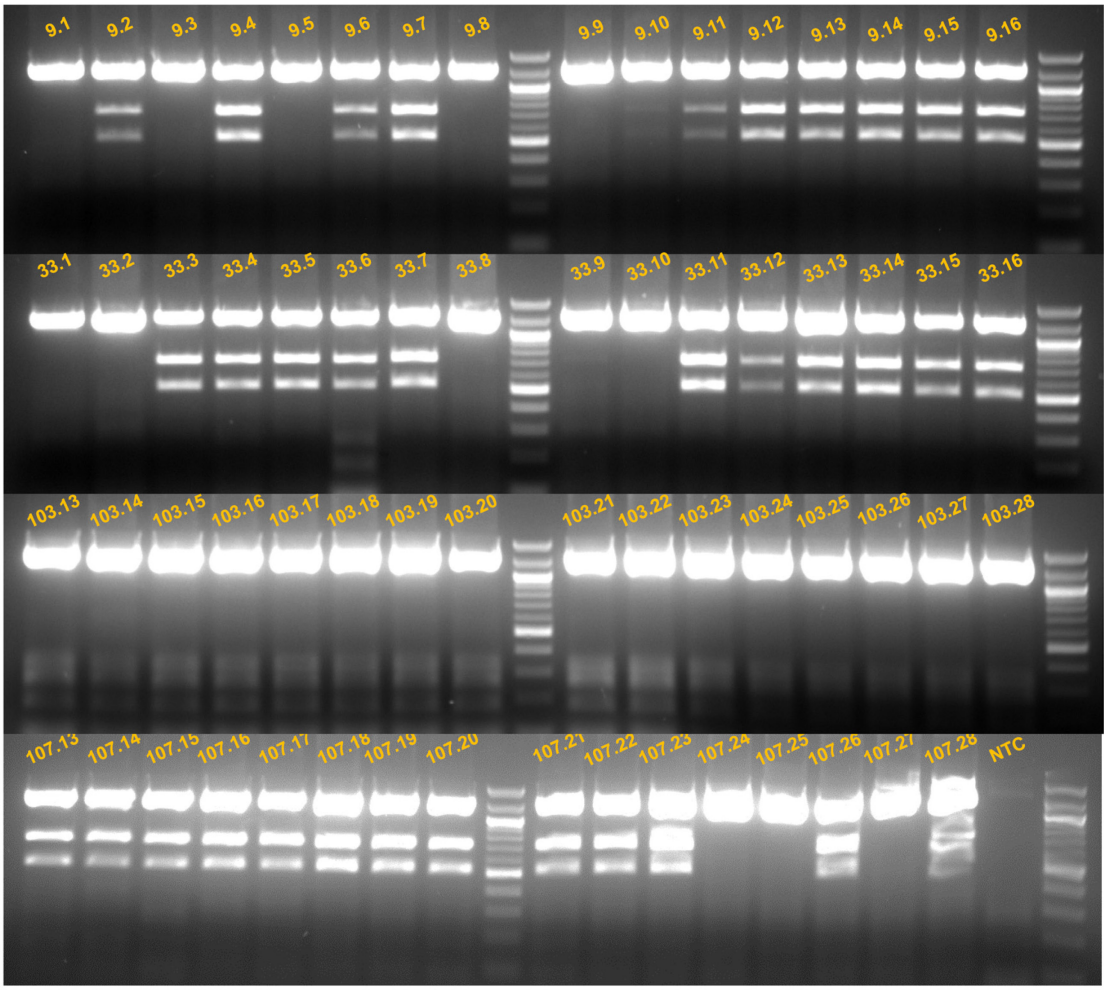

Figure 10: Agarose Gel Electrophoresis (2% Agarose) of PCR amplified products of OPRM1 Exon 1
A sample of subclones isolated from Clones 9, 33, 103, and 107 digested with BamHI illustrates heterozygous G118 clones.

2.4.3 Transfection and Isolation of Homozygous G118 Knock-In

To obtain a homozygous knock-in of the OPRM1 G118 allele, we used Lipofectamine to transfect sgRNA 4 and the ssODN to target the second un-edited allele of subclones 9.2, 9.4, 33.5, and 107.4. We repeated clonal isolation by picking 36 additional clones from each of these 4 subclones and used PCR based screening methods as described in Sections 2.2.7-2.2.9. We obtained two subclones (9.2.17, 9.2.18) which exhibited complete digestion with BamHI. PCR reaction, digestions, and sequencing was repeated for subclones 9.2.17 and 9.2.18 at different passage numbers

for confirmation of homozygous G118 knock-in (**Figure 11**). Cells were subsequently expanded and frozen down for storage.

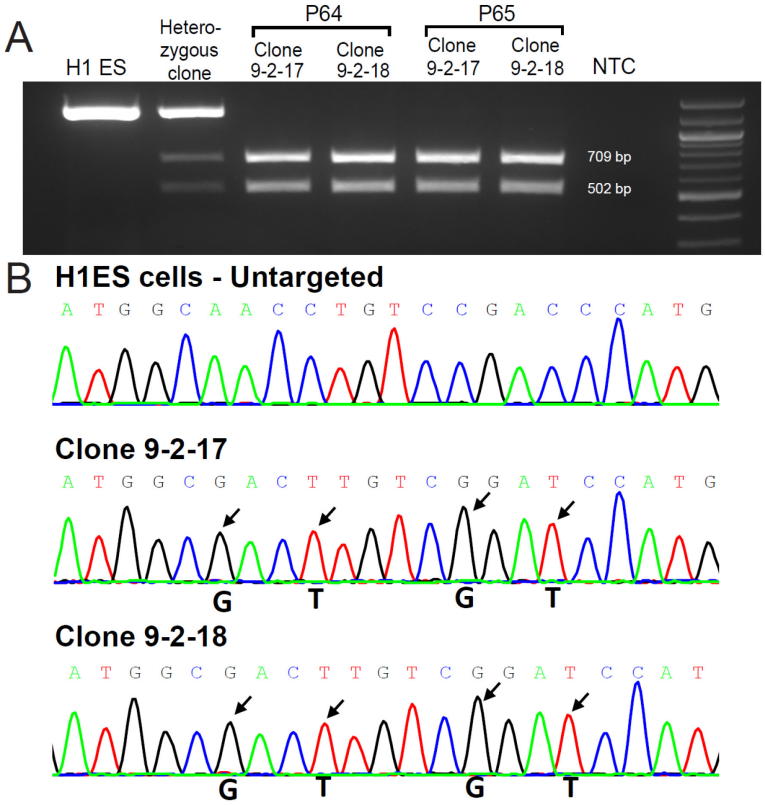

Figure 11: Successful isolation of homozygous G118 Knock-in clones from H1ES cells.
(A) Digestion of OPRM1 Exon 1 PCR products with BamHI. **(B)** Sequencing from H1ES untargeted cells and Clone 9-2-17 and 9-2-18 illustrating successful homozygous knock in of G118, BamHI enzyme sites, and PAM silent mutation into Wild type OPRM1 gene.

2.5 Off-Target Screening

Although the targeting specificity of Cas9 is thought to be strictly controlled by the 20-nt guide sequence of the sgRNA and the presence of an adjacent PAM sequence, potential off-target cleavage by Cas9 could still occur on DNA sequences with 3-5 base mismatches on the sgRNA sequence (149, 150). To detect off-target alterations in our isolated homozygous knock-in cells, we screened for off-target activity in 13 of the 16 predicted off-target sites from the Optimized CRISPR Design Tool. We first PCR

amplified these regions of interest and sequenced each PCR product for both Clones 9-2-17 and 9-2-18. Off-target PCR samples were sequenced and aligned to the reference H1 ES cell genome and sequences were compared 20 bp on either side of the of the putative cutting site. No trace of insertions or deletions were detected in either subclone at any of the putative off-target locations (**Figure 12**).

A

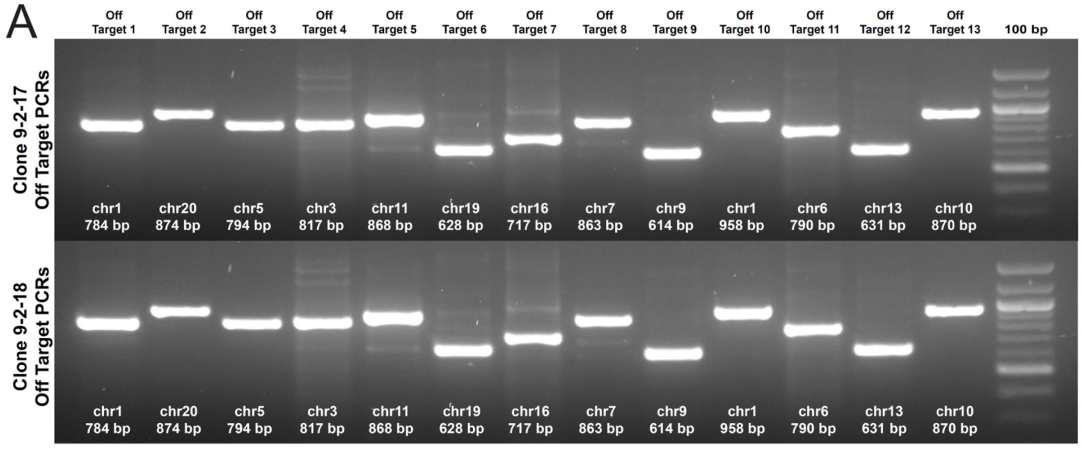

B

	Sequence	Score	Mismatches	UCSC gene	Locus	9-2-17	9-2-18
1	TGGGACCCCATGGGTCGGAGAGG	1.5	3MMs [2:8:20]		chr1:+1891752	No	No
2	GAGGTCCGCAGGGGTCGGACCGG	0.8	4MMs [1:2:5:11]	**NM_000961** prostaglandin I2 (prostacyclin) synthase (PTGIS)	chr20:+48184805	No	No
3	CGGGACCGCGTGGGTCGGAGAAG	0.7	4MMs [1:2:10:20]	**NM_001258437** threonyl-tRNA synthetase (TARS)	chr5:+33441347	No	No
4	CAGGACCCCATGGGTCAGACCAG	0.6	4MMs [1:2:8:17]	**NM_001146314** abhydrolase domain containing 14B (ABHD14B)	chr3:-52003567	No	No
5	GCAGAACGCAAGGGTCGGACCGG	0.5	4MMs [1:3:6:11]	**NM_033388** autophagy related 16 like 2 (ATG16L2)	chr11:-72533601	No	No
6	TGGGACAGCCTGGGGCGGACGAG	0.3	4MMs [2:7:10:15]	**NM_138401** multivesicular body subunit 12A (MVB12A)	chr19:-17535553	No	No
7	TCACACCGCATGGGTCGGCAGGG	0.2	4MMs [3:4:19:20]		chr16:-2339262	No	No
8	TCGGGCGGCACGGGTCGGCCTGG	0.2	4MMs [5:7:11:19]	**NM_007270** FK506 binding protein 9 (FKBP9)	chr7:-32997119	No	No
9	TCTGACAGCATGTGTCGGAAAAG	0.2	4MMs [3:7:13:20]		chr9:-104499103	No	No
10	TGGGACAGCCTGGGTGGGACCAG	0.2	4MMs [2:7:10:16]		chr1:-111736919	No	No
11	TTGGAAAGCATGGGTAGGACAGG	0.1	4MMs [2:6:7:16]		chr6:+466493	No	No
12	TAGGACCCCATGGGTATGACAAG	0.1	4MMs [2:8:16:17]	**NM_153456** heparan sulfate 6-O-sulfotransferase 3 (HS6ST3)	chr13:-97488229	No	No
13	TCAGACTGCATGGGCCGGCCTAG	0.1	4MMs [3:7:15:19]	**NR_037164** ankyrin repeat and SOCS box containing 13 (ASB13)	chr10:-5681502	No	No

Figure 12: Off-Target Screening in H1 ES A118G Knock-in Clones.
(A) PCR products amplifying first 13 off-target sites as predicted by MIT CRIPSR Design Tool in Clone 9-2-17 and 9-2-18 **(B)** Chart listing first 13 genome-wide off-target sites as predicted by MIT CRISPR Design Tool, score, number of mismatches from on-target locus, UCSC gene, gene locus.

2.6 Gene Correction Using Alternative CRISPR/Cas9 Strategy

With the help of RURDR Infinite Biologics ®, we derived another set of isogenic human stem cell lines by engineering one human subject iPS cell line (03SF) which is a homozygous minor allele (G118) carrier to homozygous major alleles (A118) using an alternative CRISPR/Cas9 gene editing strategy (**Figure 13**). Briefly, a CRISPR targeting site was found using ZiFit software (151). A 200 nt homologous recombination donor oligo was designed to convert minor to major allele, inactivate the CRISPR site, and introduce a HpaI site for screening. The gRNA was synthesized by PCR and in vitro transcription (GeneArt Precision gRNA Synthesis Kit, Life Technologies) (152), mixed with synthetic Cas9 protein (Life Technologies), donor oligo, and the mixture was electroporated into iPS cells (Amaxa nucleofector, Lonza) along with a GFP expression plasmid (pGFP-Max, Lonza). One day later, cells were dissociated with Accutase and GFP-expressing cells were collected by FACS and plated at about 5,000 cells per well in a 96-well plate on irradiated MEFs. By 7-10 days, colonies were visible and hand-picked for screening. Three iPS cell clones were selected: C12, which had no evidence of editing to be used as a negative control; D11 and A10, which both had homozygous edits to produce rs1799971 major allele (AA). Sequencing confirmed these edits and that all predicted off-target sites were unchanged.

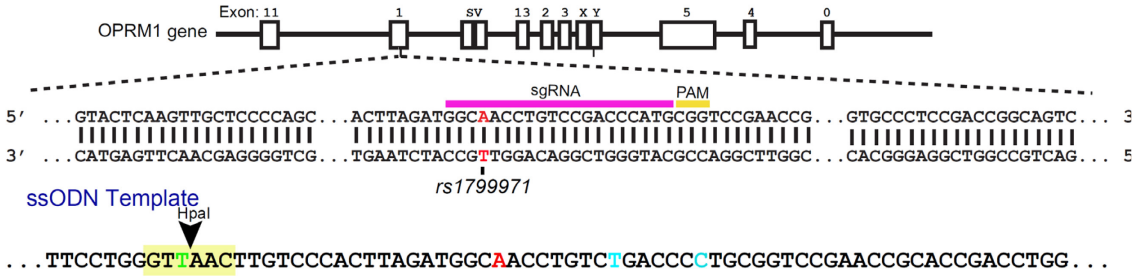

Figure 13: Alternative CRISPR/Cas9 gene targeting strategy to correct 03SF patient line.
We designed an alternative sgRNA targeting OPRM1 exon 1 and a 200 nt template strand to knock-in homozygous A118 alleles into the 03SF patient cell line (originally homozygous G118).

2.7 Discussion

The combination of human stem cells, genome engineering, and neuronal differentiation techniques gives us the opportunity to more rigorously and faithfully model psychiatric diseases such as addiction in disease relevant human cell types. The ability to modify single base pairs and introduce disease-causing mutations in human pluripotent stem cells allows the creation of genetically controlled model systems in human specific model systems. This will eliminate the interaction between background genetic variations in human stem cell lines and reveal new insights into the pathophysiology of psychiatric diseases such as addiction.

2.7.1 Advantages of CRISPR Genome Engineering

The most important advantages of CRISPR/Cas9 technology over other genome editing strategies is its simplicity as well as efficiency in making targeted modifications to the genome. CRISPR/Cas9 technology has multiple advantages over traditional genome engineering technologies such as Zinc finger nucleases (ZFN) (153-155) or Transcription activator-like effector nucleases (TALENs) (156, 157). ZFN and TALENs involve tethering the catalytic domains of endonuclease to DNA-binding proteins for inducing DNA double-stranded breaks (DSBs) at specific genomic loci (155). The Cas9 endonuclease, on the other hand, is much simpler and is guided to genomic loci of interest by small guide RNAs through Watson and Crick base pairing. Thus it has three key advantages over other systems: **(1)** Since target specificity depends on a ribonucleotide complex instead of protein and DNA interactions, sgRNAs can be designed cheaply and easily to target any genomic sequence with high specificity. **(2)** CRISPR is highly efficient so genetic modifications can be made efficiently by directly introducing sgRNAs and Cas9 protein into cells of interest, thus eliminating the long and laborious cloning steps. **(3)** CRISPR allows for more high throughout and multiplexed

gene editing, meaning mutations in multiple genes can be introduced simultaneously by using multiple sgRNAs (134).

With the use of two independent CRISPR/Cas9 genome engineering strategies, we have successfully isolated two sets of isogenic human stem cell lines to directly compare mutant and control cells with identical genetic backgrounds (**Figure 14**). One set of isogenic lines involved knocking in homozygous G118 alleles into a homozygous A118 H1ES cells (**Figure 14A**), while the other corrected homozygous G118 alleles from a human subject derived iPS cell line to homozygous A118 alleles (**Figure 14B**). By using two complementary and independently executed CRISPR/Cas9 gene targeting strategies, we are able to isolate the synaptic effect of the MOR N40D SNP in human neurons, giving higher sensitivity to detect functional differences between N40 and D40 in phenotypic analyses. Studying MOR N40D phenotypes across both patient-derived cells and two sets of genome-edited cells generated using independent targeting strategies would greatly substantiate the validity of any observed phenotypes and would directly demonstrate that the observed MOR effect is due to the N40D variant and not some background genetic variation from the subjects. CRISPR/Cas9 engineering thus enables direct genotype-phenotype associations of human genes.

Additionally, our dual approach of using complementary gene targeting strategies helps circumvent other key concerns of disease modeling. Initial concerns with patient derived human stem cells were the influence of background genetic variation on the elucidation of clear phenotypes. However, there is a similar concern that either the genetic background of the H1ES cell line or off-target cutting may confer some bias that may selectively enhance or abolish a key phenotype of N40D. Thus, using two sets of isogenic cell lines minimizes the chance of interpreting a phenotype from an off-target genomic locus as opposed to an on-target locus, and allows us to cross-validate key phenotypes in two sets of isogenic lines of different genetic backgrounds, and thus

preventing the possibility of isolating artefactual readouts. Moreover, the fact that we used one ES cell line and one iPS cell line helps to control for the potential biases incurred by the iPS cell generation process, such as retention of epigenetic memory or the effects of cellular origin on differentiation capabilities, which may confound disease phenotypes (5).

2.7.2 Comparison of CRISPR Strategies

Each set of isogenic lines was generated using independent strategies, each of which have their own distinct advantages. First, these lines exhibited different delivery methods of the active CRISPR complex. We used the PX459 plasmid to deliver Cas9 under a Cbh promoter to the H1ES cell line whereas recombinant Cas9 protein in combination with its RNA portion in a ribonucleoprotein particle (RNP) was introduced into the 03SF patient cell line for genome engineering. Since plasmid DNA lasts longer inside the cells, it has the possibility of random integration into the genome as well as increased susceptibility to off-target cutting (158). However, it also has the potential for more complete modification of target DNA. On the other hand, Cas9 protein is a DNA-free system and thus eliminates the concern of DNA integration that can occur with a plasmid based system. The Cas9 protein is immediately available for editing whereas the plasmid requires transcription and translation for editing to occur. Lastly, the Cas9 protein exhibits a fast turnover within the cell which means this shortens the length of time that the genome is exposed to the CRISPR complex, which has been shown to reduce the likelihood of off-target cutting (159-161). Thus, the 03SF patient derived stem cell line is likely to be of greater utility for disease modeling purposes.

Moreover, the isolation of isogenic clones was conducted differently with each set of isogenic lines. The H1ES cell targeted cell lines used the parental H1ES cell line as an isogenic control whereas the 03SF targeted clones used a passage-matched cell

line that remained untargeted following transfection and subcloning. Although the 03SF stem cell lines underwent greater number of passages than the H1ES cell lines, the fact that they were harvested from the same passage and had undergone identical experimental manipulations makes this set of lines more appropriate for making head-to-head phenotypic comparisons.

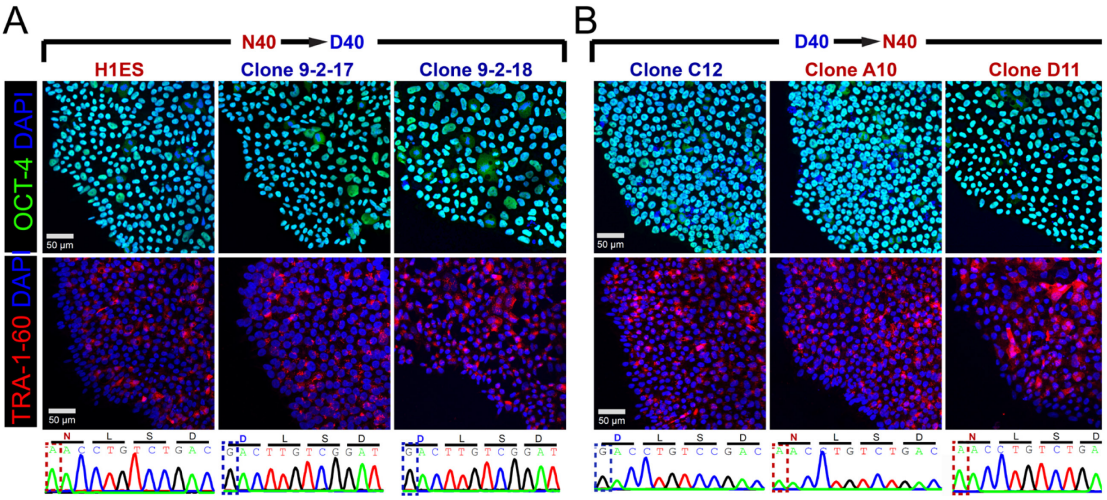

Figure 14: Characterization of two OPRM1 A118G isogenic stem cell lines. **(A)** Oct4 (green), Tra-1-60 (red), and Dapi (blue) immunofluorescence for H1ES gene-targeted clones depicting pluripotency following by sequencing confirming homozygous knock-in **(B)** Oct4 (green), Tra-1-60 (red), and Dapi (blue) immunofluorescence for 03SF gene-targeted clones depicting pluripotency followed by sequencing confirming homozygous knock-in.

2.7.3 Off-Target Detection

The Cas9 nuclease can be programmed to induce DSBs at almost any location in the genome. However DSBs trigger DNA damage response pathways that repair breaks by either nonhomologous end-joining (NHEJ) or homology-directed repair (HDR). NHEJ disrupts coding sequencing and regulatory DNA elements involved in regulated gene expression.

However, a major caveat to this approach is the fact that Cas9 may bind and cleave genomic loci other than the intended target (162). Although the targeting

specificity of Cas9 is thought to be controlled by the 20-nt sgRNA sequence and the presence of the PAM, the high frequency of off-target cutting could occur on DNA sequences with 3-5 bp mismatches in the part of the sgRNA sequence distal to the PAM (158). These can result from the prolonged expression of Cas9 after cell division. Since DNA repair and NHEJ activity can occur differently at different genomic loci, this can increase genetic mutation rates and mosaic mutations. Thus, precise control of Cas9 nuclease expression at the level of transcription and translation is required to reduce mosaic mutations (161, 163).

In both sets of isogenic cell lines, we did not detect any signs of off-target cutting activity by Cas9 by PCR and sequencing (**Figure 12**). However, a potential caveat is that off-target cutting may have occurred in sites outside of the predicted off-target sites. Thus, recent studies report methods for more reliable detection of off-target DSBs produced by Cas9. One potential method relies on the use of a foreign DNA bait sequence into off-target DSBs whereas other methods developed involve detection of endogenous genomic sequence translocations into the intended cleavage site (162). Other methods include Digenome-seq, which is an *in vitro* Cas9-digested whole-genome sequencing method to profile off target effects in human cells (164). Thus, finding a sensitive and comprehensive method to detect these off-target cutting sites is crucial to establishing CRISPR/Cas9 engineering as a reliable technology for disease modeling purposes.

2.7.4 Strategies to Minimize Off-Target Effects

There are numerous strategies to minimize off-target effects by Cas9 endonuclease. First, truncating the 3’ end of the sgRNA and shortening the region complementary to the target site at the 5’ end by 3 nt or adding to G nucleotides to the 5’ end of the sgRNA is thought to decrease off-target cutting by as much as 5000 fold,

(165-167). Another strategy is to titrate the concentration of the CRISPR complex (Cas9 and sgRNA) that is delivered to the cells, which has been shown to increase specificity (158). However, both these strategies have been shown to simultaneously decrease on-target cutting efficiencies. Thus, optimization of both Cas9 and sgRNA designs are needed to improve specificity of on-target cutting without decreasing cleavage efficiency. A last strategy would involve using the D10 mutant nickase version of Cas9 which is paired with two sgRNAs that each cleave one DNA strand. This strategy has been shown to reduce off-target activity by 50-1500 fold in cell lines without sacrificing cleavage efficiency (168). Despite the fact that there are many mechanistic questions about the use of CRISPR based genome engineering technologies, it is no doubt that the technology will help refine and enhance our studies toward understanding the mechanisms contributing to neuropsychiatric diseases.

Chapter 3: MOR N40D Differentially Regulates Neuronal Excitability and Synaptic Transmission

3.1 Introduction

The MOR mediates the reinforcing effects of natural stimuli as well as drugs of abuse. It is expressed in brain regions such as the ventral tegmental area (VTA) and the nucleus accumbens (NAc) (45) and is the primary site of action of endogenous opioid peptides including β-endorphin, met-enkephalin, and endomorphins that modulate euphoria (4, 6, 46). Because of its critical role in mediating reward and positive reinforcement, the MOR is also an indirect target of alcohol, nicotine, opioids and other drugs of abuse (50, 51). MOR mediated synaptic alterations in the VTA, NAc and other reward-associated brain regions may represent a key underlying mechanism of the reinforcing aspects of drug abuse (6). Nevertheless, how the MOR regulates synaptic transmission in a human neuronal model is unclear.

Due to their role in mediating reward, it is not surprising that genetic variants of MORs are linked to addiction and other reward related behaviors. Particularly, the A118G single nucleotide polymorphism (SNP) in OPRM1, rs1799971, is a non-synonymous gene variant which replaces an asparagine (N) to an aspartate (D) at N-terminal position 40 (N40D), and is associated with drug dependence phenotypes in humans(77). For example, the MOR N40D gene variant has been linked in various clinical studies to alcohol dependence (38-40, 42, 43, 78-82), nicotine reward (83), and smoking relapse (83-85), suggesting it has a physiologic function in the modulation of MOR signaling in reward. Additionally, of the many non-synonymous amino acid substitutions in the coding region of the human MOR, the N40D SNP is of particular importance because it has the highest overall allelic frequency of all OPRM1 coding region variants, as much as 10-12% in Caucasian populations and up to 50% in certain

Asian and Indian populations (44). Despite its high prevalence and physiologic relevance, its role in the modulation of synaptic plasticity in the brain is largely unknown.

The considerable work investigating the functional consequences of MOR N40D and its role in addiction behavior has not defined the precise cellular and synaptic mechanisms underpinning the differential effects of MOR N40D. Although the G allele was originally thought to cause increased binding affinity for endogenous ligand β-endorphin(102), subsequent studies reported conflicting results that affinity for MOR ligands vary by cell line (104, 105). Moreover, different cell lines may differ in the availability of G proteins and signaling molecules. This suggests that the physiological relevance of differential signaling profiles exhibited by MOR N40D variants in heterologous overexpression systems and immortalized cell lines is highly questionable, making direct comparisons between different expression systems problematic. Although there are two mouse models for the MOR N40D genetic variant, studies using either of these two mouse lines have provided ambiguous results about the functional consequences of the SNP (91, 94-96). To understand the physiologic role of MOR N40D in its contribution to addiction behavior, it is critical to address its role in MOR mediated synaptic mechanisms in the brain.

In order to fill the gap in studies done in the mouse and heterologous systems, we generated human induced neuronal (iN) cells from iPS cells derived from subjects carrying homozygous alleles for either MOR N40 or D40 in order to better dissect the role of MOR N40D in a physiologically relevant and human-specific model system. Strikingly, we found that D40 MOR human neurons exhibit a stronger suppression of inhibitory synaptic release in the presence of MOR-specific agonist DAMGO compared to N40 human neurons. In order to control for the possibility of individual genetic background variation between subject cell lines, we used CRISPR/Cas9 gene targeting to generate two sets of isogenic human stem cell lines: one pair with a 118GG knock-in

into a well-characterized human embryonic stem (ES) cell line and the other by converting a minor allele carrier (118GG, D40) into a major allele carrier (118AA, N40). Remarkably, the synaptic regulations of MOR activation in the isogenic lines recapitulate those of neurons generated from different human subjects. This study exemplifies the use of patient-specific iPS cells as well as gene targeted isogenic stem cell lines to advance our understanding of the fundamental cellular and synaptic alterations associated with MOR N40D in human neuronal context.

3.2 Materials and Methods

3.2.1 Human induced pluripotent stem cell generation and maintenance

Seven iPS cell lines were used in the initial phenotypic analyses of this study. Each of these seven iPS lines were derived from multiple individuals carrying homozygous alleles for either MOR N40 (n=4) or MOR D40 (n=3). These iPS cells were reprogrammed from primary human lymphocytes selected from a study of nicotine dependence (COGEND) using the Fagerström test of nicotine addiction and were generated by RUCDR Infinite Biologics® using Sendai viral mediated gene transduction of OKSM.

Human induced iPS cells and ES cells were maintained at 37°C, 5% CO_2, and cultured feeder-free on Matrigel ® Matrix (Corning Life Sciences)-coated 6-well plates or 10cm dishes in mTeSR medium (STEMCELL Technologies). The mTeSR media was refreshed daily, and the cells were passaged once a week for maintenance as well as neuronal differentiation. For passaging, the cells of each line were passaged by dissociation into single cells. To passage, mTeSR medium was removed, and the wells were washed with Minimal Essential Media (MEM, Gibco), 1 mL for 6-well plate, and 5 mL for 10cm dish. The MEM was then aspirated, and replaced with 1mL of Accutase™

(STEMCELL Technologies), 1 mL for 6-well plate and 5 mL for 10cm dish, and incubated at 37°C for 5 minutes to allow cells to dissociate from the dish. The dissociated stem cells were subsequently collected into a 15mL conical tube, remnant cells were collected in MEM and added to the conical tube. iPSCs were then collected into a pellet at 1000 RPM for 5 minutes, using a tabletop centrifuge. Supernatant was removed and cells were resuspended in 1mL of mTeSR media containing 5μM ROCK inhibitor (Stemolecule™ Y27632, Stemgent). A sample of this resuspension was diluted 1:10 and used for counting on a hemocytometer. Using estimation of cell density, 150,000 cells were plated into a 6-well plate for maintenance and 500,000 cells were plated into each well of a 6-well plate for neuronal differentiation.

3.2.2 Glial cell preparation and maintenance

Glial cell monolayer cultures were prepared using mouse pups that are 0-4 days old of the C57BL/6J Mus musculus strain and cultures were prepared as previously described (169). Both male and female mice will be used. To isolate glial cells, brains of P0-P4 pups were dissected, meninges was removed and the brain was stored in 2mL of HBSS on ice. Subsequently, 1mg/mL of trypsin was dissolved in HBSS and was added to the brain and incubated at 37°C for 20 minutes and the tube was agitated every 5 minutes to ensure penetration of trypsin solution throughout the brain. The brain was brought into the tissue culture hood, trypsin solution was aspirated, and the brain was washed twice with DMEM with 10% Fetal Bovine Serum (FBS) with 1% PenStrep to remove excess trypsin. A fresh 1 mL of DMEM with 10% FBS and 1% PenStrep was added to the tube and the tissue was dissociated into single cells using a pipette. The dissociated tissue was then passed through a sterile 70μm nylon cell strainer (Falcon ®) in order to remove debris and dead cells. The elutant containing strained cells was

subsequently cultured in DMEM media with 10% FBS and PenStrep in T75 flasks and cultured in 37°C and 5% CO_2.

3.2.3 Lentivirus preparation

We utilized HEK 293T cells to package replication incompetent lentiviral vectors, which we used to infect human stem cells for neuronal differentiation. A calcium phosphate transfection method was used to deliver both packaging vectors as well as plasmids containing transcription factors of interest. These HEK 293T cells were passaged 1:4 into 15 cm tissue culture dishes the day before calcium phosphate transfection was to be done. The HEK 293T cells were transfected when they were at 60% confluency. On the day of transfection, we mixed the three packaging vector components RRE (0.75µg), REV (9.1µg), VSV-g (13.77µg), with 22.4µg of the lentiviral expression vector expressing the transcription factor of interest. Next, we added 105 µl of a 2.5M Calcium Chloride solution and then totaled this mixture to 1.5mL using sterile water. We subsequently added this DNA, Calcium and water mixture to a 2X HBS solution while holding this on a vortex. The 2X HBS solution contained 50mM HEPES (pH 7.05), 1.4mM anhydrous Na_2HPO_4, and 280mM NaCl. This mixture of calcium causes the DNA calcium mixture to precipitate with the phosphate to form small enough calcium phosphate crystals to enter into the HEK 293T cells. This calcium phosphate DNA crystals of total of 3mL was added onto the 15cm dishes containing HEK 293 T cells.

After 12 hours of transfection, the media was aspirated and replaced with mTeSR media. The transfected HEK 293T cells were then incubated with this culture media for a total of 24 hours, upon which the media carrying the lentivirus of interest was collected and spun in a tabletop centrifuge for 1500g for 10 minutes at 4°C to

remove any dead cells and debris. The virus was immediately placed on ice, and aliquoted into 1mL or 0.5mL aliquots in Eppendorf tubes, and stored in the -80°C freezer for future use.

3.2.4 Generation and maintenance of iN cells

Induced neuronal (iN) cells were produced from iPS cells by forced expression of cell lineage transcription factors as described previously (116). On day -2, iPS cells of each cell line were dissociated using Accutase ® (Innovative Cell Technologies) as described in section 4.2.1 and collected, and centrifuged at 1000 RPM for 5 minutes on a tabletop centrifuge. The cells are plated at a density of 50,000 cells/cm^2 either in 6-well plates or 10cm dishes for neuronal differentiation. The iPS cells are plated in a lentiviral cocktail with mTeSR media containing 100µl/mL Ascl1, 100µl/mL Dlx2, and 100µl/mL rtTA lentivirus. On day 0 approximately 12-15 hours after lentiviral infection, the virus cocktail is replaced with Neurobasal ® media containing 2µg/mL Doxycycline and 5µM ROCK inhibitor to induce expression of cell lineage transcription factors. On Day 1, we conduct drug selection using 1µg/mL of Puromycin (ThermoFisherScientific) and 100µg/mL Hygromycin (ThermoFisher Scientific) for 48 hours or as needed. On day 3, 30,000 mouse glial cells are plated onto 10mm glass coverslips, each placed in an individual well of a 24-well plate. On day 4 of neuronal induction, iN cells are dissociated using Accutase and 150,000 iN cells are plated onto the 10mm coverslips carrying mouse glial cells and are allowed to mature for 5 weeks at which point we conduct functional analyses. The iN cells are half-fed every 3-4 days in Neurobasal® media containing Gem21 NeuroPlex™ Serum Free Supplement (Gemini), L-glutamine (Gibco), 2 µg/ml Doxycycline (MP Biomedicals), 10 ng/ml BDNF, 10 ng/ml GDNF, 10 ng/ml NT3 (Shenandoah Biotechnology Inc™).

3.2.5 Gene expression analysis using qPCR

For quantitative analysis of gene expression, total RNA from three independently generated batches of iN cells for each cell line was isolated using TRIzol® Reagent from Thermo Fisher Scientific according to manufacturer's instructions. Briefly, 0.1mL TRIzol™/cm^2 is added to the iN cell cultures, and the sample is homogenized using a pipette and stored at -20°C until RNA isolation is performed. For RNA isolation, sample is thawed and an equal volume of Chloroform is added to the homogenate, and it is centrifuged using a tabletop microcentrifuge at 14000 RPM for 10 minutes. The homogenate then separates into three layers: an upper aqueous layer containing RNA, an interphase, and a lower organic layer which contains the DNA and proteins). The upper aqueous later which contains the RNA is transferred to a new Eppendorf tube, and the RNA is precipitated using isopropanol. The precipitated RNA is then washed to remove impurities and then re-suspended in RNAse free water to use for cDNA generation.

The isolated RNA is then reverse-transcribed using. Human-specific Taqman probes were purchased from ThermoFisher Scientific for OPRM1 (Hs01053957_m1), MAP2 (Hs00258900_m1), Tuj1 (Hs00964962_g1), VGAT (Hs00369773_m1), GAD1 (Hs01065893_m1), TH (Hs01002182_m1) and qPCR was conducted as per manufacturer's instructions. Undifferentiated iPS cells, ES cells, and mouse astrocytes were used as negative controls. A sample of total RNA of a healthy human brain as well as Human Thalamus from Biochain ® was used as a positive control. Relative RQ values were obtained by normalizing expression levels to the C12 iN condition.

3.2.6 Immunocytochemistry and Confocal imaging

The iN cells from each condition that are plated onto glass coverslips are fixed with 4% paraformaldehyde for 15 minutes are room temperature. Next, cells are washed once with 1mL of PBS and then stored in 2 mL of PBS at 4°C until they are ready for immunocytochemical analysis. After fixation, the cells are incubated in 0.1% Triton-X-100 diluted in PBs for 10 minutes at room temperature. Subsequently, they are blocked in 4% bovine serum albumin (BSA) with 1% normal goat serum in PBS for 1 hour at room temperature on an orbital shaker. Next, primary antibodies are diluted according to manufacturer's instructions in the same blocking buffer and added to the cells. The primary antibody is incubated for 1 hour at room temperature or overnight at 4°C, which is then followed by three washes with PBS at room temperature. Next, the secondary antibodies are diluted at 1:500 in the same blocking buffer and applied to the iN cells for 1 hour at room temperature while being shaken on an orbital shaker. The iN cells are washed 3 times in PBS at room temperature. The final wash is done in deionized water, and the coverslip is then mounted upside down onto a glass slide with one drop of Mounting Media containing DAPI to stain the nuclei (Fluoroshield™). The dilutions of the primary antibodies were determined according to manufacturer's instructions as well as experimentation on iN cells. Antibodies used include: mouse anti Oct4 (Millipore Sigma MAB4401, 1:2000), mouse anti Tra-1-60 (Millipore Sigma MAB4360, 1:1000), mouse anti MAP2 (Sigma-Aldrich M1406, 1:500), rabbit anti MAP2, (Sigma-Aldrich M3696, 1:500), rabbit anti Synapsin (e028, 1:3000), rabbit anti VGAT (Millipore Sigma AB5062P, 1:2000), Gad-67 (Abcam ab26116, 1:500), β3 Tubulin (BioLegend 801201, 1:2000).

3.2.7 Electrophysiological analysis of iN cells

After 35 days following replating of iN cells onto mouse glial cells, whole cell patch clamp recordings were conducted as described previously (115, 169). Following 35 days of maturation on mouse glial cells, coverslips with iN cells were transferred to a HEPES based external solution consisting of (in mM): 140 NaCl, 5 KCl, 2 $CaCl_2$, 2 $MgCl_2$, 10 HEPES, 10 Glucose. The pH of the solution was adjusted to 7.4 using NaOH and osmolarity was measured to be in the 290-300 mOsm range. For all recordings, a K-Gluconate internal solution was used, which consisted of (in mM): 126 K-Gluconate, 4 KCl, 10 HEPES, 4 ATP-Mg, 0.3 GTP-Na_2, 10 Phosphocreatine. The pH of the solution was adjusted to 7.2 with KOH and osmolarity was measured to be in the 270-290 mOsm range.

Spontaneous inhibitory postsynaptic currents (sIPSCs) were recorded at a holding potential of 0 mV in voltage-clamp mode with K-Gluconate internal solution. Miniature IPSCs were also recorded at 0 mV in the presence of tetrodotoxin (1 μM). All synaptic recordings were analyzed with Clampfit 10.7 by Molecular Devices using Template search feature and each event was manually examined for inclusion. Current responses were recorded under a low-pass filter at 2 kHz and at a sampling rate of 5 kHz. Intrinsic action potential firing properties of the iN cells were recorded at I=0 at resting membrane potential without any current injection, in a bath solution containing 50 μM Picrotoxin and 20 μM CNQX.

Evoked action potential recordings were performed under the current clamp recording mode on Clampex 10.5 by Molecular Devices. For induced action potentials, membrane potentials were maintained around -65 mV, and current was injected in a step-wise manner (from -20 to +75 pA, 5pA increments) to elicit action potentials. For the ramp protocol, 0-200pA of current was injected in a 500 ms duration. Current responses

were recorded under a low-pass filter at 2 kHz and at a sampling rate of 5 kHz. All recordings were analyzed off-line with Clampfit 10.7 by Molecular Devices. The template search feature was used and each event was manually examined for inclusion.

3.2.8 DAMGO response

To study the response of sIPSCs to DAMGO, individual iN cells were patched and a HEPES external solution containing 10μM DAMGO was applied acutely by direct perfusion into the recording chamber using a peristaltic pump during synaptic recordings. All DAMGO response experiments are analyzed using normalization. The frequency of sIPSC events (Hz) following DAMGO perfusion is divided by the frequency of events occurring prior to DAMGO perfusion for each individual cell. Normalized data is represented in bar graphs with normalized values depicted as dots next to the averages. Only one neuron was recorded per coverslip for all DAMGO response experiments.

3.2.9 Statistical analysis

Summary graphs of frequency and amplitude are shown for individual cell lines as well as pooled data of either the four N40 patients (red bars) and three D40 patients (blue bars). Data are depicted as means ± SEM. Numbers of cells/Number of independently generated cultures analyzed are depicted in bars. Statistical significance between N40 and D40 conditions was evaluated by Student's T test (*$p<0.05$, **$p<0.01$, ***$p<0.001$).

3.3 Experimental Results

3.3.1 Using Human Subject Derived iPS Cells to Study MOR N40D

To investigate the role of the A118G SNP in MOR function in a human context, we obtained iPS cells from multiple individuals carrying homozygous alleles for either MOR N40 (expressing OPRM1 118AA) or MOR D40 (expressing OPRM1 118GG). These iPS cells were reprogrammed from cryopreserved primary lymphocytes selected from a study of nicotine dependence (COGEND) using the Fagerström test of nicotine addiction and were generated by RUCDR ® Infinite Biologics. To control for background genetic variability, all subjects selected are of European descent from whom a phenotypic history of alcohol and nicotine addiction is well documented and have passed a genotypic screen for SNPs in other nicotinic acetylcholine receptor subunits also associated with addiction behaviors (**Figure 15**). Pluripotency of all seven iPS cell lines are confirmed by immunocytochemistry of OCT4 and Tra-1-60 (**Figure 16A**), and we confirmed the homozygous A118 or G118 alleles of each line by sequencing (**Figure 16B**).

Cell lines	sex	rs880395	rs16969968	rs1799971	rs8192475	rs12914008	rs56218866	Nic. Dep.	Alc Dep.
37SB	F	GG	GG	AA	GG	GG	TT	no	no
73SB	F	GG	GG	AA	GG	GG	TT	no	yes
66SF	M	GG	GG	AA	GG	GG	TT	no	no
41SE	M	GG	GG	AA	GG	GG	TT	no	no
43SD	M	GG	GG	GG	GG	GG	TT	no	no
03SF	M	AA	GG	GG	GG	GG	TT	yes	yes
88SA	F	AA	GG	GG	GG	GG	TT	no	no

Figure 15: Human subject-derived iPS cell lines carrying homozygous A118 or G118 alleles are homozygous for other addiction associated SNPs.

3.3.2 MOR N40D Does Not Affect Neuronal Differentiation and Function

To study MOR N40D in a human neuronal context, we derived inhibitory induced neuronal (iN) cells from all 7 iPS cell lines by lentiviral mediated ectopic expression of the transcription factors Ascl1 and Dlx2, from an established protocol (170). We confirmed neuronal and functional maturation in the iN cells by ICC for MAP2, β3-tubulin, and Synapsin (**Figure 16C**, **Figure 17A**). MAP2 positive iN cells also co-stained for GAD67 (**Figure 17B**) and exhibited punctate staining for vesicular GABA transporter (VGAT) (**Figure 16D**), confirming inhibitory neuronal identity. Gene expression analysis for OPRM1, TH and VGAT in N40 and D40 iN cells (**Figure 18A**) reveals that the N40D SNP has no effect on receptor mRNA expression. Further gene expression analysis for neuronal maturation markers including MAP2, Tuj1, and GAD1 further confirm similar differentiation status and inhibitory neuronal identity of iN cells (**Figure 18B**). While the mean expression levels of these differentiation markers exhibit subject-to-subject variability, pooled data by genotype illustrates there exists no significant difference between corresponding N40 and D40 iN cells.

To examine whether neurons generated from iPS cells of N40 and D40 subject lines are functionally comparable under baseline conditions, we performed whole cell patch-clamp recordings of neurons after 5 weeks of re-plating onto mouse astrocytes. Induced neuronal cells from all subject-derived cell lines exhibit intrinsic membrane properties that are similar among different subject cell lines (**Figure 17C-E**) and can fire repetitive spontaneous action potentials (APs) (**Figure 17F**). We also tested the intrinsic excitability of the inhibitory iN cells by inducing APs using current injections and found that the intrinsic neuronal excitability is unchanged by OPRM1 genotype under baseline conditions (**Figure 16E-G**). Similarly, no significant difference in spontaneous and miniature inhibitory post synaptic currents (IPSCs) were observed by genotype (**Figure 16H-M**). On the basis of patch clamping data and ICC data, we conclude that the

OPRM1 A118G SNP does not lead to major changes in non-synaptic properties of human neurons. The neurons generated from subject iPS cell lines are of similar functional maturation and differentiation.

3.3.3 MOR D40 iN cells exhibit altered sensitivity to MOR activation by DAMGO

There have been numerous studies (77, 96, 97, 102-107) examining the functional consequences of MOR N40D on receptor activation in overexpression models and in knock-in mice harboring MOR N40D, but no functional or electrophysiological analyses on cultured neurons have been conducted, specifically not in a human neuronal context. The only available functional data is from overexpression in heterologous model systems (Section 1.3.2.3 Heterologous expression systems), which give little insight into how the N40D SNP affects MOR signaling or neuronal function at a synaptic level when expressed at endogenous levels in a human system. To gauge whether N40 and D40 iN cells may respond differently to MOR activation, we used a MOR-specific agonist DAMGO ([D-Ala^2, N-MePhe^4, Gly-ol]-enkephalin) to study its role modulating synaptic release. In both N40 and D40 iN cells, DAMGO suppressed sIPSCs in a dose-dependent manner (**Figure 19A**). However, the suppression of sIPSC frequency was more robust in D40 iN cells compared to N40 iN cells in multiple repeated experiments (**Figure 19B-C**) with no significant difference in sIPSC amplitude by genotype (**Figure 19D-E**). To confirm that the differential response in the Dose-response curve is not a residual effect of prolonged agonist exposure, we applied a single concentration of 10μM DAMGO (**Figure 19F-G**) to N40 and D40 iN cells and found a similar trend, illustrating that the differential response is likely to be due to genotype-dependent differential regulation of MOR signaling.

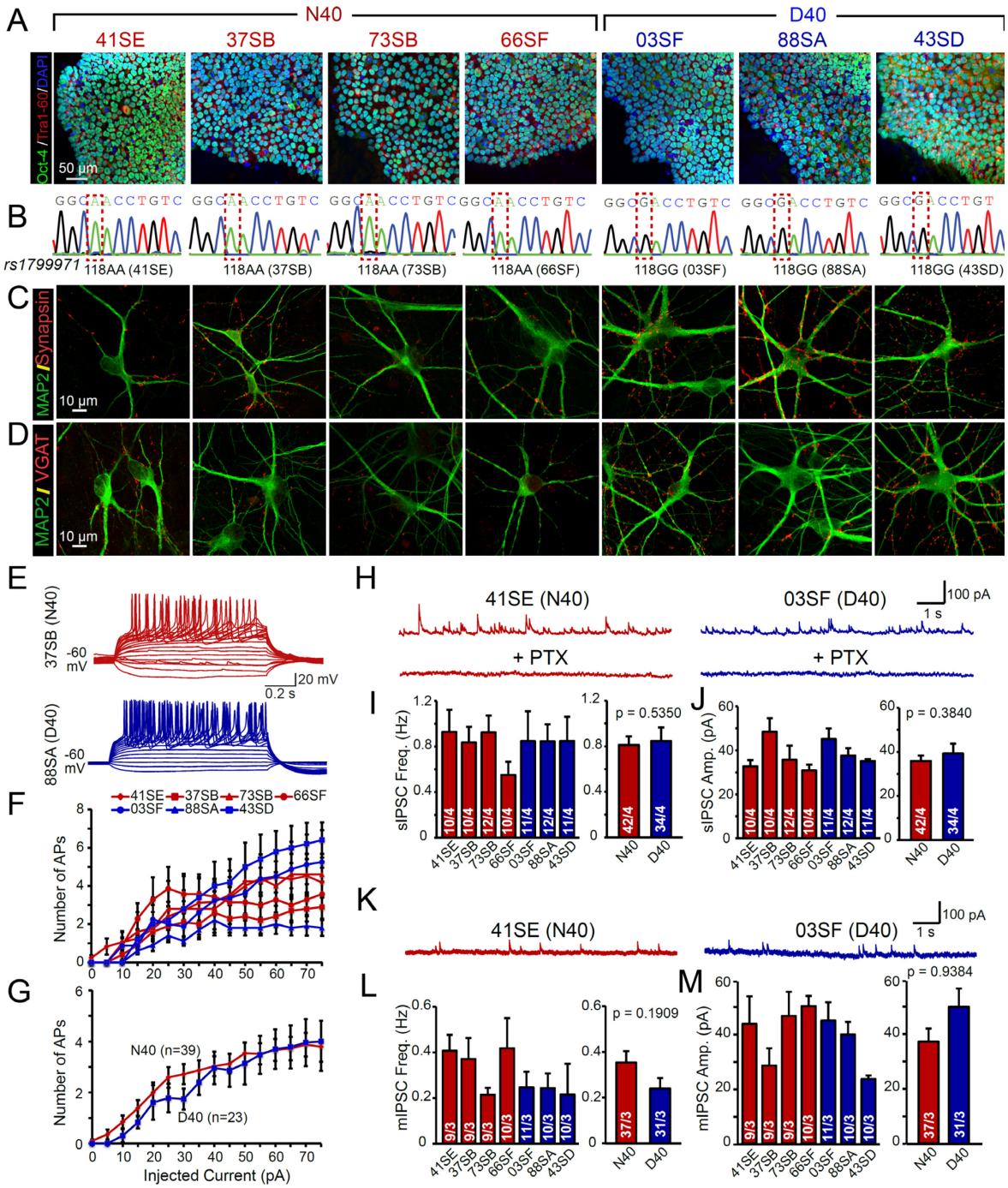

Figure 16: Functionally mature inhibitory human neurons generated from subject-derived iPS cell lines carrying homozygous alleles for OPRM1 A118G.
(A) Oct4 (green), Tra 1-60 (red), and Dapi (blue) ICC for N40 and D40 subject iPS cells. **(B)** Sequencing confirming homozygous A118 or G118 genotype of human iPS cell lines. **(C)** MAP2 (green) and Synapsin (red) ICC of iN cells generated from N40 and D40 subject iPS cells. **(D)** MAP2 (green) and VGAT (red) ICC of iN cells generated from N40 and D40 subject iPS cells. **(E)** Representative traces of induced action potentials of N40 and D40 iN cells. **(F-G)** Quantification of induced action potentials. **(H-I)** Both N40 and D40 iN cells exhibit PTX sensitive spontaneous IPSCs; Frequency and amplitude of sIPSCs in iN cells are unaffected by MOR N40D substitution. **(K-M)** Frequency and amplitude of miniature IPSCs in iN cells are unaffected by MOR N40D substitution.

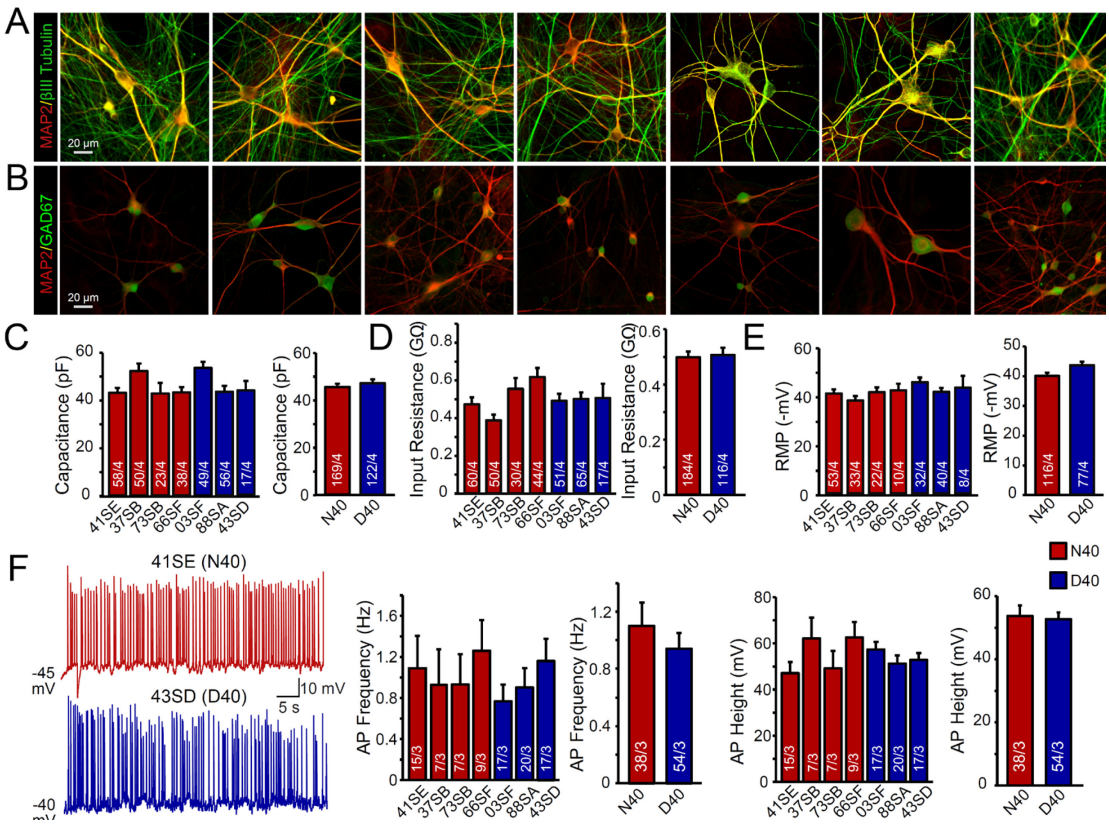

Figure 17: OPRM1 N40D SNP does not impair inhibitory neuronal differentiation or neuronal function at baseline conditions.

(A) MAP2 and βIII-tubulin ICC of inhibitory iN cells differentiated from human iPS cell subject lines to illustrate expression of markers of neuronal maturation **(B)** MAP2 and GAD67 ICC of inhibitory iN cells confirm inhibitory neuronal subtype. **(C-E)** N40 and D40 iPS cell derived iN cells exhibit similar intrinsic membrane properties (Capacitance, Input resistance, and Resting Membrane Potential (RMP)) illustrating similar maturation status **(I)** Representative traces of spontaneous action potentials recorded from one A118 (N40) and one G118 (D40) iN cell line. Summary graphs illustrate that N40 and D40 iNs exhibit similar spontaneous action potential firing frequency and amplitude**.**

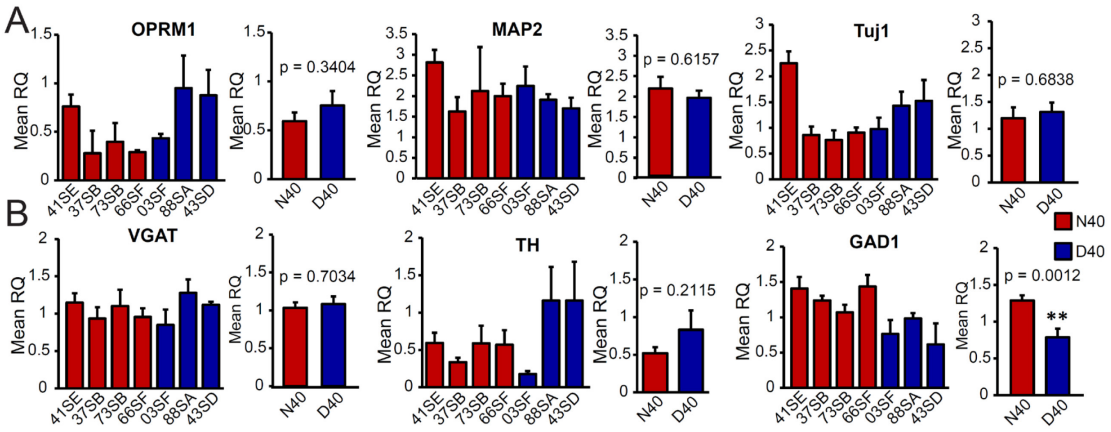

Figure 18: MOR N40D does not affect OPRM1 gene expression or markers of inhibitory neuronal identity.

(A) Relative mRNA levels of OPRM1 as well as markers of neuronal maturation (MAP2, Tuj1) measured by quantitative RT-PCR. **(B)** Relative mRNA levels of inhibitory subtype specificity (GAD1, TH, VGAT) measured by quantitative RT-PCR; mRNA levels are normalized to Synapsin I. Data are represented as means of three independently differentiated batches of iNs from each patient iPS cell line.

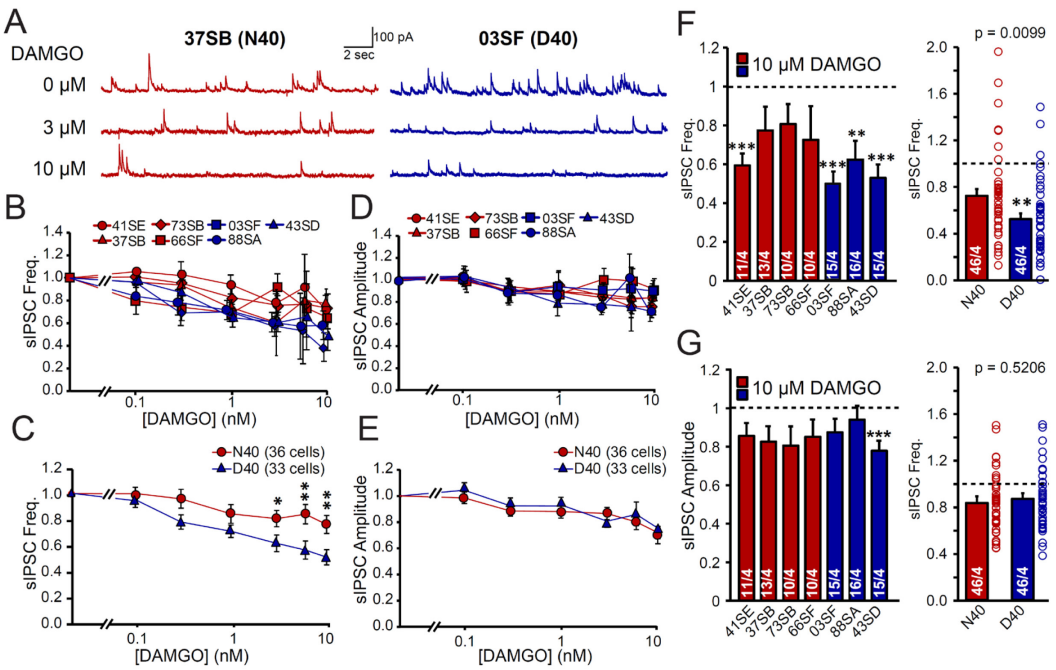

Figure 19: DAMGO exerts stronger suppression of inhibitory synaptic transmission in human iNs carrying D40 MOR variants than those carrying N40 MOR.

(A) Representative traces of sIPSCs recorded to increasing concentrations of DAMGO in N40 and D40 iN cells **(B)** Quantification of inhibition of sIPSC frequency in individual subject derived N40 and D40 iN cells **(C)** Merged data of the four N40 and three D40 subject lines illustrates that D40 iN cells exhibit stronger suppression of IPSC frequency compared to N40 iN cells **(D)** Quantification of inhibition of sIPSC amplitude in individual subject derived N40 and D40 iN cells **(E)** Merged data shows DAMGO causes no difference in sIPSC amplitude by genotype **(F)** Normalized data of iN cells shows frequency response to a single concentration of 10µM DAMGO **(G)** Normalized data of iN cells Amplitude response to a single concentration of 10µM DAMGO.

3.3.4 Isogenic human neurons recapitulate differential DAMGO response

Using the same differentiation technique, we converted each of the isogenic lines into inhibitory iN cells which stain positive for MAP2, Synapsin and VGAT (**Figure 20A-B**). Similarly, these iN cells derived from both sets of isogenic cell lines exhibit similar intrinsic membrane properties, such as membrane capacitance and input resistance (**Figure 20F-G**). Also, they exhibit sIPSCs whose frequency and amplitude do not differ by genotype (**Figure 20H-I**). Furthermore, we detected no differences at baseline levels in spontaneous AP frequency and amplitude, along with other AP properties including firing threshold, time to peak, resting membrane potential, half-width, rise and decay time between corresponding N40 and D40 iN cells derived from the iPS cell line derived isogenic lines (**Figure 21**). This illustrates that the N40D SNP does not alter synaptogenesis or functional maturation in the isogenic human neurons, and that the MOR N40D SNP has no consequence on iN cell maturation or synaptic transmission at baseline levels.

Moreover, as analyzed by qPCR, the two sets of isogenic lines exhibit less variability in OPRM1 gene expression than the patient lines, and also exhibit expression levels that are similar to what is observed in a normal human thalamus (**Figure 20C**). These iN cells also express similar expression levels of markers of inhibitory neuronal subtype (GAD1 and VGAT) (**Figure 20D-E**). This data demonstrates that the two sets of isogenic human stem cell lines can be efficiently converted into human neurons for phenotype level analyses to carefully dissect the cellular and functional synaptic consequences of MOR N40D.

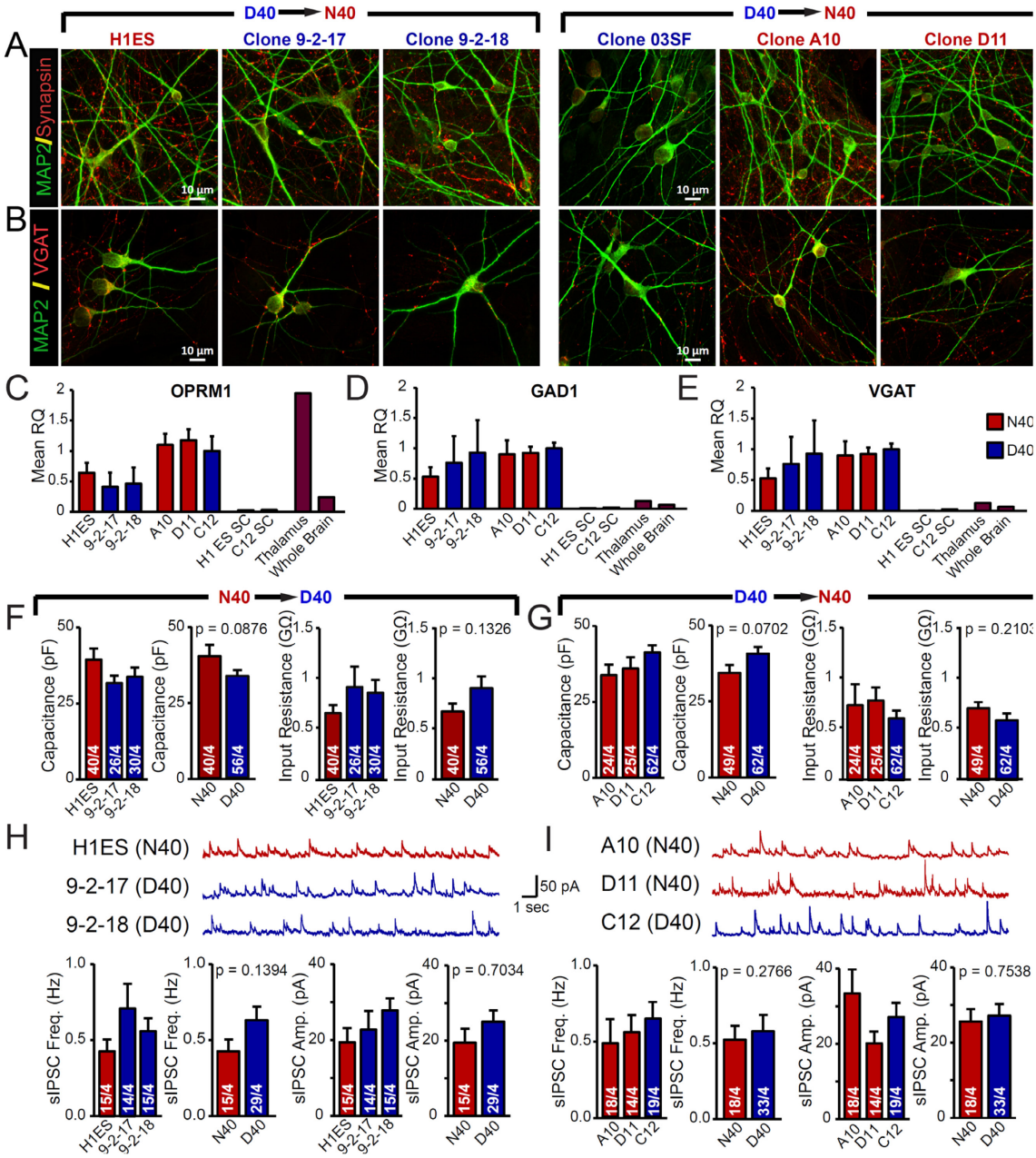

Figure 20: OPRM1 N40D SNP does not impair neuronal differentiation, intrinsic neuronal parameters or neuronal function in isogenic human neurons.
(A) ICC for MAP2 (green) and Synapsin (red) of iN cells produced from gene-targeted ESCs and iPS cells. **(B)** ICC for MAP2 (green) and VGAT (red) of iN cells produced from gene-targeted ESCs and iPS cells. **(C-E)** Relative mRNA levels of OPRM1 as well as markers inhibitory subtype specificity (GAD1, VGAT) measured by quantitative RT-PCR; mRNA levels are normalized to Synapsin I. Data are represented as means of three independently differentiated batches of iNs from each patient iPSC line**. (F-G)** N40 and D40 isogenic iN cells exhibit similar intrinsic membrane properties (Capacitance, Input resistance) at baseline levels, illustrating similar maturation status. **(H-I)** Both N40 and D40 iN cells exhibit sIPSCs whose frequency and amplitude are unaffected by MOR N40D substitution.

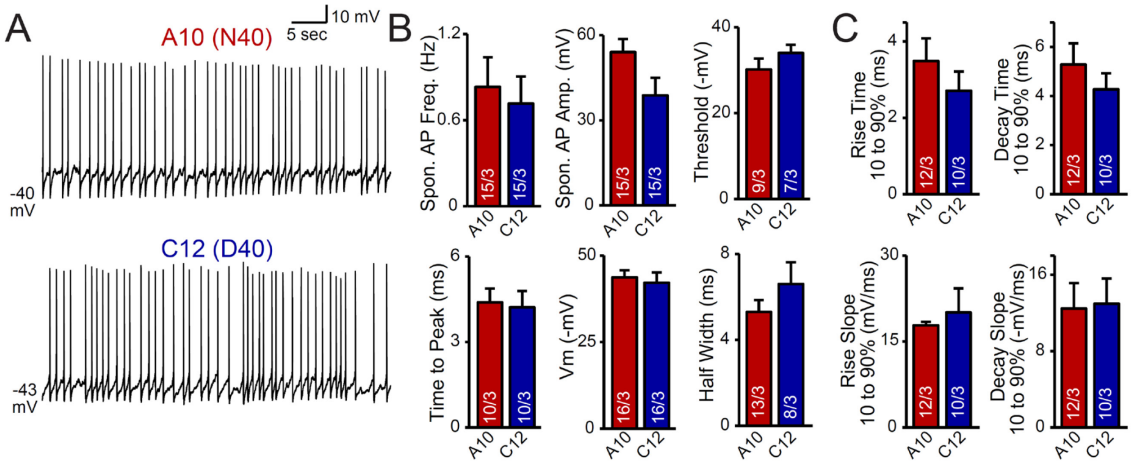

Figure 21: OPRM1 N40D SNP does not impair AP properties in N40 and D40 iN cells at baseline levels.
(A) Representative traces of spontaneous action potentials fired by A10 (N40) iN cells and C12 (D40) iN cells **(B)** Quantification of action potential properties at baseline levels between A10 (N40) and C12 (D40) iN cells shows N40D does not alter Spontaneous AP frequency, amplitude, threshold, time to peak, resting membrane potential, and half width **(C)** Quantification of action potential rise and decay kinetics at baseline levels between A10 (N40) and C12 (D40) iN cells shows N40D does not alter Rise Time, Decay time, Rise slope, or decay slope.

Using this highly controlled system of isogenic cell lines, we then assessed the reproducibility of the DAMGO response phenotype we observed in the patient lines. We studied the effect of DAMGO on sIPSCs in both sets of isogenic cell lines, and observed a similar decrease in sIPSC frequency following acute DAMGO application, with a stronger inhibition in D40 iN cells compared to N40 iN cells, with no effect on amplitude (**Fig 3J-O**). Furthermore, to validate that the effect of DAMGO was mediated by MOR, we applied Naltrexone, a broad spectrum MOR antagonist, and found that the synaptic suppression caused by DAMGO could be reversed (**Figure 23**). Overall, these results suggest that the N40D isogenic neurons recapitulate the findings obtained with N40 and D40 subject-derived neurons. Therefore, D40 MOR mediated signaling in human neurons is likely stronger than that of N40 human neurons. This indicates that the N40D variant alone explains the differential signaling effect and that it was likely not due to unknown variant(s) elsewhere in the subjects' genomes.

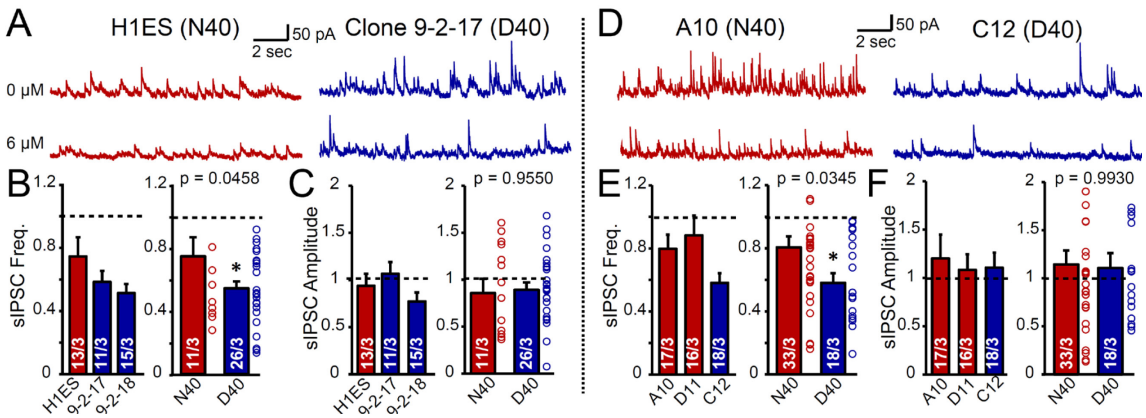

Figure 22: Human neurons from two sets of independently targeted isogenic human stem cell lines for OPRM1 A118G validate differential DAMGO response observed in patient cell lines.
(A) Sample traces of sIPSCs from one N40 and one D40 isogenic H1ES cell line. **(B-C)** Quantification of sIPSC Frequency and Amplitude shows DAMGO has stronger suppression of inhibitory synaptic transmission in Clone 9-2-17 and 9-2-18 (carrying MOR D40) compared to parent H1ES cell derived iN cells with no genotype specific effect on sIPSC amplitude**. (D)** Sample traces of sIPSCs from one N40 and one D40 isogenic iPS cell lines. **(E-F)** Quantification of sIPSC Frequency and Amplitude shows DAMGO has stronger suppression of inhibitory synaptic transmission in Clone C12 (carrying D40) compared to clone A10 and D11 iN cells with no genotype specific effect on sIPSC amplitude**.**

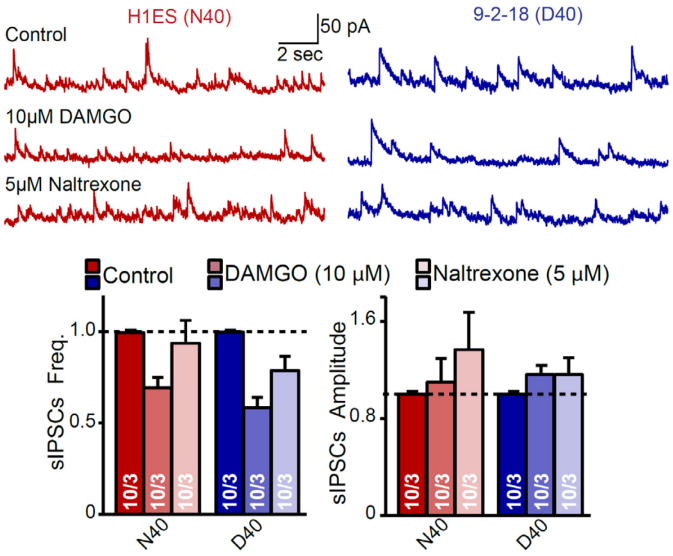

Figure 23: Naltrexone reverses the DAMGO synaptic inhibition phenotype in both N40 and D40 iN cells.
(A) Sample traces of sIPSCs of N40 and D40 iN cells **(B)** Quantification of sIPSC Frequency and amplitude following 10µM DAMGO and 5µM Naltrexone.

3.3.5 MOR N40D SNP confers more robust decrease in excitability following DAMGO

To explore the mechanistic basis of the DAMGO-induced decrease in spontaneous activity, we focused the remaining analyses on one pair of isogenic cells, the C12 and A10 cell lines. We used the expression of mature synapse marker synapsin, functional synaptic releases indicated by sIPSCs and intrinsic membrane properties as metrics to judge the differentiation quality of all iN cells. We selected the C12 and A10 cell lines for further mechanistic studies on the basis that these metrics were most similar at baseline levels, allowing us to make appropriate phenotypic comparisons.

We then examined the effect of DAMGO on the intrinsic excitability of iN cells carrying N40D MOR variants. Upon application of 10 μM DAMGO, we found that D40 iN cells fire significantly fewer induced APs compared to N40 iN cells (**Figure 24A-B**), with no effect on AP amplitude or AP firing threshold (**Figure 24C**) or other AP properties including Time to reach peak and Time to reach threshold (data not shown). This is supported by an immediate and more robust decrease in spontaneous AP firing frequency following DAMGO application in D40 compared to N40 iN cells (**Figure 24D**) an effect which is sustained over the course of several minutes (**Figure 24E**). This sustained decrease in AP frequency is paralleled by a rapid hyperpolarization of iN cells N40 and D40 iN cells upon DAMGO application **(Figure 24F)**. This effect was found to be significantly more robust in D40 iN cells compared to N40 iN cells in the first minute following DAMGO application. No difference in other spontaneous AP properties such as AP Rise time, decay time or half width were detected by DAMGO application between N40 and D40 iN cells (data not shown). However, we did observe a slight increase in the after hyperpolarization potential (AHP) in the D40 iN cells compared to the N40 iN cells (**Figure 25**). These data indicate the functional differences between N40 and D40 iN

cells are at least in part mediated by a preferential decrease in excitability in D40 iN cells compared to N40 iN cells, likely mediated by alterations in the G-protein coupled signaling cascade.

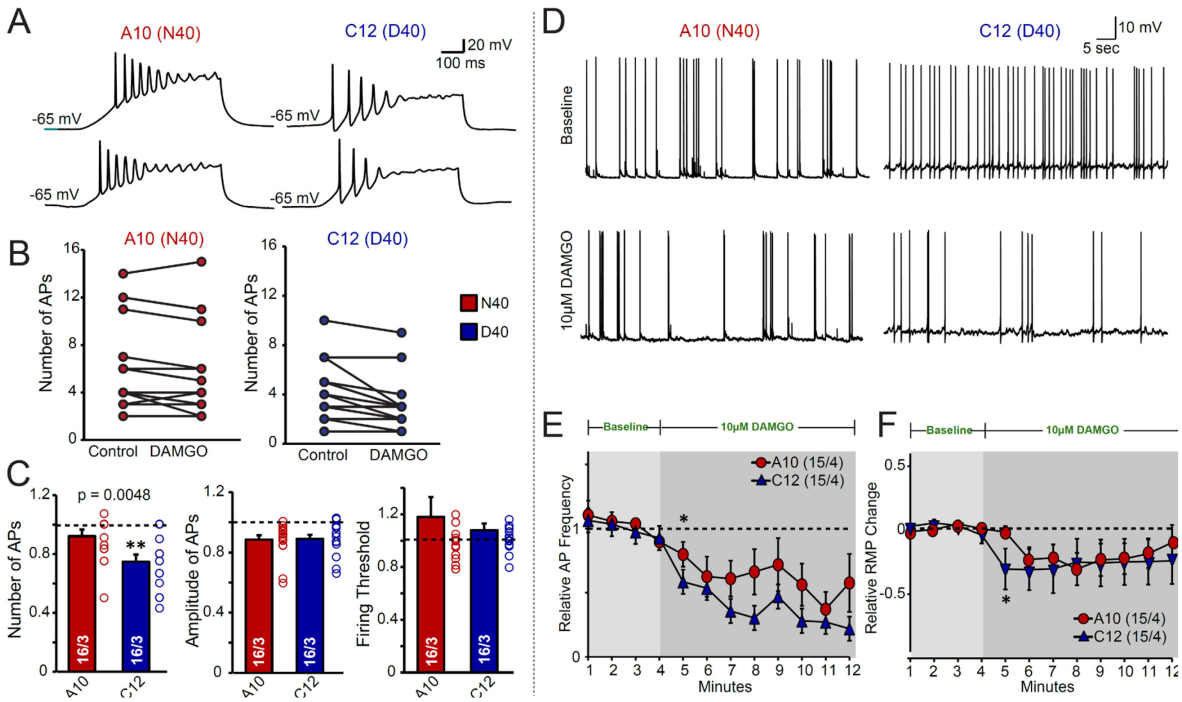

Figure 24: DAMGO preferentially decreases intrinsic excitability in D40 MOR iN cells compared to N40 MOR iN cells.
(A) Representative traces of repetitive action potentials generated from depolarizing current injections in one N40 (A10) cell line derived iN and one D40 (C12) cell line derived iN, and their response to DAMGO**. (B)** Quantification of number of action potentials fired before and after DAMGO application in N40 and D40 iNs**. (C)** Summary graphs of DAMGO effect on AP Number, Amplitude, and firing threshold (Data normalized to before DAMGO application) reveals DAMGO preferentially decreases intrinsic excitability of D40 iNs but not N40 iNs with no effect on Amplitude or Firing Threshold**. (D)** Representative traces depicting the effect of DAMGO on spontaneous action potential firing in one D40 (C12) and one N40 (A10) cell line derived iN**. (E)** Quantification of number of spontaneous action potentials fired before and after DAMGO application in N40 and D40 iNs represented as a timecourse**. (F)** Quantification of number of resting membrane potential before and after DAMGO application in N40 and D40 iNs represented as a timecourse**.**

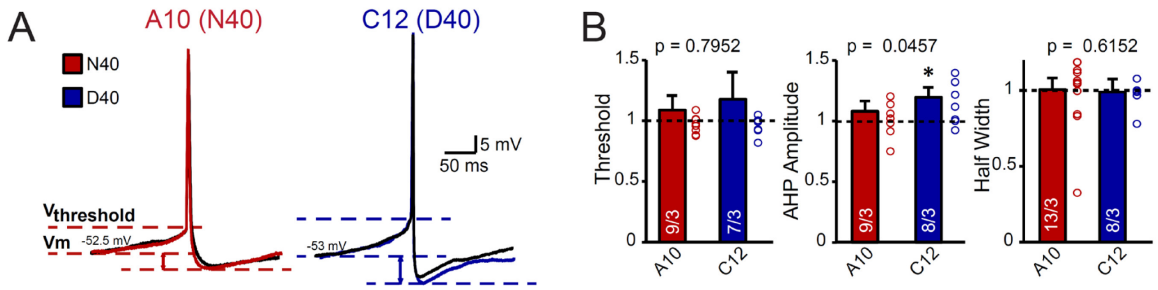

Figure 25: D40 iN Cells Exhibit Preferential Increase in AHP Amplitude Following DAMGO

(A) Representative traces of individual Action Potentials before and after DAMGO in N40 and D40 iNs. **(B)** Summary graphs depicting that DAMGO has no effect on Firing threshold or half width, but preferentially increases the AHP amplitude in D40 iN cells compared to N40 iN cells.

3.3.6 MOR D40 iN Cells Exhibit Decreased Synaptic Release Upon Receptor Activation

In order to understand whether the reduced neuronal excitability following DAMGO is compounded by reduced synaptic release, we asked whether MOR activation by DAMGO alters synapse function by measuring its effect on mIPSCs in both N40 and D40 iN cells. We found that DAMGO application more robustly decreases mIPSC frequency in D40 iN cells compared to N40 iN cells (**Figure 26**). This change in mIPSC frequency suggests a decrease in synaptic release following DAMGO application that is more profound in D40 iN cells compared to N40 iN cells. This suggests that this DAMGO induced decrease in excitability is superimposed by a synapse-specific effect, i.e. a stronger reduction in synaptic release probability mediated by presynaptic MOR at the nerve terminal in D40 MOR carrier inhibitory neurons.

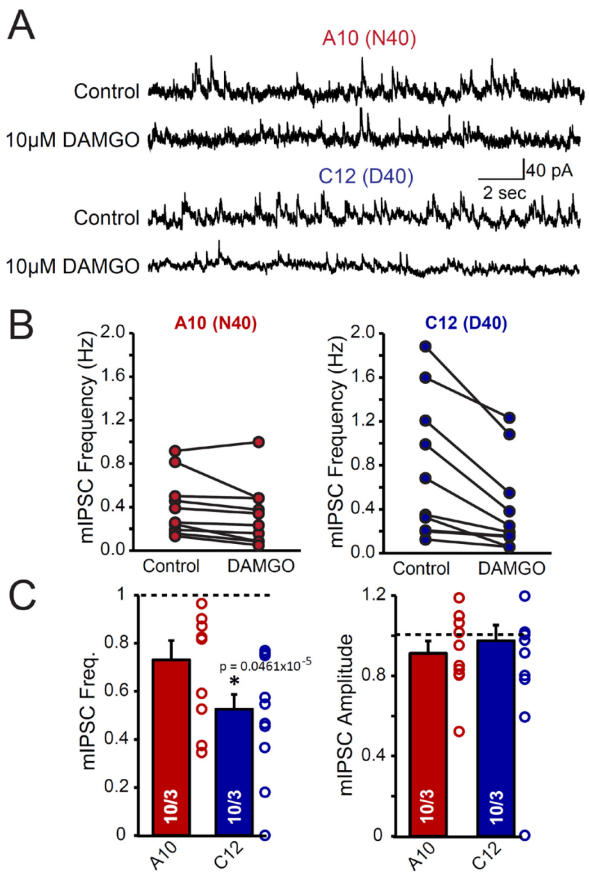

Figure 26: DAMGO preferentially decreases synaptic release in D40 MOR iN Cells Compared to N40 MOR iN Cells.
(A) Representative traces of mIPSCs in A10 (N40) iNs and C12 (D40) iNs and their response to DAMGO. **(B)** Quantification of number mIPSC frequency before and after DAMGO application in N40 and D40 iNs**. (C)** Summary graphs of DAMGO effect on mIPSC Frequency and amplitude in A10 (N40) iNs and C12 (D40) iNs normalized to before DAMGO application illustrate that DAMGO decreases synaptic release in D40 iNs to a greater extent than in N40 iNs with no corresponding effect on amplitude**.**

3.4 Discussion

The N40D SNP in the MOR has been linked to addiction and other reward related behaviors. Despite countless studies attempting to understand the functional consequences of the MOR N40D SNP in heterologous expression systems and A112G knockin mice (Discussed in Section 1.3.2 Functional Characterization of MOR N40D), the underlying cellular mechanisms of the MOR N40D SNP in the modulation of synaptic and function in the human brain and its relevance to human reward behaviors is largely unknown. These contradictory results in the literature strongly suggest not only species-specific but also context-specific mechanisms in the modulation of MOR signaling, necessitating the need for a human neuronal model to elucidate the appropriate mechanisms. Thus, our study provides the first experimental evidence detailing the electrophysiological consequences of the N40D SNP on MOR activation in its endogenous human neuronal context.

3.4.1 Caveats of Modeling N40D in Human Stem Cells

The novelty of using human iN cells to understand synaptic pathology of addiction is that these cells carry the genetic signatures of the patients from which they were derived. While this may serve as an attractive alternative to knock-in mouse models, the vast phenotypic and genetic heterogeneity between subjects exhibiting drug dependence and addiction can pose limitations in understanding the role of disease-associated human SNPs, such as MOR N40D (171). Moreover, the differentiation status of an iN cell *in vitro* does not likely mimic the adult neurons found within a network in the human or the identical subtype specificity of the neurons in the brain's endogenous reward circuitry. In fact, there is evidence that iPS cell lines exhibit variability in

reprogramming and in the efficiencies of neural differentiation (171, 172), which brings into question the validity of direct comparisons between subject derived neurons.

In spite of these limitations, we have been able to generate neurons with no distinguishable differentiation or maturation abnormalities and have been able to isolate a consistent and reproducible synaptic phenotype across neurons generated from multiple individuals carrying either homozygous D40 or N40 alleles at the MOR. To consolidate these findings further, we employed CRISPR/Cas9 genome-editing to knock-in homozygous D40 alleles into a well characterized H1 ES cell line and correct the homozygous D40 alleles in one subject iPS cell line. This generated two sets of isogenic stem cell lines for highly controlled mechanistic analyses. Isolating identical DAMGO mediated responses across both patient derived iN cells as well as two sets of genome targeted cells generated using independently executed targeting strategies substantiates the validity of the isolated synaptic phenotypes and directly demonstrates that the observed MOR effect is due to the N40D variant and not some other genetic variation in the backgrounds of subjects.

3.4.2 Synaptic Role of MOR N40D in Human Neurons

MORs are localized in different subcellular compartments, namely the soma, dendrites and synaptic terminals and each have distinct functional roles. Activation of MORs localized in the somatodendritic decrease the excitability of the neuron. However, presynaptic MORs are involved in inhibiting neurotransmitter release (54). Thus, MORs regardless of their localization function to decrease downstream excitation of the postsynaptic neuron, as is seen in their role in the mesolimbic dopamine pathway (**Figure 1**). However, regulation of MORs in different cellular compartments can vary dramatically. For example, presynaptic MORs fail to exhibit acute desensitization

whereas postsynaptic MORs located on the soma or dendrites exhibit acute desensitization and internalization (173, 174).

In our human iN cells, we observed distinct synaptic consequences of acute MOR activation by DAMGO. Specifically, we observed an increased sIPSC response to DAMGO in D40 iN cells compared to N40 iN cells, which was highly consistent between both human subject-derived as well as gene-targeted isogenic iN cells (**Figure 19, Figure 22**). We subsequently identified that this increased DAMGO response to spontaneous activity is caused by a more robust inhibition of neuronal excitability. This excitability effect is most likely to be mediated by postsynaptic MORs, whose activation modulates ion channel regulation to hyperpolarize the neuron. An immediate consequence of MOR signaling is G-protein mediated inhibition of presynaptic calcium channels and activation of G protein-activated, inwardly rectifying K^+ (GIRK) channels to cause overall reduction of neuronal excitability (46). Correspondingly, we observed a rapid hyperpolarization immediately upon DAMGO application and a coincident decrease in intrinsic action potential firing frequency, ultimately resulting in a more robust decrease in neuronal excitability in D40 iNs compared to N40 iNs (**Figure 24**).

Careful observation of the timescale of these events (RMP drops within 1 minute of MOR activation, AP frequency drops within 1 minute) allows us to speculate on the precise mechanisms mediating these effects. Reduced excitability is likely to be mediated by downstream effectors that are recruited within milliseconds following activation (54). Thus, the most likely explanation is that D40 iN cells exhibit decreased GIRK channel signaling or Ca^{2+} channel function, which is known to occur within milliseconds of receptor activation and halt upon receptor desensitization (occurs within 1 minute). This decreased excitability is sustained over a period of eight minutes following activation, suggesting that differential ion channel regulation may be mediating only the initial 1 minute of this phenotype.

We thus subsequently studied DAMGO's effect on synaptic release and similarly observed a more robust drop in mIPSC frequency in D40 iN cells, suggesting that the sustained decrease in excitability over the span of 8 minutes may be compounded by a decrease in synaptic release, which is likely mediated by presynaptic MORs. Given that pre-synaptic MORs fail to exhibit acute desensitization, this effect is likely to be more prolonged as seen on the time-course. This could be further confirmed by plotting the mIPSC frequency response to DAMGO as a time-course.

Further experiments need to be conducted in order to elucidate the precise signaling pathways that are altered by MOR N40D. Specifically, direct electrophysiological measurements of GIRK channels as well as calcium channel function in response to MOR agonists can elucidate the synaptic mechanisms underlying MOR function. An additional key next step would be to understand whether the reduced excitability and synaptic release phenotypes associated with MOR N40D hold true for the endogenously released β-endorphin or exogenous opioid agonists, such as morphine, which have addictive capability.

3.4.3 Role of N-linked glycosylation in MOR N40D function

N-linked glycosylation is a common post-translational modification of GPCRs that occurs at the consensus sequence Asn-Xaa-Ser/Thr (175). MOR N40D SNP abolishes 1 of 5 putative N-linked glycosylation sites at the N-terminus of the receptor, which potentially plays a role in the functional impact of the SNP (104). Based on our results, it is likely that loss of glycosylation has two roles in MOR function: **(1)** To enhance acute signaling in previously naïve cells (**Figure 19, Figure 22**). **(2)** To differentially regulate MOR trafficking and recycling following DAMGO pre-exposures (**Figure 29, Figure 31**, See

4.4.2 Role of glycosylation on receptor expression and trafficking). Here we explore the potential role of glycosylation in these two aspects of MOR regulation.

To date, there has been minimal work investigating the role of the N-terminus in MOR function. One study examined the binding affinities of various mu ligands in truncated MORs lacking 64 amino acids from the N-terminus overexpressed in HEK 293 cells. They found that these receptors exhibit 3.5-fold decreases in affinity to naloxone and a 6-fold decrease in affinity for morphine (176). Similarly, the affinities for opioid peptide agonists including DAMGO or β-endorphin were also decreased from 3 to 8-fold from the deletion (176). However, a definitive role for the N-terminus in stabilizing the active conformation of the human MOR and its role in opioid receptor mediated signaling processes has yet to be thoroughly investigated.

The possibility that single amino acid substitutions can lead to profound changes in GPCR signaling and disease associations have already been demonstrated for other GPCRs. For example, loss of an N-terminal glycosylation site in the rhodopsin GPCR from the N15S polymorphism is the cause of retinitis pigmentosa in humans which is likely due to the destabilization of the S15 rhodopsin (177, 178). In fact, the N15S mutation has been shown to disrupt protein folding and binding of rhodopsin to its ligand 11-cis-retinal chromophore (177). Moreover, the R389G and the S49G SNPs in the β_1-adrenergic receptor have been shown to enhance activation of the cAMP/PKA and influence β1AR trafficking, respectively, ultimately causing a predisposition to cardiomyopathic decompensation (134).

While it is unlikely that the N40D SNP directly affects the ligand binding affinity or G protein coupling, our data suggests that the glycosylation affects the functioning of the N-terminus in such a way that signaling is enhanced. Some experimental evidence in the literature also supports this notion that the glycosylation has an inhibitory effect on ligand

efficacy. For example, the X ray crystal structure of the MOR bound to the morphinan agonist BU72 revealed that the N-terminus forms a lid over the ligand binding pocket in the MOR, allowing a few amino acids to penetrate into the ligand binding pocket to contact the ligand (179). Thus, it is possible that a loss of glycosylation from the N-terminus would enhance this interaction of the N-terminus with the agonist. This would potentially stabilize a slightly different active conformation of the MOR that promotes enhanced receptor efficacy upon acute agonist binding.

Another study supports this notion by showing that the glycosylated side chains of the Nterminus undergo a conformational change upon agonist binding (180). In fact, the involvement of N-glycosylation in the positioning of the N-terminus is supported by recent crystallographic studies that show that the polysaccharide chains of individual receptors within a dimer wrap around each other in the basal state (181). Using conformation-sensitive monoclonal antibodies that can differentially recognize receptor activation states, one study revealed that agonist treatment leads to the movement of the N-terminus in each protomer away from each other within a MOR homodimer (180). Thus, it is possible that a loss of glycosylation in D40 MORs abolishes these coordinated conformational changes observed upon receptor activation, ultimately affecting receptor signaling efficacies.

These studies collectively suggest that N-terminal glycosylation of the MOR may have an inhibitory effect on MOR activation through its interaction with the ligand. They also suggest a structural basis for the importance of glycosylation on MOR function that potentially contribute to differential signaling observed by N40D. In order to definitively determine the role of glycosylation on MOR function, crystal structures of activated A118 and G118 MORs would be required to reveal the functional consequences. In the absence of those studies, it is difficult to mechanistically explain the precise molecular interactions that mediate these acute signaling differences.

In summary, this study provides a significant advance in our understanding of the underlying neurobiological mechanisms underlying N40D MOR variants in human neuronal context. In addition, our study uses human neuronal cells to reveal the novel observation that the highly prevalent MOR N40D SNP produces functional alterations at the level of the synapse. This study illustrates the use of patient-specific stem cells to unravel the impact of OPRM1 gene variants in humans and will ultimately help devise patient-specific therapeutic interventions based on OPRM1 genotype for those suffering from drug and alcohol dependence.

Chapter 4 Role of MOR N40D SNP in modulating long term tolerance

4.1 Introduction

Prolonged or repeated administration of opiates produces adaptive changes in the nervous system that leads to reduced drug potency or efficacy, which is the consequence of drug tolerance. Short term and long term tolerance at the mu opioid receptor refers to the loss of responsiveness to an agonist after prolonged exposures (54). Traditionally, it has been understood that internalization of mu opioid receptors following activation by an efficacious ligand results in a reduced number of functional MORs at the cell surface and has long been thought to be the cellular correlate of tolerance to opiate drugs (54). Although we understand the mechanisms of opioid receptor desensitization in great detail, the functional consequences and the mechanisms of neuronal adaptation to prolonged opioid exposure are still poorly understood.

There have been many approaches to understanding the molecular and cellular underpinnings of the development of tolerance. For instance, various studies have induced tolerance to opioids using chronic treatment of animals and then examined what adaptations were incurred (182). Another approach is to find ways to perturb hypothesized mechanisms using pharmacologic or genetic manipulations and examine how this may affect opioid tolerance in either cell culture or animal models. These approaches have identified a multitude of mechanisms that may be contributing to opioid tolerance in vitro, but have failed to identify any individual consistent regulatory mechanism.

Moreover, long term adaptations induced in iN cells from prolonged MOR activation have more long lasting changes at the synaptic level. While the literature has explored the molecular and cellular underpinnings of tolerance, surprisingly little is

known about how MOR N40D SNP may cause long-term changes by altering synaptic function and plasticity, ultimately contributing to the development of tolerance at the mu opioid receptor. Understanding the cellular, synaptic and network level changes that occur downstream of receptor activation are key to understanding long term tolerance at the MOR. Various studies have been done to understand how opioids induce short-term plasticity of MOR function that may serve as precursors to the development of tolerance. For example, it is possible that long term tolerance at the MOR is induced by receptor to effector coupling and downregulation of receptors that persists even hours and days following removal of an agonist (183). Moreover, it is possible that intracellular signaling mechanisms in neurons expressing MOR may develop adaptations to chronic agonist exposure. Lastly, it is also possible that neuronal circuitry related adaptations may occur to offset the chronic agonist mediated signaling that occurs during drug adaptation. A clear synaptic role for MOR N40D on development of long-term tolerance has yet to be explored in human neurons. Thus, it is important to understand the adaptive changes in cellular and synaptic function induced by chronic agonist treatment.

Using human iN cells derived from human stem cells, we investigated the impact of prolonged MOR activation on neuronal and synaptic function and intrinsic membrane properties. We found that short-term activation of mu opioid receptor by DAMGO abolishes both N40 and D40 iN cells' ability to respond to DAMGO whereas long-term MOR activation induced differential changes in synaptic function in N40 and D40 iN cells. These experiments not only provide the first experimental evidence of MOR mediated changes in long term tolerance in human neurons, but also illustrate a level of synaptic adaptation exhibited by neurons, which could provide an important link to understanding the synaptic plasticity mechanisms in the reward circuit.

4.2 Materials and Methods

4.2.1 Human induced pluripotent stem cell generation and maintenance

The seven iPS cell lines that were used in the initial phenotypic analyses of this study were derived from multiple individuals carrying homozygous alleles for either MOR N40 (n=4) or MOR D40 (n=3). These iPS cells were reprogrammed from primary human lymphocytes selected from a study of nicotine dependence (COGEND) using the Fagerström test of nicotine addiction and were generated by RUCDR Infinite Biologics® using Sendai viral mediated gene transduction of OKSM.

Human iPS and ES cells were maintained at 37°C, 5% CO_2, and cultured feeder-free on Matrigel ® Matrix (Corning Life Sciences)-coated 6-well plates or 10cm dishes in mTeSR medium (STEMCELL Technologies). The mTeSR media was refreshed daily, and the cells were passaged once a week for maintenance as well as neuronal differentiation. For passaging, the cells of each line were passaged by dissociation into single cells. To passage, mTeSR medium was removed, and the wells were washed with Minimal Essential Media (MEM, Gibco), 1 mL for 6-well plate, and 5 mL for 10cm dish. The MEM was then aspirated, and replaced with 1mL of Accutase™ (STEMCELL Technologies), 1 mL for 6-well plate and 5 mL for 10cm dish, and incubated at 37°C for 5 minutes to allow cells to dissociate from the dish. The dissociated stem cells were subsequently collected into a 15mL conical tube, remnant cells were collected in MEM and added to the conical tube. iPSCs were then collected into a pellet at 1000 RPM for 5 minutes, using a tabletop centrifuge. Supernatant was removed and cells were resuspended in 1mL of mTeSR media containing 5μM ROCK inhibitor (Stemolecule™ Y27632, Stemgent). A sample of this resuspension was diluted 1:10 and used for counting on a hemocytometer. Using estimation of cell density, 150,000 cells were

plated into a 6-well plate for maintenance and 500,000 cells were plated into each well of a 6-well plate for neuronal differentiation.

4.2.2 Glial cell preparation and maintenance

Glial cell monolayer cultures were prepared using mouse pups that are 0-4 days old of the C57BL/6J Mus musculus strain and cultures were prepared as previously described (169). Both male and female mice will be used. To isolate glial cells, brains of P0-P4 pups were dissected, meninges was removed and the brain was stored in 2mL of HBSS on ice. Subsequently, 1mg/mL of trypsin was dissolved in HBSS and was added to the brain and incubated at 37°C for 20 minutes and the tube was agitated every 5 minutes to ensure penetration of trypsin solution throughout the brain. The brain was brought into the tissue culture hood, trypsin solution was aspirated, and the brain was washed twice with DMEM with 10% Fetal Bovine Serum (FBS) with 1% PenStrep to remove excess trypsin. A fresh 1 mL of DMEM with 10% FBS and 1% PenStrep was added to the tube and the tissue was dissociated into single cells using a pipette. The dissociated tissue was then passed through a sterile 70µm nylon cell strainer (Falcon ®) in order to remove debris and dead cells. The elutant containing strained cells was subsequently cultured in DMEM media with 10% FBS and PenStrep in T75 flasks and cultured in 37°C and 5% CO_2.

4.2.3 Lentivirus preparation

We utilized HEK 293T cells to package replication incompetent lentiviral vectors, which we used to infect human stem cells for neuronal differentiation. A calcium phosphate transfection method was used to deliver both packaging vectors as well as plasmids containing transcription factors of interest. These HEK 293T cells were

passaged 1:4 into 15 cm tissue culture dishes the day before calcium phosphate transfection was to be done. The HEK 293T cells were transfected when they were at 60% confluency. On the day of transfection, we mixed the three packaging vector components RRE (0.75µg), REV (9.1µg), VSV-g (13.77µg), with 22.4µg of the lentiviral expression vector expressing the transcription factor of interest. Next, we added 105 µl of a 2.5M Calcium Chloride solution and then totaled this mixture to 1.5mL using sterile water. We subsequently added this DNA, Calcium and water mixture to a 2X HBS solution while holding this on a vortex. The 2X HBS solution contained 50mM HEPES (pH 7.05), 1.4mM anhydrous Na_2HPO_4, and 280mM NaCl. This mixture of calcium causes the DNA calcium mixture to precipitate with the phosphate to form small enough calcium phosphate crystals to enter into the HEK 293T cells. This calcium phosphate DNA crystals of total of 3mL was added onto the 15cm dishes containing HEK 293T cells.

After 12 hours of transfection, the media was aspirated and replaced with mTeSR media. The transfected HEK 293T cells were then incubated with this culture media for a total of 24 hours, upon which the media carrying the lentivirus of interest was collected and spun in a tabletop centrifuge for 1500g for 10 minutes at 4°C to remove any dead cells and debris. The virus was immediately placed on ice, and aliquoted into 1mL or 0.5mL aliquots in Eppendorf tubes, and stored in the -80°C freezer for future use.

4.2.4 Generation and maintenance of iN cells

Induced neuronal (iN) cells were produced from iPS cells by forced expression of cell lineage transcription factors as described previously (116). On day -2, iPS cells of each cell line were dissociated using Accutase ® (Innovative Cell Technologies) as described in section 4.2.1 and collected, and centrifuged at 1000 RPM for 5 minutes on

a tabletop centrifuge. The cells are plated at a density of 50,000 cells/cm^2 either in 6-well plates or 10cm dishes for neuronal differentiation. The iPS cells are plated in a lentiviral cocktail with mTeSR media containing 100µl/mL Ascl1, 100µl/mL Dlx2, and 100µl/mL rtTA lentivirus. On day 0 (approximately 12-15 hours after lentiviral infection), the virus cocktail is replaced with Neurobasal ® media containing 2µg/mL Doxycycline and 5µM ROCK inhibitor to induce expression of cell lineage transcription factors. On Day 1, we conduct drug selection using 1µg/mL of Puromycin (ThermoFisherScientific) and 100µg/mL Hygromycin (ThermoFisher Scientific) for 48 hours or as needed. On day 3, 30,000 mouse glial cells are plated onto 10mm glass coverslips, each placed in an individual well of a 24-well plate. On day 4 of neuronal induction, iN cells are dissociated using Accutase and 150,000 iN cells are plated onto the 10mm coverslips carrying mouse glial cells and are allowed to mature for 5 weeks at which point we conduct functional analyses. The iN cells are half-fed every 3-4 days in Neurobasal® media containing Gem21 NeuroPlex™ Serum Free Supplement (Gemini), L-glutamine (Gibco), 2 µg/ml Doxycycline (MP Biomedicals), 10 ng/ml BDNF, 10 ng/ml GDNF, 10 ng/ml NT3 (Shenandoah Biotechnology Inc™).

4.2.5 Electrophysiological analysis of iN cells

After 5 weeks of maturation on mouse glial cells, whole cell patch clamp recordings were conducted as described previously (115, 169). Coverslips with iN cells were transferred to a HEPES based external solution consisting of (in mM): 140 NaCl, 5 KCl, 2 $CaCl_2$, 2 $MgCl_2$, 10 HEPES, 10 Glucose. The pH of the solution was adjusted to 7.4 using NaOH and osmolarity was measured to be in the 290-300 mOsm range. For all recordings, a K-Gluconate internal solution was used, which consisted of (in mM): 126 K-Gluconate, 4 KCl, 10 HEPES, 4 ATP-Mg, 0.3 GTP-Na_2, 10 Phosphocreatine. The pH

of the solution was adjusted to 7.2 with KOH and osmolarity was measured to be in the 270-290 mOsm range.

Spontaneous inhibitory postsynaptic currents (sIPSCs) were recorded at a holding potential of 0 mV in voltage-clamp mode with K-Gluconate internal solution. Current responses were recorded under a low-pass filter at 2 kHz and at a sampling rate of 5 kHz. All synaptic recordings were analyzed off-line with Clampfit 10.7 by Molecular Devices. The template search feature was used and each event was manually examined for inclusion.

4.2.6 DAMGO Pre-Exposures

To understand MOR function after short term and long-term tolerance at the MOR, we pre-exposed N40 and D40 iN cells to DAMGO to understand how this would affect the DAMGO response phenotypes. For 1-day pre-exposures, DAMGO was diluted in neuronal culture medium at a concentration of 10μM and added to coverslips carrying iN cells 24 hours prior to the electrophysiological experiments. For 7-day pre-exposures, DAMGO was diluted and added to the neurons in the same manner; however, the DAMGO containing culture medium was refreshed daily for 7 days prior to recordings. At the time the recordings were to be done, coverslips were removed from the DAMGO containing culture medium and brought to the recording chamber in HEPES bath solution for electrophysiological analyses (4.2.5 Electrophysiological analysis of iN cells) and DAMGO responses (4.2.7 DAMGO response). The iN cells were tested for their ability to respond to DAMGO re-application following pre-exposures (**Figure 27**).

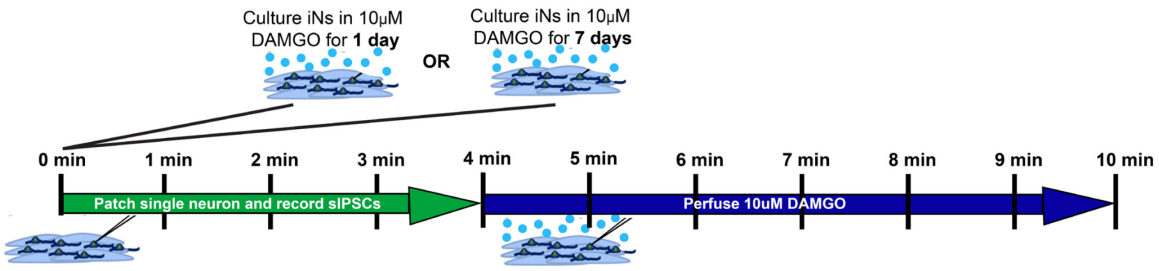

Figure 27: Experimental paradigm to study short-term and long-term tolerance.

4.2.7 DAMGO response

To study the response of sIPSCs to DAMGO, individual iN cells were patched and a HEPES external solution containing 10μM DAMGO was applied acutely by direct perfusion into the recording chamber using a peristaltic pump during synaptic recordings. All DAMGO response experiments are analyzed using normalization. The frequency of sIPSC events (Hz) following DAMGO perfusion is divided by the frequency of events occurring prior to DAMGO perfusion for each individual cell. Normalized data is represented in bar graphs with normalized values depicted as dots next to the averages. Only one neuron was recorded per coverslip for all DAMGO response experiments.

4.2.8 Statistical analysis

Summary graphs of frequency and amplitude are shown for individual cell lines as well as pooled data of either the four N40 patients (red bars) and three D40 patients (blue bars). Data are depicted as means ± SEM. Numbers of cells/Number of independently generated cultures analyzed are depicted in bars. Statistical significance between N40 and D40 conditions was evaluated by Student's T test (*$p<0.05$, **$p<0.01$, ***$p<0.001$).

4.3 Experimental Results

While MOR desensitization can be observed within seconds to minutes following receptor activation, tolerance at the MOR results from multiple regulatory processes that develop over several hours or days following receptor activation (54). Tolerance results from adaptive mechanisms to restore normal neuronal function following more prolonged and repeated MOR activation and can occur at the cellular, synaptic and network levels. To dissect the role of N40D in modulating the development of tolerance, we pre-exposed N40 and D40 human neurons to 10μM DAMGO for either 1 day or 7 days to induce short-term and long-term tolerance, respectively (4.2.6 DAMGO Pre-Exposures).

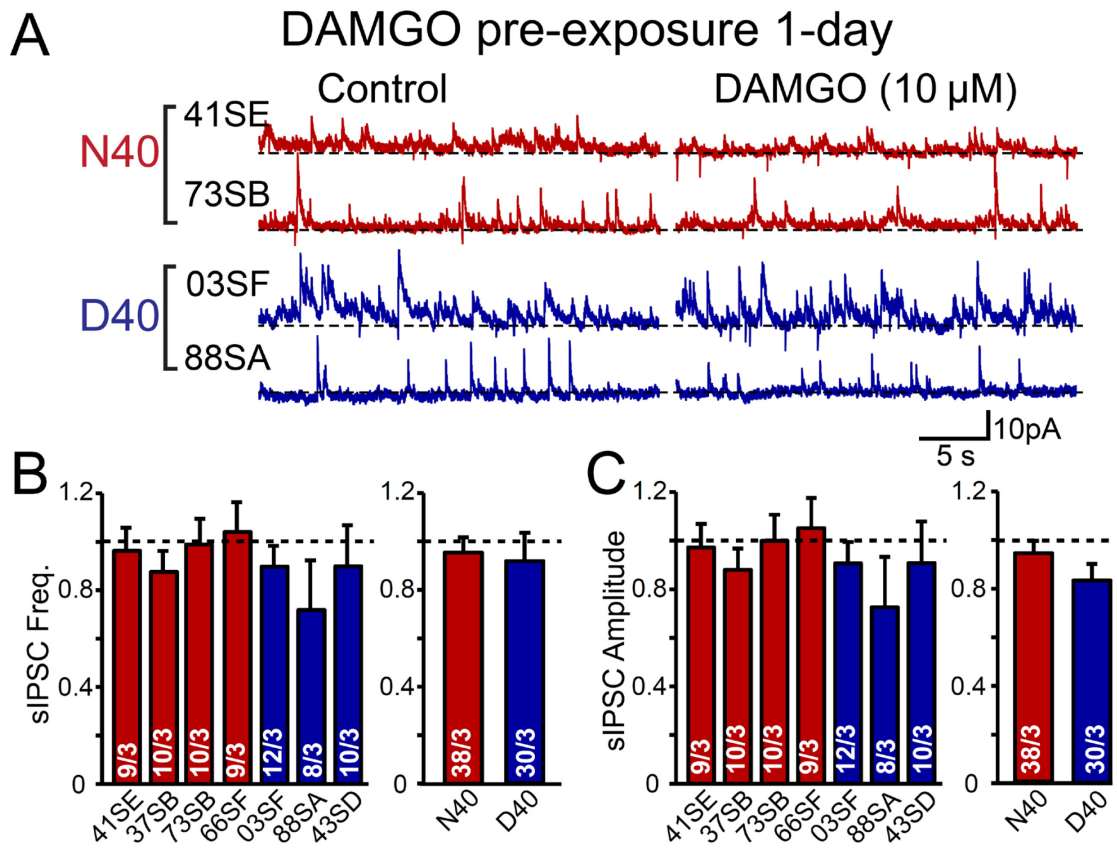

Figure 28: Role of MOR N40D SNP on Short Term Tolerance at the MOR
(A) Sample traces of sIPSCs response to DAMGO in N40 and D40 iN cells pre-exposed to DAMGO for 1 day. **(B)** Quantification of normalized sIPSC frequency following 10μM DAMGO re-application. **(C)** Quantification of normalized sIPSC amplitude following 10μM DAMGO re-application.

Following pre-exposures, we tested the ability of iN cells to respond to DAMGO re-application. Interestingly, we found that just one day of DAMGO pre-exposure abolishes DAMGO sensitivity in human neurons (**Figure 28A**). The suppression of inhibitory synaptic release observed by reduced sIPSC frequency in naïve cultures is no longer seen in either N40 or D40 iN cells after a 1 day pre-exposure paradigm (**Figure 28B**). No effect was seen on sIPSC amplitude in either genotype (**Figure 28C**). These results suggest that both N40 and D40 iN cells are desensitized to re-application of DAMGO following 1 day DAMGO pre-exposure, likely due to MOR internalization.

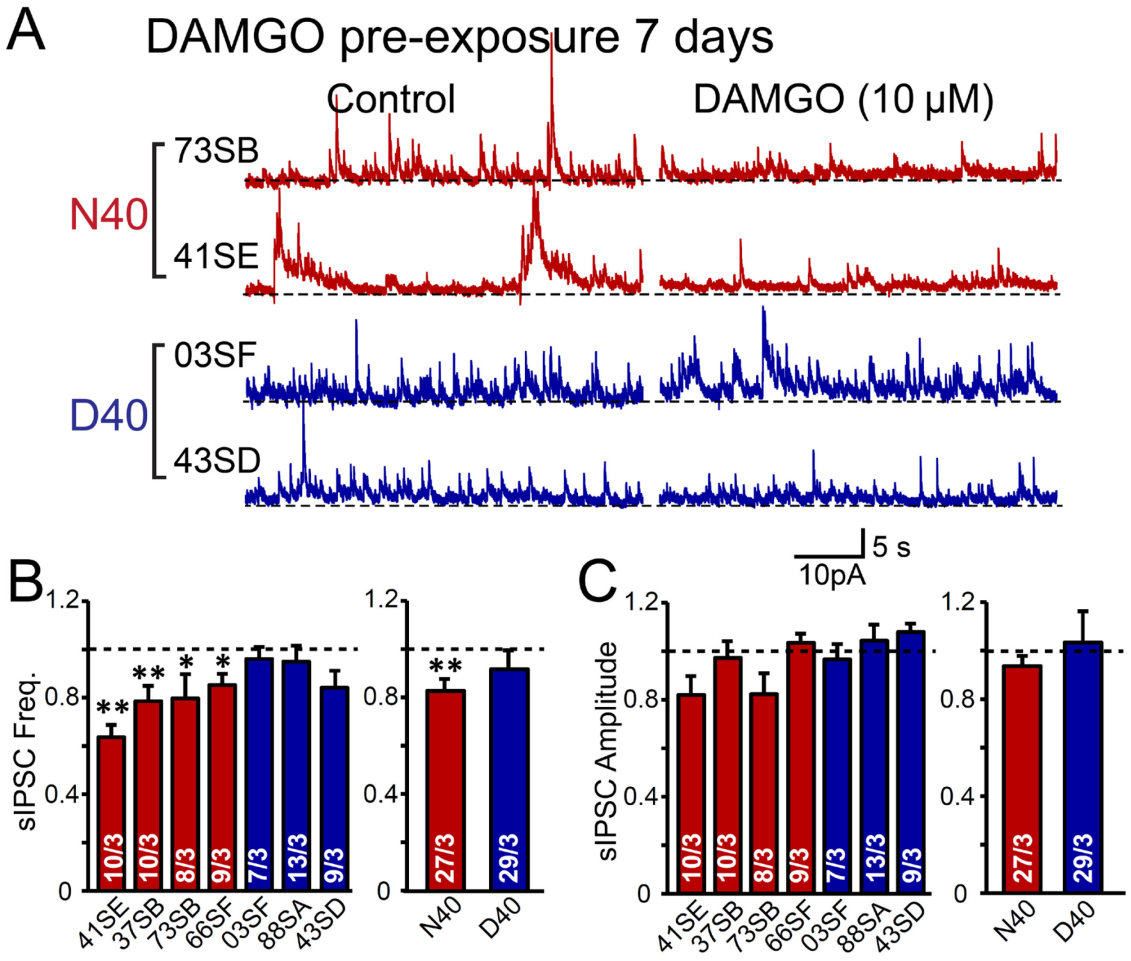

Figure 29: Synaptic suppression in iN cells following 7 day DAMGO pre-exposure. **(A)** Sample traces of sIPSCs response to DAMGO in N40 and D40 iN cells pre-exposed to DAMGO for 7 days. **(B)** Quantification of normalized sIPSC frequency following 10μM DAMGO application. **(C)** Quantification of normalized sIPSC amplitude following 10μM DAMGO application.

Interestingly, after 7-days of DAMGO pre-exposure, N40 iN cells regained partial DAMGO sensitivity to DAMGO re-application (**Figure 29A-B**). This suggests that following MOR de-sensitization, receptors are re-inserted to the cell surface. However, the suppression of inhibitory synaptic release is less robust in 7-day DAMGO pre-exposed iN cells (approx. 30% suppression) compared to iN cells that are naïve to DAMGO treatment seen in Chapter 3 (approx. 50% suppression), which suggests only partial MOR membrane re-insertion (**Figure 29B**Figure 19). In contrast to N40 iN cells, D40 subject derived iN cells pre-exposed to 7 days of DAMGO exhibited no signs of re-sensitization (**Figure 29A**), suggesting negligible MOR membrane re-insertion. No effect was seen on sIPSC amplitude in either genotype (**Figure 29C**). These differential responses to DAMGO following short-term and long-term tolerance suggests that while both N40 and D40 MORs are capable of internalization, D40 expressing iN cells exhibit differential regulation of long-term tolerance at the MOR. These data also suggest that there is a differential effect based on the length of DAMGO pre-exposure.

In order to validate these results observed in the patient derived iN cells, we repeated both the 1 day and 7 day pre-exposure paradigms on the H1ES cell G118 knock-in cell line. Using this more controlled system, we expected to not only be able to recapitulate the effects observed with the patient cell lines, but also potentially elucidate this phenotype with greater resolution. Interestingly, we observed a suppression of sIPSC frequency in N40 iN cells with no observed response in D40 iN cells, similar to what was observed in the patient cell lines. However, this effect was observed after both 1-day and 7-day pre-exposure paradigms, suggesting there is no difference based on the length of DAMGO pre-exposure (**Figure 29A-B, Figure 30A-B**). One-day pre-exposed N40 iN cells also exhibited a statistically significant decrease in sIPSC amplitude (**Figure 30C**) whereas no amplitude effect was observed following 7-day DAMGO pre-exposure (**Figure 31C**).

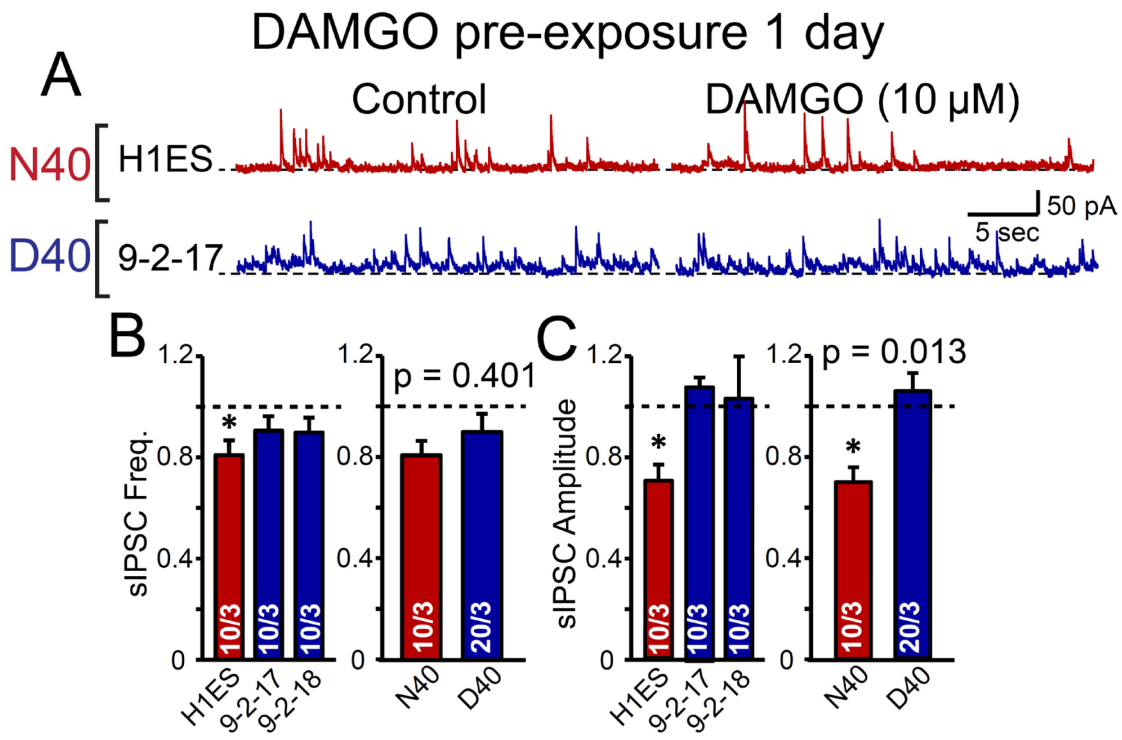

Figure 30: MOR N40DD differentially regulates short term tolerance at the MOR
(A) Sample traces of sIPSCs of N40 and D40 isogenic iN cells pre-exposed to DAMGO for 7 days **(B)** Quantification of sIPSC Frequency following 10μM DAMGO normalized to baseline **(C)** Quantification of sIPSC Amplitude following 10μM DAMGO normalized to baseline.

4.4 Discussion

In Chapter 3, we discussed how N40D affects "acute tolerance" or desensitization which can be observed rapidly in seconds or minutes following agonist binding. Here, we discuss tolerance which occurs upon more prolonged agonist exposure of days and weeks following MOR activation. MOR mediated mechanisms of tolerance can manifest at the level of receptor signaling, neuronal function, or network level changes. Though the specific mechanisms have not been fully resolved, the MOR N40D SNP has potential role in influencing each these processes.

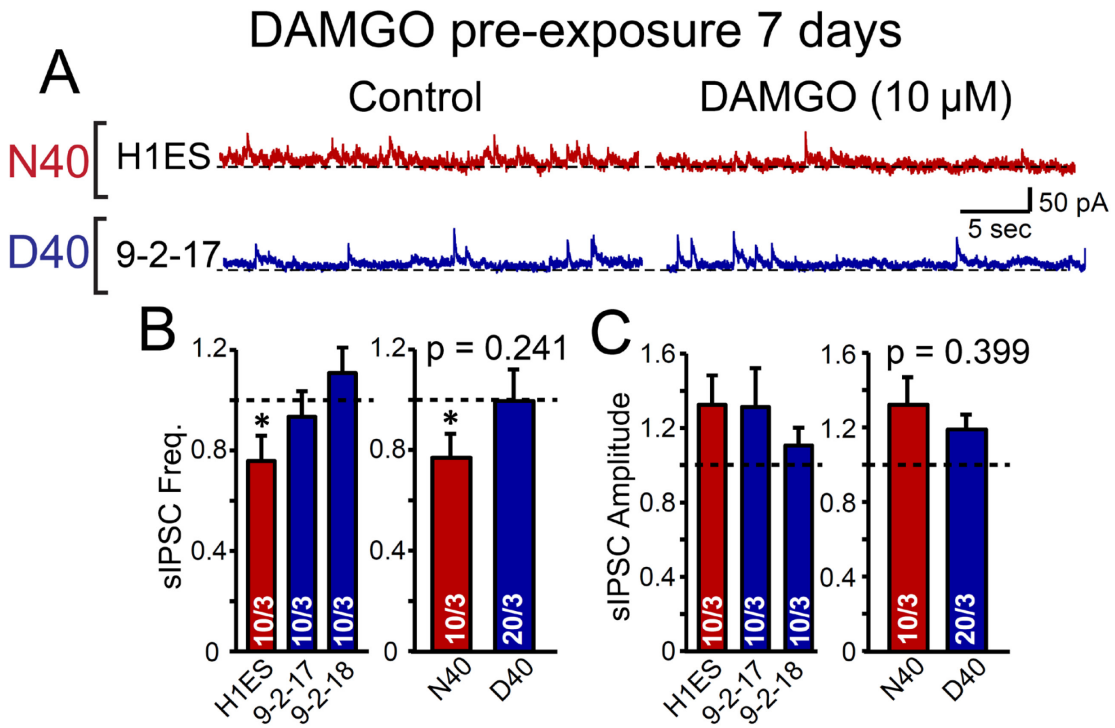

Figure 31: MOR N40D differentially regulates long-term tolerance at the MOR. **(A)** Sample traces of sIPSCs in N40 and D40 isogenic iN cells pre-exposed to DAMGO for 7 days **(B)** Quantification of sIPSC Frequency following 10μM DAMGO normalized to baseline **(C)** Quantification of sIPSC Amplitude following 10μM DAMGO normalized to baseline.

4.4.1 Caveats of Using Human iN Cells to Study MOR Tolerance

Here we used seven patient derived iN cell lines along with one set of isogenic lines to understand the impact of prolonged MOR activation on synaptic regulation. There are multiple reasons for the phenotypic differences observed between the patient iPS cells and isogenic cell lines upon chronic DAMGO exposures. First, the impact of genetic background of the H1ES cell line cannot be discounted and as it potentially influenced the phenotype observed at the synaptic level. Additionally, the lack of difference between 1 and 7 day pre-exposures in the isogenic cell lines suggests that differential effect between N40 and D40 may not be a robust phenotype that is penetrant on all genetic backgrounds. To clarify this issue, future work would need to repeat this experiment in multiple isogenic cell lines, which would determine conclusively whether

the length of DAMGO exposure plays a role in the development of tolerance. Moreover, conducting DAMGO pre-exposures by exposing iN cells for 1 hour, 6 hours, 12 hours, etc. can further elucidate the timescale at which MOR tolerance develops in human cells.

4.4.2 Role of glycosylation on receptor expression and trafficking

It is thought that the N40D SNP destroys N-linked glycosylation at the N-terminus of the MOR, which has been predicted to affect the trafficking and expression of MORs (99, 184). During the migration of MORs from the endoplasmic reticulum (ER) to the trans-Golgi network (TGN), mature G protein coupled receptors (GPCRs) undergo glycosylation and attain a mature status, allowing them to migrate from the TGN to their final destination at the plasma membrane (175). Studies examining the functional role of glycosylation of family A GPCRs have shown that loss of glycosylation affects receptor cell surface expression (185, 186). However, given that we observed enhanced signaling efficacy in D40 iN cells (**Figure 19, Figure 22**), this is unlikely to be the case in N40D function at least in our human iN cells.

Following agonist mediated desensitization and endocytosis, receptors can either be downregulated through degradation, or recycled back to the cell surface. This dynamic cycle of desensitization, endocytosis and resensitization is a rapid way to titrate signaling through the MOR in the presence of opioid exposure (183). Thus, it is possible that glycosylation plays a role in the de-sensitization and re-sensitization processes following DAMGO pre-exposures in which D40 iN cells exhibited reduced signaling efficacy following prolonged treatment. It is possible that D40 MORs exhibit decreased stability and are more prone to degradation compared to N40 MORs. One recent study showed that the half-life of mature D40 MOR was significantly lower than that of N40

MOR (99) suggestive of the idea that N-linked glycans are important for the overall stability of MORs. In fact, this has been shown to be true for other glycoproteins as well (187-189).

Thus, it is likely that D40 MORs exhibit defective receptor recycling, faster protein degradation, or slower protein synthesis after prolonged agonist exposure compared to N40 MORs that might account for the defective re-sensitization of D40 iN cells after the 7-day DAMGO pre-exposure paradigm (**Figure 32**).

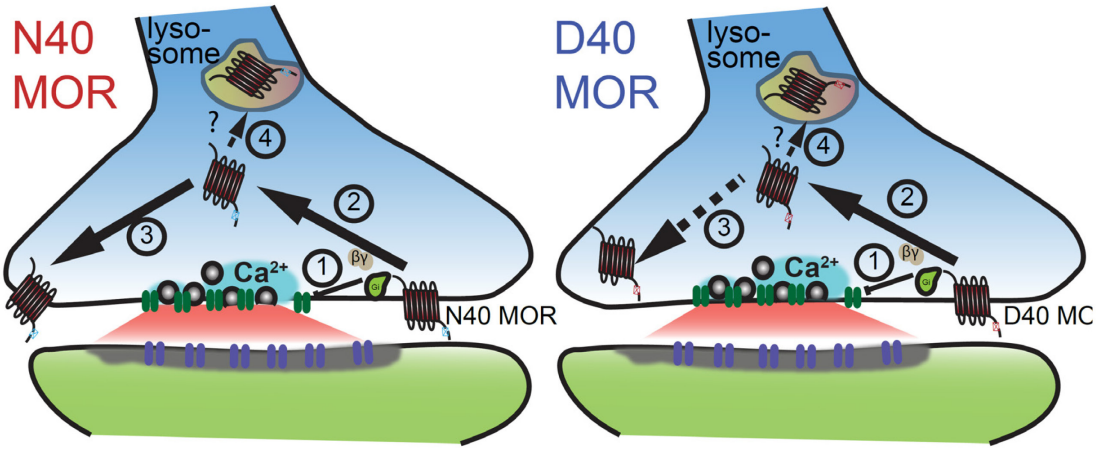

Figure 32: Hypothesized Mechanism Underlying Synaptic Alterations Caused by MOR N40D.
Both MOR N40 and D40 are desensitized following activation by an efficacious agonist. However, it is possible that N40D affects MOR coupling to downstream effectors (1), rates of internalization (2) and re-sensitization (3), or protein stability and degradation (4). *Figure courtesy of Dr. Zhiping Pang.*

4.4.3 Downstream signaling

Moreover, an alternative mechanism to explain the development of long-term tolerance is reduced coupling of MORs to their downstream effectors. This can occur through a loss of coupling to activation of GIRK channels, voltage gated calcium channels, inhibition of adenylate cyclase (AC) or stimulation of MAPK pathways. For

example, GTPγS binding experiments reflect decreased activity following chronic morphine treatment in both the brain (190, 191) and cultured cells (192). MORs have been similarly found to be uncoupled from GIRK channels and voltage gated calcium channels in SH-SY5Y cells (192).

Chronic stimulation of MORs such as in our 1-day and 7-day DAMGO exposure paradigms (**Figure 27**) can lead to a homeostatic adjustment of these downstream signaling pathways, which is a possible explanation for the synaptic consequences of tolerance we observed in MOR expressing neurons. It is unlikely, however, that the MOR N40D SNP would directly affect the functional uncoupling of MORs from downstream effectors given that receptor-effector coupling is primarily mediated through residues in the C-terminal tail of MOR. Whether N40D affects receptor stability and desensitization and re-sensitization processes thus remains unknown.

4.4.4 Synaptic Regulation of MOR N40D in Long-term Tolerance

Long term adaptive processes are involved in mediating the cellular and synaptic effects following long term opioid exposure. Understanding MOR mediated synaptic regulation in long-term tolerance is mechanistically complex due to the differential roles of presynaptic and postsynaptic MOR function. First, repeated and chronic administration of MOR agonists such as morphine are shown to induce considerable tolerance to MOR mediated inhibition of neurotransmitter release (193). These synaptic effects may be mediated by a cAMP dependent regulation (194). Thus, following chronic opioid administration, opioids cause inhibition by a cAMP mediated mechanism. Whether N40D differentially mediates cAMP inhibition and whether this may contribute to the pre-synaptic effect observed upon long-term DAMGO exposure is unknown.

Chapter 5: Conclusions and Future Directions

5.1 Synopsis of Findings

Understanding how functional genetic variation in the human population contributes to addiction behaviors has been particularly challenging. However, recent advances in human stem cell based disease models has allowed for the study of addiction risk associated gene variants in a human neuronal system. Thus, in this study, we have taken advantage of the iPS cell technology to generate patient derived human neurons *in vitro* to understand the molecular and synaptic consequences of the N40D SNP in the MOR as well as the D398N SNP in CHRNA5 (**Appendix**). Additionally, to study the functional consequences of the MOR N40D SNP in a system highly controlled for background genetic variation, we used CRISPR/Cas9 mediated gene targeting to: **(1)** knock-in homozygous D40 alleles into H1ES cells; **(2)** correct the homozygous D40 alleles in 03SF iPS cell subject line into N40 alleles, and thus generated two sets of isogenic stem cell lines for highly controlled mechanistic analyses.

The N40D SNP produced no distinguishable differentiation or maturation abnormalities in the human neurons as they did not alter baseline sIPSC, mIPSC frequency and amplitude or neuronal excitability. Moreover, the SNP did not alter the intrinsic electrical properties of human neurons or their synapse numbers. Instead, the key phenotype of MOR N40D in human neurons was that of differential response to MOR activation by DAMGO, which is a result that was highly consistent between both human subject-derived iN cells as well as gene-targeted isogenic iN cells. We subsequently identified that this increased DAMGO response to spontaneous activity is caused by a more robust inhibition of neuronal excitability and synaptic release in D40 iN cells compared to N40 iN cells. The elucidation of identical phenotypes in inhibitory iN cells carrying different genetic backgrounds strengthens the claim that DAMGO does

indeed cause a more robust inhibition of excitability and synaptic release in D40 expressing neurons. Our study extends to understand the role of the SNP in the regulation of long-term tolerance at the MOR. We found that that N40 and D40 expressing iN cells differentially respond to acute DAMGO administration upon long term pre-exposures to DAMGO. These suggest an alternative role for the MOR in differentially regulating MOR recycling that may contribute to the development of long-term tolerance.

To dissect the functional consequences of CHRNA5 D398N in human neurons, we used iPS cells derived from subjects homozygous for either the D398 or N398 alleles and generated either dopaminergic neurons or glutamatergic neurons to test their functional responses to nicotine. The SNP did not alter the intrinsic electrical properties of human neurons or their capacity to generate action potentials. Moreover, mRNA expression of nicotinic acetylcholine receptor subunits was unchanged between N398 and D398 expressing neurons. These results collectively suggest that the SNP does not affect the differentiation or maturation status of the iN cells. However, we did observe that the CHRNA5 N398 expressing dopaminergic and glutamatergic iN cells exhibited a greater excitatory postsynaptic current response to acute nicotine application. To determine the potential regulatory processes that may contribute to the differential nicotine response between D398 and N398 iN cells, we probed gene expression differences using RNASeq and identified that neuroactive ligand-receptor interactions, calcium signaling, and axon guidance pathways were enriched due to the D398N SNP. Thus, our results suggest that human neurons with the N398 variant would exhibit an enhanced response to initial nicotine exposure, potentially increasing subsequent cravings for nicotine.

Our studies in both MOR N40D and CHRNA5 D398N provide the first experimental evidence detailing the electrophysiological consequences of these SNPs

on receptor activation in their endogenous human neuronal context. This study provides a significant advance in our understanding of the underlying neurobiological mechanisms underlying risk associated SNPs for addiction in human neurons, ultimately giving insight into the functional alterations at the level of the synapse. This studies illustrate the use of patient-specific stem cells to unravel the impact of gene variants in humans and will ultimately help devise patient-specific therapeutic interventions based on genotype for those suffering from drug and alcohol dependence.

5.2 Alternative Considerations

5.2.1 Caveats of Human Stem Cell Disease Modeling

Human iPS cell models serve as an invaluable tool to dissect the molecular and cellular defects underlying neuropsychiatric disorders and serve as powerful platforms for drug screening. However, there are important limitations to this approach which should be considered (172). For example, the iPS cells may retain epigenetic memory from the donor cell type from which they were derived (124). DNA methylation studies in both mouse and human iPS cell lines have shown clear evidence of such an epigenetic memory, which then correlates with differentiation efficiencies in vitro (126, 195). This clearly has multiple consequences on induced neuronal disease modeling, particularly that different cell lines may have different neuronal differentiation capabilities. While this a valid concern, we have been sure to do multiple levels of analyses characterizing both the induced pluripotent stem cells for pluripotency through immunohistochemistry (**Figure 14, Figure 15**). We have also extensively characterized the iN cells, and validated that the neurons exhibit similar differentiation capabilities based on their synapse formation potential, electrophysiological properties, intrinsic membrane

properties, as well as gene expression of markers (**Figure 16, Figure 17, Figure 18**) to ensure we are making valid phenotypic conclusions.

Moreover, chromosomal abnormalities are a key problem in human stem cells passaged enzymatically for multiple passages (196, 197). These may cause abnormalities in phenotypes observed at later iPS cells passages, especially in cells that have undergone gene targeting considering that they are of higher passage number. To circumvent this, we keep iPS cells in culture only for a limited number of passages upon which we thaw a fresh lower passage vial for continued analyses. In spite of these limitations of using human stem cells, we accept these caveats considering that there is no alternative human model for studying neuropsychiatric disease mechanisms.

5.2.2 Using Human iN cells to Model Risk-Associated SNPs for Addiction

The iN cell technology represents a powerful tool for investigating human neuron function in that it is scalable and controllable and much cheaper than studies done directly on human subjects (198). Many disease associated SNPs, including MOR N40D and CHRNA5 D398N, have been characterized in mouse models as well as heterologous expression systems but these studies frequently yield confusing and even contradictory results about the functional consequences of the SNPs. Thus, the power of using human neurons derived from human subject derived iPS cells lies in the ability to study the function of endogenous levels of receptors expressed in a disease relevant cell type. Since our goal was to analyze the functional differences between the major and minor alleles of CHRNA5 and MOR SNPs, we used cell lines derived from subjects that were unrelated to each other. The concern with this strategy is that more subtle phenotypic differences would be diluted by the inherent variability between individual cell lines as well as the background genetic variation of different subjects. Thus, in both the

MOR N40D and CHRNA5 studies, we have tested a reasonable number of human subject-specific iPS cell lines that helps capture sufficient variability while still enabling the isolation of clear phenotypic differences between the major and minor alleles. The MOR N40D study has the added advantage that we generated two sets of isogenic lines that each differ in only a single locus using CRISPR/Cas9 mediated gene targeting.

Despite the attractiveness of using human neurons for understanding opioid receptor signaling in the human brain, there are several caveats that must be considered. For example, the developmental state of neurons differentiated from iPS cells resembles that of fetal brain neurons, making this a problem to model adult disorders such as addiction (199). There are, however, new technologies aimed to mimic cellular maturation and aging which can be useful to study diseases that emerge later in life (200). Moreover, current protocols for generating neuronal subtypes typically yield a heterogeneous population of neurons, which may reveal varying phenotypes for a given disease (170, 201). For clinical as well as disease modeling purposes, it would be important to generate iN cells with region-specificity and neurotransmitter-specificity. To study MOR N40D, we have used transcription factors Ascl1 and Dlx2 to generate iN cells of inhibitory neuronal subtype, which are a mixed population of calbindin, calretinin, and parvalbumin neurons (170). On the other hand, to understand other addiction risk associated SNPs such as CHRNA5 D398N, we have differentiated iPS cells into midbrain dopamine or glutamatergic neurons and tested their functional responses to nicotine (**Appendix**). To mimic the midbrain dopaminergic neuronal induction, we used a previously published small molecule based dual SMAD inhibition protocol to generate midbrain-like dopaminergic neurons (202). Greater than 75% of the MAP2 and TUJ1 positive neurons also express TH, indicative of mature dopamine neurons; however, dual SMAD cultures contained a small population of serotonergic (5-HT positive) as well as inhibitory (GAD6 positive) neurons. While the neurons we generated using either

lentivirus mediated overexpression or small molecule differentiation are of similar maturation and differentiation status, their heterogeneous subtypes will add unnecessary complexity to the isolation of specific disease phenotypes associated with either MOR N40D or CHRNA5 D398N and increase the variability in responses to either DAMGO or nicotine that we observe from electrophysiological experiments.

Another key caveat is that the neurons we generate are cultured as a monolayer *in vitro*, and do not fully recapitulate the network connectivity found in a 3D environment of the brain. In fact, most neuropsychiatric disorders such as addiction manifest as circuit level changes in neural function (6). To recapitulate an *in vivo* environment, we co-culture mouse glial cells along with the iN cells because they are important for long term survival and synaptogenesis (203). In order to study circuit level changes of MOR N40D, it would be optimal to use co-culture systems with GABAergic and Dopaminergic neuronal subtypes or 3-dimensional organoids which would recapitulate circuit level interactions (164, 204). Regardless of these key considerations, we believe these limitations are acceptable caveats considering the fact that human iN cells are currently the most sophisticated approach we have to understand physiological and pathological processes of human disease-specific SNPs such as MOR N40D or CHRNA5 D398N in a human neuronal model system.

5.2.3 Agonist Specificity of MOR Function

The MOR is activated by numerous endogenous opioid peptides as well as synthetic opiates. Thus, the MOR exhibits functional selectivity or biased agonism, which is the phenomenon whereby different ligands can stabilize slightly different conformational states of the receptor thereby resulting in differential activation of cell signaling pathways within an identical cellular background (58). For example, some

opioid ligands such as etorphine can reduce receptor reserve by receptor internalization and downregulation (182) whereas the alkaloid agonists fentanyl and methadone cause only partial internalization and only when present at high concentrations (61). Morphine, on the other hand, induces only weak desensitization and little to no endocytosis despite its efficacy in mediated G-protein activation (54). Other studies have even reported that morphine induced internalization occurs in dendrites but not somas of NAc neurons, suggesting regulatory mechanisms differ based on neuronal compartment (205). One key caveat is whether the differential regulatory mechanisms we observed in human iN cells due to the MOR N40D SNP can be extrapolated to endogenous ligands β-endorphin or exogenously administered morphine. Thus, the differential regulatory mechanisms induced by MOR N40D SNP, whether it be the acute response to MOR activation or the effects of long-term tolerance at the MOR, may be ligand dependent. Thus, future experiments would necessitate an analysis of MOR mediated synaptic function using an array of multiple ligands of different signaling efficacies and functions.

5.3 Future Directions

Alcoholism and drug abuse in general have a substantial genetic component. In fact, single amino acid substitutions have been shown to modify the responsiveness of individuals to alcohol and influence drug abuse in humans (2, 41, 79, 91, 206-211). The past several years have yielded tremendous advances in large scale SNP genotyping technologies such as Genome Wide Association Studies (GWAS) that have allowed for identification of risk associated genetic variants that contribute to addiction (122). In spite of this, our understanding of the cellular and molecular mechanisms underlying candidate genetic variants for alcoholism remains poor.

Moreover, we also now understand that addiction is highly polygenic with each individual SNP contributing in a small but additive fashion to addiction vulnerability (122).

Thus, isolating distinct phenotypes from individual genetic variants may be only a precursor to understanding the genetic influences of alcoholism. Studies examining the mechanisms underlying candidate genes implicated in alcoholism have largely examined GABAergic system genes (such as GABRA3) (212). Few studies have examined the interactive effects of GABAergic genes that have been implicated in alcoholism and MOR N40D which also has strong associations to alcohol vulnerability. Given that the primary target of alcohol and other addictive drugs is the synapse, studies examining the interactive role of MOR signaling and alcohol on synaptic transmission are required.

Furthermore, we must also consider the comorbidity of nicotine addiction and alcohol use disorders. Concurrent alcohol and tobacco use may be due to multiple mechanisms that include genes involved in regulating different brain chemical systems. Our work understanding the mechanisms of risk associated SNPs in CHRNA5 and the OPRM1 uniquely identifies synaptic and cellular changes that may underlie the the comorbid disorders. A key next step would be in understanding the combinatorial mechanisms of CHRNA5 D398N and MOR N40D as well as other prevalent genetic variants that may lead to predisposition for substance abuse. Moreover, investigating mechanisms of cross-tolerance and cross-sensitization to both alcohol and nicotine and how functional genetic variation in genes may influence these processes will help to understand the development or maintenance of addiction behaviors. Future studies will also require more system and circuit level analyses of the interactive effects of multiple genetic variants to thoroughly dissect how genetic predisposition may influence dopaminergic signaling in the brain and how this may contribute to the development of addiction. This will more definitively resolve how genotypic heterogeneity can lead to phenotypic diversity in the human population and will lead to a broader understanding of its role in contributing to alcoholism and addiction vulnerability.

References

1. Ramchandani VA, Umhau J, Pavon FJ, Ruiz-Velasco V, Margas W, Sun H, Damadzic R, Eskay R, Schoor M, Thorsell A, Schwandt ML, Sommer WH, George DT, Parsons LH, Herscovitch P, Hommer D, Heilig M. A genetic determinant of the striatal dopamine response to alcohol in men. Mol Psychiatry. 2011;16(8):809-17. doi: 10.1038/mp.2010.56. PubMed PMID: 20479755; PMCID: PMC2925052.
2. Berrettini W. Opioid pharmacogenetics of alcohol addiction. Cold Spring Harb Perspect Med. 2013;3(7). doi: 10.1101/cshperspect.a012203. PubMed PMID: 23729643; PMCID: PMC3685876.
3. Knapman A, Connor M. Cellular signalling of non-synonymous single-nucleotide polymorphisms of the human mu-opioid receptor (OPRM1). Br J Pharmacol. 2015;172(2):349-63. doi: 10.1111/bph.12644. PubMed PMID: 24527749; PMCID: PMC4292952.
4. Nestler EJ. Is there a common molecular pathway for addiction? Nat Neurosci. 2005;8(11):1445-9. doi: 10.1038/nn1578. PubMed PMID: 16251986.
5. Robinton DA, Daley GQ. The promise of induced pluripotent stem cells in research and therapy. Nature. 2012;481(7381):295-305. doi: 10.1038/nature10761. PubMed PMID: 22258608; PMCID: PMC3652331.
6. Kauer JA, Malenka RC. Synaptic plasticity and addiction. Nat Rev Neurosci. 2007;8(11):844-58. doi: 10.1038/nrn2234. PubMed PMID: 17948030.
7. Goldman D, Oroszi G, Ducci F. The genetics of addictions: uncovering the genes. Nat Rev Genet. 2005;6(7):521-32. doi: 10.1038/nrg1635. PubMed PMID: 15995696.
8. Joffe ME, Grueter CA, Grueter BA. Biological substrates of addiction. Wiley Interdiscip Rev Cogn Sci. 2014;5(2):151-71. doi: 10.1002/wcs.1273. PubMed PMID: 24999377; PMCID: PMC4078878.
9. Koob GF, Le Moal M. Drug addiction, dysregulation of reward, and allostasis. Neuropsychopharmacology. 2001;24(2):97-129. doi: 10.1016/S0893-133X(00)00195-0. PubMed PMID: 11120394.
10. Di Chiara G, Bassareo V, Fenu S, De Luca MA, Spina L, Cadoni C, Acquas E, Carboni E, Valentini V, Lecca D. Dopamine and drug addiction: the nucleus accumbens shell connection. Neuropharmacology. 2004;47 Suppl 1:227-41. doi: 10.1016/j.neuropharm.2004.06.032. PubMed PMID: 15464140.
11. Nestler EJ. Molecular basis of long-term plasticity underlying addiction. Nat Rev Neurosci. 2001;2(2):119-28. doi: 10.1038/35053570. PubMed PMID: 11252991.
12. Volkow ND, Fowler JS, Wang GJ, Swanson JM. Dopamine in drug abuse and addiction: results from imaging studies and treatment implications. Mol Psychiatry. 2004;9(6):557-69. doi: 10.1038/sj.mp.4001507. PubMed PMID: 15098002.
13. Wise RA. Dopamine, learning and motivation. Nat Rev Neurosci. 2004;5(6):483-94. doi: 10.1038/nrn1406. PubMed PMID: 15152198.
14. Hyman SE, Malenka RC, Nestler EJ. Neural mechanisms of addiction: the role of reward-related learning and memory. Annu Rev Neurosci. 2006;29:565-98. doi: 10.1146/annurev.neuro.29.051605.113009. PubMed PMID: 16776597.
15. Garzon M, Pickel VM. Ultrastructural localization of enkephalin and mu-opioid receptors in the rat ventral tegmental area. Neuroscience. 2002;114(2):461-74. PubMed PMID: 12204215.
16. Johnson SW, North RA. Opioids excite dopamine neurons by hyperpolarization of local interneurons. J Neurosci. 1992;12(2):483-8. PubMed PMID: 1346804.

17. Spanagel R, Herz A, Shippenberg TS. Opposing tonically active endogenous opioid systems modulate the mesolimbic dopaminergic pathway. Proc Natl Acad Sci U S A. 1992;89(6):2046-50. PubMed PMID: 1347943; PMCID: PMC48593.
18. Bergevin A, Girardot D, Bourque MJ, Trudeau LE. Presynaptic mu-opioid receptors regulate a late step of the secretory process in rat ventral tegmental area GABAergic neurons. Neuropharmacology. 2002;42(8):1065-78. PubMed PMID: 12128008.
19. Manzoni OJ, Williams JT. Presynaptic regulation of glutamate release in the ventral tegmental area during morphine withdrawal. J Neurosci. 1999;19(15):6629-36. PubMed PMID: 10414991.
20. Tanda G, Di Chiara G. A dopamine-mu1 opioid link in the rat ventral tegmentum shared by palatable food (Fonzies) and non-psychostimulant drugs of abuse. Eur J Neurosci. 1998;10(3):1179-87. PubMed PMID: 9753186.
21. Di Chiara G. Nucleus accumbens shell and core dopamine: differential role in behavior and addiction. Behav Brain Res. 2002;137(1-2):75-114. PubMed PMID: 12445717.
22. Paladini CA, Roeper J. Generating bursts (and pauses) in the dopamine midbrain neurons. Neuroscience. 2014;282:109-21. doi: 10.1016/j.neuroscience.2014.07.032. PubMed PMID: 25073045.
23. Volkow ND, Morales M. The Brain on Drugs: From Reward to Addiction. Cell. 2015;162(4):712-25. doi: 10.1016/j.cell.2015.07.046. PubMed PMID: 26276628.
24. Everitt BJ, Robbins TW. From the ventral to the dorsal striatum: devolving views of their roles in drug addiction. Neurosci Biobehav Rev. 2013;37(9 Pt A):1946-54. doi: 10.1016/j.neubiorev.2013.02.010. PubMed PMID: 23438892.
25. Black KJ, Koller JM, Campbell MC, Gusnard DA, Bandak SI. Quantification of indirect pathway inhibition by the adenosine A2a antagonist SYN115 in Parkinson disease. J Neurosci. 2010;30(48):16284-92. doi: 10.1523/JNEUROSCI.2590-10.2010. PubMed PMID: 21123574; PMCID: PMC3008651.
26. Volkow ND, Baler RD. NOW vs LATER brain circuits: implications for obesity and addiction. Trends Neurosci. 2015;38(6):345-52. doi: 10.1016/j.tins.2015.04.002. PubMed PMID: 25959611.
27. Goldstein RZ, Volkow ND. Dysfunction of the prefrontal cortex in addiction: neuroimaging findings and clinical implications. Nat Rev Neurosci. 2011;12(11):652-69. doi: 10.1038/nrn3119. PubMed PMID: 22011681; PMCID: PMC3462342.
28. Alwi ZB. The Use of SNPs in Pharmacogenomics Studies. Malays J Med Sci. 2005;12(2):4-12. PubMed PMID: 22605952; PMCID: PMC3349395.
29. Ramensky V, Bork P, Sunyaev S. Human non-synonymous SNPs: server and survey. Nucleic Acids Res. 2002;30(17):3894-900. PubMed PMID: 12202775; PMCID: PMC137415.
30. Buhler KM, Gine E, Echeverry-Alzate V, Calleja-Conde J, de Fonseca FR, Lopez-Moreno JA. Common single nucleotide variants underlying drug addiction: more than a decade of research. Addict Biol. 2015;20(5):845-71. doi: 10.1111/adb.12204. PubMed PMID: 25603899.
31. Genomes Project C, Auton A, Brooks LD, Durbin RM, Garrison EP, Kang HM, Korbel JO, Marchini JL, McCarthy S, McVean GA, Abecasis GR. A global reference for human genetic variation. Nature. 2015;526(7571):68-74. doi: 10.1038/nature15393. PubMed PMID: 26432245; PMCID: PMC4750478.
32. Welter D, MacArthur J, Morales J, Burdett T, Hall P, Junkins H, Klemm A, Flicek P, Manolio T, Hindorff L, Parkinson H. The NHGRI GWAS Catalog, a curated

resource of SNP-trait associations. Nucleic Acids Res. 2014;42(Database issue):D1001-6. doi: 10.1093/nar/gkt1229. PubMed PMID: 24316577; PMCID: PMC3965119.

33. Bierut LJ, Stitzel JA, Wang JC, Hinrichs AL, Grucza RA, Xuei X, Saccone NL, Saccone SF, Bertelsen S, Fox L, Horton WJ, Breslau N, Budde J, Cloninger CR, Dick DM, Foroud T, Hatsukami D, Hesselbrock V, Johnson EO, Kramer J, Kuperman S, Madden PA, Mayo K, Nurnberger J, Jr., Pomerleau O, Porjesz B, Reyes O, Schuckit M, Swan G, Tischfield JA, Edenberg HJ, Rice JP, Goate AM. Variants in nicotinic receptors and risk for nicotine dependence. Am J Psychiatry. 2008;165(9):1163-71. doi: 10.1176/appi.ajp.2008.07111711. PubMed PMID: 18519524; PMCID: PMC2574742.
34. Saccone SF, Hinrichs AL, Saccone NL, Chase GA, Konvicka K, Madden PA, Breslau N, Johnson EO, Hatsukami D, Pomerleau O, Swan GE, Goate AM, Rutter J, Bertelsen S, Fox L, Fugman D, Martin NG, Montgomery GW, Wang JC, Ballinger DG, Rice JP, Bierut LJ. Cholinergic nicotinic receptor genes implicated in a nicotine dependence association study targeting 348 candidate genes with 3713 SNPs. Hum Mol Genet. 2007;16(1):36-49. doi: 10.1093/hmg/ddl438. PubMed PMID: 17135278; PMCID: PMC2270437.
35. Ramirez-Latorre J, Yu CR, Qu X, Perin F, Karlin A, Role L. Functional contributions of alpha5 subunit to neuronal acetylcholine receptor channels. Nature. 1996;380(6572):347-51. doi: 10.1038/380347a0. PubMed PMID: 8598930.
36. Fowler CD, Tuesta L, Kenny PJ. Role of alpha5* nicotinic acetylcholine receptors in the effects of acute and chronic nicotine treatment on brain reward function in mice. Psychopharmacology (Berl). 2013. Epub 2013/08/21. doi: 10.1007/s00213-013-3235-1. PubMed PMID: 23958943.
37. Sciaccaluga M, Moriconi C, Martinello K, Catalano M, Bermudez I, Stitzel JA, Maskos U, Fucile S. Crucial role of nicotinic alpha5 subunit variants for Ca2+ fluxes in ventral midbrain neurons. FASEB J. 2015;29(8):3389-98. doi: 10.1096/fj.14-268102. PubMed PMID: 25911614; PMCID: PMC4511205.
38. Miranda R, Ray L, Justus A, Meyerson LA, Knopik VS, McGeary J, Monti PM. Initial evidence of an association between OPRM1 and adolescent alcohol misuse. Alcohol Clin Exp Res. 2010;34(1):112-22. doi: 10.1111/j.1530-0277.2009.01073.x. PubMed PMID: 19860800; PMCID: PMC3691683.
39. Koller G, Zill P, Rujescu D, Ridinger M, Pogarell O, Fehr C, Wodarz N, Bondy B, Soyka M, Preuss UW. Possible association between OPRM1 genetic variance at the 118 locus and alcohol dependence in a large treatment sample: relationship to alcohol dependence symptoms. Alcoholism, clinical and experimental research. 2012;36(7):1230-6. doi: 10.1111/j.1530-0277.2011.01714.x. PubMed PMID: 22309038.
40. Enoch MA. Genetic influences on the development of alcoholism. Curr Psychiatry Rep. 2013;15(11):412. doi: 10.1007/s11920-013-0412-1. PubMed PMID: 24091936; PMCID: PMC4159132.
41. Enoch MA. Genetic influences on response to alcohol and response to pharmacotherapies for alcoholism. Pharmacology, biochemistry, and behavior. 2013. doi: 10.1016/j.pbb.2013.11.001. PubMed PMID: 24220019.
42. Ehlers CL, Lind PA, Wilhelmsen KC. Association between single nucleotide polymorphisms in the mu opioid receptor gene (OPRM1) and self-reported responses to alcohol in American Indians. BMC Med Genet. 2008;9:35. doi: 10.1186/1471-2350-9-35. PubMed PMID: 18433502; PMCID: PMC2386778.

43. Ray LA, Hutchison KE. A polymorphism of the mu-opioid receptor gene (OPRM1) and sensitivity to the effects of alcohol in humans. Alcohol Clin Exp Res. 2004;28(12):1789-95. PubMed PMID: 15608594.
44. Kreek MJ, Bart G, Lilly C, LaForge KS, Nielsen DA. Pharmacogenetics and human molecular genetics of opiate and cocaine addictions and their treatments. Pharmacol Rev. 2005;57(1):1-26. doi: 10.1124/pr.57.1.1. PubMed PMID: 15734726.
45. Gardon O, Faget L, Chu Sin Chung P, Matifas A, Massotte D, Kieffer BL. Expression of mu opioid receptor in dorsal diencephalic conduction system: new insights for the medial habenula. Neuroscience. 2014;277:595-609. doi: 10.1016/j.neuroscience.2014.07.053. PubMed PMID: 25086313; PMCID: PMC4164589.
46. Al-Hasani R, Bruchas MR. Molecular mechanisms of opioid receptor-dependent signaling and behavior. Anesthesiology. 2011;115(6):1363-81. doi: 10.1097/ALN.0b013e318238bba6. PubMed PMID: 22020140; PMCID: PMC3698859.
47. Jordan B, Devi LA. Molecular mechanisms of opioid receptor signal transduction. Br J Anaesth. 1998;81(1):12-9. PubMed PMID: 9771268.
48. Kieffer BL, Gaveriaux-Ruff C. Exploring the opioid system by gene knockout. Prog Neurobiol. 2002;66(5):285-306. PubMed PMID: 12015197.
49. Mitchell JM, O'Neil JP, Janabi M, Marks SM, Jagust WJ, Fields HL. Alcohol consumption induces endogenous opioid release in the human orbitofrontal cortex and nucleus accumbens. Sci Transl Med. 2012;4(116):116ra6. doi: 10.1126/scitranslmed.3002902. PubMed PMID: 22238334.
50. Contet C, Kieffer BL, Befort K. Mu opioid receptor: a gateway to drug addiction. Curr Opin Neurobiol. 2004;14(3):370-8. doi: 10.1016/j.conb.2004.05.005. PubMed PMID: 15194118.
51. Gerrits MA, Lesscher HB, van Ree JM. Drug dependence and the endogenous opioid system. Eur Neuropsychopharmacol. 2003;13(6):424-34. PubMed PMID: 14636958.
52. Manglik A, Kruse AC, Kobilka TS, Thian FS, Mathiesen JM, Sunahara RK, Pardo L, Weis WI, Kobilka BK, Granier S. Crystal structure of the micro-opioid receptor bound to a morphinan antagonist. Nature. 2012;485(7398):321-6. doi: 10.1038/nature10954. PubMed PMID: 22437502; PMCID: PMC3523197.
53. Serohijos AW, Yin S, Ding F, Gauthier J, Gibson DG, Maixner W, Dokholyan NV, Diatchenko L. Structural basis for mu-opioid receptor binding and activation. Structure. 2011;19(11):1683-90. doi: 10.1016/j.str.2011.08.003. PubMed PMID: 22078567; PMCID: PMC3217204.
54. Williams JT, Ingram SL, Henderson G, Chavkin C, von Zastrow M, Schulz S, Koch T, Evans CJ, Christie MJ. Regulation of mu-opioid receptors: desensitization, phosphorylation, internalization, and tolerance. Pharmacol Rev. 2013;65(1):223-54. doi: 10.1124/pr.112.005942. PubMed PMID: 23321159; PMCID: PMC3565916.
55. Connor M, Christie MD. Opioid receptor signalling mechanisms. Clin Exp Pharmacol Physiol. 1999;26(7):493-9. PubMed PMID: 10405772.
56. Alexander SP, Benson HE, Faccenda E, Pawson AJ, Sharman JL, Spedding M, Peters JA, Harmar AJ, Collaborators C. The Concise Guide to PHARMACOLOGY 2013/14: G protein-coupled receptors. Br J Pharmacol. 2013;170(8):1459-581. doi: 10.1111/bph.12445. PubMed PMID: 24517644; PMCID: PMC3892287.

57. Kenakin T. Functional selectivity and biased receptor signaling. J Pharmacol Exp Ther. 2011;336(2):296-302. doi: 10.1124/jpet.110.173948. PubMed PMID: 21030484.
58. Thompson GL, Kelly E, Christopoulos A, Canals M. Novel GPCR paradigms at the mu-opioid receptor. Br J Pharmacol. 2015;172(2):287-96. doi: 10.1111/bph.12600. PubMed PMID: 24460711; PMCID: PMC4292946.
59. Schmid CL, Kennedy NM, Ross NC, Lovell KM, Yue Z, Morgenweck J, Cameron MD, Bannister TD, Bohn LM. Bias Factor and Therapeutic Window Correlate to Predict Safer Opioid Analgesics. Cell. 2017;171(5):1165-75 e13. doi: 10.1016/j.cell.2017.10.035. PubMed PMID: 29149605; PMCID: PMC5731250.
60. Arden JR, Segredo V, Wang Z, Lameh J, Sadee W. Phosphorylation and agonist-specific intracellular trafficking of an epitope-tagged mu-opioid receptor expressed in HEK 293 cells. J Neurochem. 1995;65(4):1636-45. PubMed PMID: 7561859.
61. Keith DE, Anton B, Murray SR, Zaki PA, Chu PC, Lissin DV, Monteillet-Agius G, Stewart PL, Evans CJ, von Zastrow M. mu-Opioid receptor internalization: opiate drugs have differential effects on a conserved endocytic mechanism in vitro and in the mammalian brain. Mol Pharmacol. 1998;53(3):377-84. PubMed PMID: 9495801.
62. Sternini C, Spann M, Anton B, Keith DE, Jr., Bunnett NW, von Zastrow M, Evans C, Brecha NC. Agonist-selective endocytosis of mu opioid receptor by neurons in vivo. Proc Natl Acad Sci U S A. 1996;93(17):9241-6. PubMed PMID: 8799185; PMCID: PMC38626.
63. Rodriguez-Munoz M, de la Torre-Madrid E, Sanchez-Blazquez P, Garzon J. Morphine induces endocytosis of neuronal mu-opioid receptors through the sustained transfer of Galpha subunits to RGSZ2 proteins. Mol Pain. 2007;3:19. doi: 10.1186/1744-8069-3-19. PubMed PMID: 17634133; PMCID: PMC1947952.
64. Kenakin T, Watson C, Muniz-Medina V, Christopoulos A, Novick S. A simple method for quantifying functional selectivity and agonist bias. ACS Chem Neurosci. 2012;3(3):193-203. doi: 10.1021/cn200111m. PubMed PMID: 22860188; PMCID: PMC3369801.
65. Bohn LM, Lefkowitz RJ, Gainetdinov RR, Peppel K, Caron MG, Lin FT. Enhanced morphine analgesia in mice lacking beta-arrestin 2. Science. 1999;286(5449):2495-8. PubMed PMID: 10617462.
66. Raehal KM, Walker JK, Bohn LM. Morphine side effects in beta-arrestin 2 knockout mice. J Pharmacol Exp Ther. 2005;314(3):1195-201. doi: 10.1124/jpet.105.087254. PubMed PMID: 15917400.
67. Chakrabarti S, Yang W, Law PY, Loh HH. The mu-opioid receptor down-regulates differently from the delta-opioid receptor: requirement of a high affinity receptor/G protein complex formation. Mol Pharmacol. 1997;52(1):105-13. PubMed PMID: 9224819.
68. Chan KW, Duttory A, Yoburn BC. Magnitude of tolerance to fentanyl is independent of mu-opioid receptor density. Eur J Pharmacol. 1997;319(2-3):225-8. PubMed PMID: 9042594.
69. Nishino K, Su YF, Wong CS, Watkins WD, Chang KJ. Dissociation of mu opioid tolerance from receptor down-regulation in rat spinal cord. J Pharmacol Exp Ther. 1990;253(1):67-72. PubMed PMID: 2158554.
70. Yoburn BC, Billings B, Duttaroy A. Opioid receptor regulation in mice. J Pharmacol Exp Ther. 1993;265(1):314-20. PubMed PMID: 8386239.
71. Koch T, Schulz S, Schroder H, Wolf R, Raulf E, Hollt V. Carboxyl-terminal splicing of the rat mu opioid receptor modulates agonist-mediated internalization

and receptor resensitization. J Biol Chem. 1998;273(22):13652-7. PubMed PMID: 9593704.

72. Walwyn WM, Keith DE, Jr., Wei W, Tan AM, Xie CW, Evans CJ, Kieffer BL, Maidment NT. Functional coupling, desensitization and internalization of virally expressed mu opioid receptors in cultured dorsal root ganglion neurons from mu opioid receptor knockout mice. Neuroscience. 2004;123(1):111-21. PubMed PMID: 14667446.
73. Finn AK, Whistler JL. Endocytosis of the mu opioid receptor reduces tolerance and a cellular hallmark of opiate withdrawal. Neuron. 2001;32(5):829-39. PubMed PMID: 11738029.
74. He L, Fong J, von Zastrow M, Whistler JL. Regulation of opioid receptor trafficking and morphine tolerance by receptor oligomerization. Cell. 2002;108(2):271-82. PubMed PMID: 11832216.
75. Hoehe MR, Kopke K, Wendel B, Rohde K, Flachmeier C, Kidd KK, Berrettini WH, Church GM. Sequence variability and candidate gene analysis in complex disease: association of mu opioid receptor gene variation with substance dependence. Hum Mol Genet. 2000;9(19):2895-908. PubMed PMID: 11092766.
76. Drewes AM, Jensen RD, Nielsen LM, Droney J, Christrup LL, Arendt-Nielsen L, Riley J, Dahan A. Differences between opioids: pharmacological, experimental, clinical and economical perspectives. Br J Clin Pharmacol. 2013;75(1):60-78. doi: 10.1111/j.1365-2125.2012.04317.x. PubMed PMID: 22554450; PMCID: PMC3555047.
77. Mague SD, Blendy JA. OPRM1 SNP (A118G): involvement in disease development, treatment response, and animal models. Drug Alcohol Depend. 2010;108(3):172-82. doi: 10.1016/j.drugalcdep.2009.12.016. PubMed PMID: 20074870; PMCID: PMC2887703.
78. Enoch MA. Genetic influences on response to alcohol and response to pharmacotherapies for alcoholism. Pharmacol Biochem Behav. 2014;123:17-24. doi: 10.1016/j.pbb.2013.11.001. PubMed PMID: 24220019; PMCID: PMC4016188.
79. Bart G, Kreek MJ, Ott J, LaForge KS, Proudnikov D, Pollak L, Heilig M. Increased attributable risk related to a functional mu-opioid receptor gene polymorphism in association with alcohol dependence in central Sweden. Neuropsychopharmacology. 2005;30(2):417-22. doi: 10.1038/sj.npp.1300598. PubMed PMID: 15525999.
80. Nishizawa D, Han W, Hasegawa J, Ishida T, Numata Y, Sato T, Kawai A, Ikeda K. Association of mu-opioid receptor gene polymorphism A118G with alcohol dependence in a Japanese population. Neuropsychobiology. 2006;53(3):137-41. doi: 10.1159/000093099. PubMed PMID: 16679777.
81. Kim SG, Kim CM, Kang DH, Kim YJ, Byun WT, Kim SY, Park JM, Kim MJ, Oslin DW. Association of functional opioid receptor genotypes with alcohol dependence in Koreans. Alcohol Clin Exp Res. 2004;28(7):986-90. PubMed PMID: 15252283.
82. Rommelspacher H, Smolka M, Schmidt LG, Samochowiec J, Hoehe MR. Genetic analysis of the mu-opioid receptor in alcohol-dependent individuals. Alcohol. 2001;24(2):129-35. PubMed PMID: 11522434.
83. Perkins KA, Lerman C, Grottenthaler A, Ciccocioppo MM, Milanak M, Conklin CA, Bergen AW, Benowitz NL. Dopamine and opioid gene variants are associated with increased smoking reward and reinforcement owing to negative mood. Behav Pharmacol. 2008;19(5-6):641-9. doi:

10.1097/FBP.0b013e32830c367c. PubMed PMID: 18690118; PMCID: PMC2717609.

84. Lerman C, Wileyto EP, Patterson F, Rukstalis M, Audrain-McGovern J, Restine S, Shields PG, Kaufmann V, Redden D, Benowitz N, Berrettini WH. The functional mu opioid receptor (OPRM1) Asn40Asp variant predicts short-term response to nicotine replacement therapy in a clinical trial. Pharmacogenomics J. 2004;4(3):184-92. doi: 10.1038/sj.tpj.6500238. PubMed PMID: 15007373.
85. Ray R, Jepson C, Patterson F, Strasser A, Rukstalis M, Perkins K, Lynch KG, O'Malley S, Berrettini WH, Lerman C. Association of OPRM1 A118G variant with the relative reinforcing value of nicotine. Psychopharmacology (Berl). 2006;188(3):355-63. doi: 10.1007/s00213-006-0504-2. PubMed PMID: 16960700.
86. Kim SG, Kim CM, Choi SW, Jae YM, Lee HG, Son BK, Kim JG, Choi YS, Kim HO, Kim SY, Oslin DW. A micro opioid receptor gene polymorphism (A118G) and naltrexone treatment response in adherent Korean alcohol-dependent patients. Psychopharmacology (Berl). 2009;201(4):611-8. doi: 10.1007/s00213-008-1330-5. PubMed PMID: 18795264.
87. Zhang H, Luo X, Kranzler HR, Lappalainen J, Yang BZ, Krupitsky E, Zvartau E, Gelernter J. Association between two mu-opioid receptor gene (OPRM1) haplotype blocks and drug or alcohol dependence. Hum Mol Genet. 2006;15(6):807-19. doi: 10.1093/hmg/ddl024. PubMed PMID: 16476706; PMCID: PMC3164878.
88. Town T, Abdullah L, Crawford F, Schinka J, Ordorica PI, Francis E, Hughes P, Duara R, Mullan M. Association of a functional mu-opioid receptor allele (+118A) with alcohol dependency. Am J Med Genet. 1999;88(5):458-61. PubMed PMID: 10490697.
89. Schinka JA, Town T, Abdullah L, Crawford FC, Ordorica PI, Francis E, Hughes P, Graves AB, Mortimer JA, Mullan M. A functional polymorphism within the mu-opioid receptor gene and risk for abuse of alcohol and other substances. Mol Psychiatry. 2002;7(2):224-8. doi: 10.1038/sj.mp.4000951. PubMed PMID: 11840318.
90. Arias A, Feinn R, Kranzler HR. Association of an Asn40Asp (A118G) polymorphism in the mu-opioid receptor gene with substance dependence: a meta-analysis. Drug Alcohol Depend. 2006;83(3):262-8. doi: 10.1016/j.drugalcdep.2005.11.024. PubMed PMID: 16387451.
91. Chen D, Liu L, Xiao Y, Peng Y, Yang C, Wang Z. Ethnic-specific meta-analyses of association between the OPRM1 A118G polymorphism and alcohol dependence among Asians and Caucasians. Drug and alcohol dependence. 2012;123(1-3):1-6. doi: 10.1016/j.drugalcdep.2011.10.012. PubMed PMID: 22071118.
92. Ersboll AK, Ersboll BK. Epidemiological studies based on small sample sizes--a statistician's point of view. Acta Vet Scand Suppl. 2003;98:127-40. PubMed PMID: 15259786.
93. Enoch MA. The influence of gene-environment interactions on the development of alcoholism and drug dependence. Curr Psychiatry Rep. 2012;14(2):150-8. doi: 10.1007/s11920-011-0252-9. PubMed PMID: 22367454; PMCID: PMC3470472.
94. Bilbao A, Robinson JE, Heilig M, Malanga CJ, Spanagel R, Sommer WH, Thorsell A. A pharmacogenetic determinant of mu-opioid receptor antagonist effects on alcohol reward and consumption: evidence from humanized mice. Biol Psychiatry. 2015;77(10):850-8. doi: 10.1016/j.biopsych.2014.08.021. PubMed PMID: 25442002.

95. Wang YJ, Huang P, Blendy JA, Liu-Chen LY. Brain region- and sex-specific alterations in DAMGO-stimulated [(35) S]GTPgammaS binding in mice with Oprm1 A112G. Addict Biol. 2014;19(3):354-61. doi: 10.1111/j.1369-1600.2012.00484.x. PubMed PMID: 22862850; PMCID: PMC3864546.
96. Mague SD, Isiegas C, Huang P, Liu-Chen LY, Lerman C, Blendy JA. Mouse model of OPRM1 (A118G) polymorphism has sex-specific effects on drug-mediated behavior. Proc Natl Acad Sci U S A. 2009;106(26):10847-52. doi: 10.1073/pnas.0901800106. PubMed PMID: 19528658; PMCID: PMC2705603.
97. Zhang Y, Wang D, Johnson AD, Papp AC, Sadee W. Allelic expression imbalance of human mu opioid receptor (OPRM1) caused by variant A118G. J Biol Chem. 2005;280(38):32618-24. doi: 10.1074/jbc.M504942200. PubMed PMID: 16046395.
98. Chou WY, Wang CH, Liu PH, Liu CC, Tseng CC, Jawan B. Human opioid receptor A118G polymorphism affects intravenous patient-controlled analgesia morphine consumption after total abdominal hysterectomy. Anesthesiology. 2006;105(2):334-7. PubMed PMID: 16871067.
99. Huang P, Chen C, Mague SD, Blendy JA, Liu-Chen LY. A common single nucleotide polymorphism A118G of the mu opioid receptor alters its N-glycosylation and protein stability. Biochem J. 2012;441(1):379-86. doi: 10.1042/BJ20111050. PubMed PMID: 21864297; PMCID: PMC3923516.
100. Barr CS, Schwandt M, Lindell SG, Chen SA, Goldman D, Suomi SJ, Higley JD, Heilig M. Association of a functional polymorphism in the mu-opioid receptor gene with alcohol response and consumption in male rhesus macaques. Arch Gen Psychiatry. 2007;64(3):369-76. doi: 10.1001/archpsyc.64.3.369. PubMed PMID: 17339526.
101. Vallender EJ, Ruedi-Bettschen D, Miller GM, Platt DM. A pharmacogenetic model of naltrexone-induced attenuation of alcohol consumption in rhesus monkeys. Drug Alcohol Depend. 2010;109(1-3):252-6. doi: 10.1016/j.drugalcdep.2010.01.005. PubMed PMID: 20153935; PMCID: PMC2875311.
102. Bond C, LaForge KS, Tian M, Melia D, Zhang S, Borg L, Gong J, Schluger J, Strong JA, Leal SM, Tischfield JA, Kreek MJ, Yu L. Single-nucleotide polymorphism in the human mu opioid receptor gene alters beta-endorphin binding and activity: possible implications for opiate addiction. Proc Natl Acad Sci U S A. 1998;95(16):9608-13. PubMed PMID: 9689128; PMCID: PMC21386.
103. Beyer A, Koch T, Schroder H, Schulz S, Hollt V. Effect of the A118G polymorphism on binding affinity, potency and agonist-mediated endocytosis, desensitization, and resensitization of the human mu-opioid receptor. J Neurochem. 2004;89(3):553-60. doi: 10.1111/j.1471-4159.2004.02340.x. PubMed PMID: 15086512.
104. Befort K, Filliol D, Decaillot FM, Gaveriaux-Ruff C, Hoehe MR, Kieffer BL. A single nucleotide polymorphic mutation in the human mu-opioid receptor severely impairs receptor signaling. J Biol Chem. 2001;276(5):3130-7. doi: 10.1074/jbc.M006352200. PubMed PMID: 11067846.
105. Kroslak T, Laforge KS, Gianotti RJ, Ho A, Nielsen DA, Kreek MJ. The single nucleotide polymorphism A118G alters functional properties of the human mu opioid receptor. J Neurochem. 2007;103(1):77-87. doi: 10.1111/j.1471-4159.2007.04738.x. PubMed PMID: 17877633.
106. Margas W, Zubkoff I, Schuler HG, Janicki PK, Ruiz-Velasco V. Modulation of Ca2+ channels by heterologously expressed wild-type and mutant human micro-opioid receptors (hMORs) containing the A118G single-nucleotide polymorphism.

J Neurophysiol. 2007;97(2):1058-67. doi: 10.1152/jn.01007.2006. PubMed PMID: 17151221.
107. Mahmoud S, Thorsell A, Sommer WH, Heilig M, Holgate JK, Bartlett SE, Ruiz-Velasco V. Pharmacological consequence of the A118G mu opioid receptor polymorphism on morphine- and fentanyl-mediated modulation of Ca(2)(+) channels in humanized mouse sensory neurons. Anesthesiology. 2011;115(5):1054-62. doi: 10.1097/ALN.0b013e318231fc11. PubMed PMID: 21926562; PMCID: PMC3203255.
108. Takahashi K, Yamanaka S. Induction of pluripotent stem cells from mouse embryonic and adult fibroblast cultures by defined factors. Cell. 2006;126(4):663-76. doi: 10.1016/j.cell.2006.07.024. PubMed PMID: 16904174.
109. Lim SJ, Ho SC, Mok PL, Tan KL, Ong AH, Gan SC. Induced pluripotent stem cells from human hair follicle keratinocytes as a potential source for in vitro hair follicle cloning. PeerJ. 2016;4:e2695. doi: 10.7717/peerj.2695. PubMed PMID: 27867768; PMCID: PMC5111897.
110. Zhou T, Benda C, Dunzinger S, Huang Y, Ho JC, Yang J, Wang Y, Zhang Y, Zhuang Q, Li Y, Bao X, Tse HF, Grillari J, Grillari-Voglauer R, Pei D, Esteban MA. Generation of human induced pluripotent stem cells from urine samples. Nat Protoc. 2012;7(12):2080-9. doi: 10.1038/nprot.2012.115. PubMed PMID: 23138349.
111. Su RJ, Neises A, Zhang XB. Generation of iPS Cells from Human Peripheral Blood Mononuclear Cells Using Episomal Vectors. Methods Mol Biol. 2016;1357:57-69. doi: 10.1007/7651_2014_139. PubMed PMID: 25403468.
112. Takahashi K, Okita K, Nakagawa M, Yamanaka S. Induction of pluripotent stem cells from fibroblast cultures. Nat Protoc. 2007;2(12):3081-9. doi: 10.1038/nprot.2007.418. PubMed PMID: 18079707.
113. Aasen T, Raya A, Barrero MJ, Garreta E, Consiglio A, Gonzalez F, Vassena R, Bilic J, Pekarik V, Tiscornia G, Edel M, Boue S, Izpisua Belmonte JC. Efficient and rapid generation of induced pluripotent stem cells from human keratinocytes. Nat Biotechnol. 2008;26(11):1276-84. doi: 10.1038/nbt.1503. PubMed PMID: 18931654.
114. Soliman MA, Aboharb F, Zeltner N, Studer L. Pluripotent stem cells in neuropsychiatric disorders. Mol Psychiatry. 2017;22(9):1241-9. doi: 10.1038/mp.2017.40. PubMed PMID: 28322279; PMCID: PMC5582162.
115. Pang ZP, Yang N, Vierbuchen T, Ostermeier A, Fuentes DR, Yang TQ, Citri A, Sebastiano V, Marro S, Sudhof TC, Wernig M. Induction of human neuronal cells by defined transcription factors. Nature. 2011;476(7359):220-3. doi: 10.1038/nature10202. PubMed PMID: 21617644; PMCID: PMC3159048.
116. Zhang Y, Pak C, Han Y, Ahlenius H, Zhang Z, Chanda S, Marro S, Patzke C, Acuna C, Covy J, Xu W, Yang N, Danko T, Chen L, Wernig M, Sudhof TC. Rapid single-step induction of functional neurons from human pluripotent stem cells. Neuron. 2013;78(5):785-98. doi: 10.1016/j.neuron.2013.05.029. PubMed PMID: 23764284; PMCID: PMC3751803.
117. Szeto CY, Tang NL, Lee DT, Stadlin A. Association between mu opioid receptor gene polymorphisms and Chinese heroin addicts. Neuroreport. 2001;12(6):1103-6. PubMed PMID: 11338173.
118. Ebert AD, Liang P, Wu JC. Induced pluripotent stem cells as a disease modeling and drug screening platform. J Cardiovasc Pharmacol. 2012;60(4):408-16. doi: 10.1097/FJC.0b013e318247f642. PubMed PMID: 22240913; PMCID: PMC3343213.

119. Ji P, Manupipatpong S, Xie N, Li Y. Induced Pluripotent Stem Cells: Generation Strategy and Epigenetic Mystery behind Reprogramming. Stem Cells Int. 2016;2016:8415010. doi: 10.1155/2016/8415010. PubMed PMID: 26880993; PMCID: PMC4736417.
120. Rouhani F, Kumasaka N, de Brito MC, Bradley A, Vallier L, Gaffney D. Genetic background drives transcriptional variation in human induced pluripotent stem cells. PLoS Genet. 2014;10(6):e1004432. doi: 10.1371/journal.pgen.1004432. PubMed PMID: 24901476; PMCID: PMC4046971.
121. Burrows CK, Banovich NE, Pavlovic BJ, Patterson K, Gallego Romero I, Pritchard JK, Gilad Y. Genetic Variation, Not Cell Type of Origin, Underlies the Majority of Identifiable Regulatory Differences in iPSCs. PLoS Genet. 2016;12(1):e1005793. doi: 10.1371/journal.pgen.1005793. PubMed PMID: 26812582; PMCID: PMC4727884.
122. Hall FS, Drgonova J, Jain S, Uhl GR. Implications of genome wide association studies for addiction: are our a priori assumptions all wrong? Pharmacol Ther. 2013;140(3):267-79. doi: 10.1016/j.pharmthera.2013.07.006. PubMed PMID: 23872493; PMCID: PMC3797854.
123. Soldner F, Jaenisch R. Medicine. iPSC disease modeling. Science. 2012;338(6111):1155-6. doi: 10.1126/science.1227682. PubMed PMID: 23197518.
124. Bar-Nur O, Russ HA, Efrat S, Benvenisty N. Epigenetic memory and preferential lineage-specific differentiation in induced pluripotent stem cells derived from human pancreatic islet beta cells. Cell Stem Cell. 2011;9(1):17-23. doi: 10.1016/j.stem.2011.06.007. PubMed PMID: 21726830.
125. Ghosh Z, Wilson KD, Wu Y, Hu S, Quertermous T, Wu JC. Persistent donor cell gene expression among human induced pluripotent stem cells contributes to differences with human embryonic stem cells. PLoS One. 2010;5(2):e8975. doi: 10.1371/journal.pone.0008975. PubMed PMID: 20126639; PMCID: PMC2813859.
126. Kim K, Doi A, Wen B, Ng K, Zhao R, Cahan P, Kim J, Aryee MJ, Ji H, Ehrlich LI, Yabuuchi A, Takeuchi A, Cunniff KC, Hongguang H, McKinney-Freeman S, Naveiras O, Yoon TJ, Irizarry RA, Jung N, Seita J, Hanna J, Murakami P, Jaenisch R, Weissleder R, Orkin SH, Weissman IL, Feinberg AP, Daley GQ. Epigenetic memory in induced pluripotent stem cells. Nature. 2010;467(7313):285-90. doi: 10.1038/nature09342. PubMed PMID: 20644535; PMCID: PMC3150836.
127. Marchetto MC, Yeo GW, Kainohana O, Marsala M, Gage FH, Muotri AR. Transcriptional signature and memory retention of human-induced pluripotent stem cells. PLoS One. 2009;4(9):e7076. doi: 10.1371/journal.pone.0007076. PubMed PMID: 19763270; PMCID: PMC2741600.
128. Ohi Y, Qin H, Hong C, Blouin L, Polo JM, Guo T, Qi Z, Downey SL, Manos PD, Rossi DJ, Yu J, Hebrok M, Hochedlinger K, Costello JF, Song JS, Ramalho-Santos M. Incomplete DNA methylation underlies a transcriptional memory of somatic cells in human iPS cells. Nat Cell Biol. 2011;13(5):541-9. doi: 10.1038/ncb2239. PubMed PMID: 21499256; PMCID: PMC3987913.
129. Polo JM, Liu S, Figueroa ME, Kulalert W, Eminli S, Tan KY, Apostolou E, Stadtfeld M, Li Y, Shioda T, Natesan S, Wagers AJ, Melnick A, Evans T, Hochedlinger K. Cell type of origin influences the molecular and functional properties of mouse induced pluripotent stem cells. Nat Biotechnol. 2010;28(8):848-55. doi: 10.1038/nbt.1667. PubMed PMID: 20644536; PMCID: PMC3148605.

130. Stadtfeld M, Apostolou E, Akutsu H, Fukuda A, Follett P, Natesan S, Kono T, Shioda T, Hochedlinger K. Aberrant silencing of imprinted genes on chromosome 12qF1 in mouse induced pluripotent stem cells. Nature. 2010;465(7295):175-81. doi: 10.1038/nature09017. PubMed PMID: 20418860; PMCID: PMC3987905.
131. Wang F, Qi LS. Applications of CRISPR Genome Engineering in Cell Biology. Trends Cell Biol. 2016;26(11):875-88. doi: 10.1016/j.tcb.2016.08.004. PubMed PMID: 27599850; PMCID: PMC5077632.
132. Hsu PD, Lander ES, Zhang F. Development and applications of CRISPR-Cas9 for genome engineering. Cell. 2014;157(6):1262-78. doi: 10.1016/j.cell.2014.05.010. PubMed PMID: 24906146; PMCID: PMC4343198.
133. Wu X, Kriz AJ, Sharp PA. Target specificity of the CRISPR-Cas9 system. Quant Biol. 2014;2(2):59-70. doi: 10.1007/s40484-014-0030-x. PubMed PMID: 25722925; PMCID: PMC4338555.
134. Ran FA, Hsu PD, Wright J, Agarwala V, Scott DA, Zhang F. Genome engineering using the CRISPR-Cas9 system. Nat Protoc. 2013;8(11):2281-308. doi: 10.1038/nprot.2013.143. PubMed PMID: 24157548; PMCID: PMC3969860.
135. Doench JG, Hartenian E, Graham DB, Tothova Z, Hegde M, Smith I, Sullender M, Ebert BL, Xavier RJ, Root DE. Rational design of highly active sgRNAs for CRISPR-Cas9-mediated gene inactivation. Nat Biotechnol. 2014;32(12):1262-7. doi: 10.1038/nbt.3026. PubMed PMID: 25184501; PMCID: PMC4262738.
136. Fu BX, Hansen LL, Artiles KL, Nonet ML, Fire AZ. Landscape of target:guide homology effects on Cas9-mediated cleavage. Nucleic Acids Res. 2014;42(22):13778-87. doi: 10.1093/nar/gku1102. PubMed PMID: 25399416; PMCID: PMC4267615.
137. Elliott B, Richardson C, Winderbaum J, Nickoloff JA, Jasin M. Gene conversion tracts from double-strand break repair in mammalian cells. Mol Cell Biol. 1998;18(1):93-101. PubMed PMID: 9418857; PMCID: PMC121458.
138. Cong L, Ran FA, Cox D, Lin S, Barretto R, Habib N, Hsu PD, Wu X, Jiang W, Marraffini LA, Zhang F. Multiplex genome engineering using CRISPR/Cas systems. Science. 2013;339(6121):819-23. doi: 10.1126/science.1231143. PubMed PMID: 23287718; PMCID: PMC3795411.
139. Yang H, Wang H, Shivalila CS, Cheng AW, Shi L, Jaenisch R. One-step generation of mice carrying reporter and conditional alleles by CRISPR/Cas-mediated genome engineering. Cell. 2013;154(6):1370-9. doi: 10.1016/j.cell.2013.08.022. PubMed PMID: 23992847; PMCID: PMC3961003.
140. Peng Y, Clark KJ, Campbell JM, Panetta MR, Guo Y, Ekker SC. Making designer mutants in model organisms. Development. 2014;141(21):4042-54. doi: 10.1242/dev.102186. PubMed PMID: 25336735; PMCID: PMC4302887.
141. Storici F, Snipe JR, Chan GK, Gordenin DA, Resnick MA. Conservative repair of a chromosomal double-strand break by single-strand DNA through two steps of annealing. Mol Cell Biol. 2006;26(20):7645-57. doi: 10.1128/MCB.00672-06. PubMed PMID: 16908537; PMCID: PMC1636868.
142. Chen F, Pruett-Miller SM, Huang Y, Gjoka M, Duda K, Taunton J, Collingwood TN, Frodin M, Davis GD. High-frequency genome editing using ssDNA oligonucleotides with zinc-finger nucleases. Nat Methods. 2011;8(9):753-5. doi: 10.1038/nmeth.1653. PubMed PMID: 21765410; PMCID: PMC3617923.
143. Yang L, Guell M, Byrne S, Yang JL, De Los Angeles A, Mali P, Aach J, Kim-Kiselak C, Briggs AW, Rios X, Huang PY, Daley G, Church G. Optimization of scarless human stem cell genome editing. Nucleic Acids Res. 2013;41(19):9049-61. doi: 10.1093/nar/gkt555. PubMed PMID: 23907390; PMCID: PMC3799423.

144. Beumer KJ, Trautman JK, Mukherjee K, Carroll D. Donor DNA Utilization During Gene Targeting with Zinc-Finger Nucleases. G3 (Bethesda). 2013;3(4):657-64. doi: 10.1534/g3.112.005439. PubMed PMID: 23550125; PMCID: PMC3618352.
145. Harel I, Benayoun BA, Machado B, Singh PP, Hu CK, Pech MF, Valenzano DR, Zhang E, Sharp SC, Artandi SE, Brunet A. A platform for rapid exploration of aging and diseases in a naturally short-lived vertebrate. Cell. 2015;160(5):1013-26. doi: 10.1016/j.cell.2015.01.038. PubMed PMID: 25684364; PMCID: PMC4344913.
146. Shao Y, Guan Y, Wang L, Qiu Z, Liu M, Chen Y, Wu L, Li Y, Ma X, Liu M, Li D. CRISPR/Cas-mediated genome editing in the rat via direct injection of one-cell embryos. Nat Protoc. 2014;9(10):2493-512. doi: 10.1038/nprot.2014.171. PubMed PMID: 25255092.
147. Renaud JB, Boix C, Charpentier M, De Cian A, Cochennec J, Duvernois-Berthet E, Perrouault L, Tesson L, Edouard J, Thinard R, Cherifi Y, Menoret S, Fontaniere S, de Croze N, Fraichard A, Sohm F, Anegon I, Concordet JP, Giovannangeli C. Improved Genome Editing Efficiency and Flexibility Using Modified Oligonucleotides with TALEN and CRISPR-Cas9 Nucleases. Cell Rep. 2016;14(9):2263-72. doi: 10.1016/j.celrep.2016.02.018. PubMed PMID: 26923600.
148. Liang X, Potter J, Kumar S, Ravinder N, Chesnut JD. Enhanced CRISPR/Cas9-mediated precise genome editing by improved design and delivery of gRNA, Cas9 nuclease, and donor DNA. J Biotechnol. 2017;241:136-46. doi: 10.1016/j.jbiotec.2016.11.011. PubMed PMID: 27845164.
149. Fu Y, Foden JA, Khayter C, Maeder ML, Reyon D, Joung JK, Sander JD. High-frequency off-target mutagenesis induced by CRISPR-Cas nucleases in human cells. Nat Biotechnol. 2013;31(9):822-6. doi: 10.1038/nbt.2623. PubMed PMID: 23792628; PMCID: PMC3773023.
150. Schaefer KA, Wu WH, Colgan DF, Tsang SH, Bassuk AG, Mahajan VB. Unexpected mutations after CRISPR-Cas9 editing in vivo. Nat Methods. 2017;14(6):547-8. doi: 10.1038/nmeth.4293. PubMed PMID: 28557981.
151. Sander JD, Maeder ML, Reyon D, Voytas DF, Joung JK, Dobbs D. ZiFiT (Zinc Finger Targeter): an updated zinc finger engineering tool. Nucleic Acids Res. 2010;38(Web Server issue):W462-8. Epub 2010/05/04. doi: 10.1093/nar/gkq319. PubMed PMID: 20435679; PMCID: PMC2896148.
152. Liang X, Potter J, Kumar S, Zou Y, Quintanilla R, Sridharan M, Carte J, Chen W, Roark N, Ranganathan S, Ravinder N, Chesnut JD. Rapid and highly efficient mammalian cell engineering via Cas9 protein transfection. Journal of biotechnology. 2015;208:44-53. Epub 2015/05/25. doi: 10.1016/j.jbiotec.2015.04.024. PubMed PMID: 26003884.
153. Porteus MH, Baltimore D. Chimeric nucleases stimulate gene targeting in human cells. Science. 2003;300(5620):763. doi: 10.1126/science.1078395. PubMed PMID: 12730593.
154. Sander JD, Dahlborg EJ, Goodwin MJ, Cade L, Zhang F, Cifuentes D, Curtin SJ, Blackburn JS, Thibodeau-Beganny S, Qi Y, Pierick CJ, Hoffman E, Maeder ML, Khayter C, Reyon D, Dobbs D, Langenau DM, Stupar RM, Giraldez AJ, Voytas DF, Peterson RT, Yeh JR, Joung JK. Selection-free zinc-finger-nuclease engineering by context-dependent assembly (CoDA). Nat Methods. 2011;8(1):67-9. doi: 10.1038/nmeth.1542. PubMed PMID: 21151135; PMCID: PMC3018472.
155. Wood AJ, Lo TW, Zeitler B, Pickle CS, Ralston EJ, Lee AH, Amora R, Miller JC, Leung E, Meng X, Zhang L, Rebar EJ, Gregory PD, Urnov FD, Meyer BJ.

Targeted genome editing across species using ZFNs and TALENs. Science. 2011;333(6040):307. doi: 10.1126/science.1207773. PubMed PMID: 21700836; PMCID: PMC3489282.
156. Joung JK, Sander JD. TALENs: a widely applicable technology for targeted genome editing. Nat Rev Mol Cell Biol. 2013;14(1):49-55. doi: 10.1038/nrm3486. PubMed PMID: 23169466; PMCID: PMC3547402.
157. Christian M, Cermak T, Doyle EL, Schmidt C, Zhang F, Hummel A, Bogdanove AJ, Voytas DF. Targeting DNA double-strand breaks with TAL effector nucleases. Genetics. 2010;186(2):757-61. doi: 10.1534/genetics.110.120717. PubMed PMID: 20660643; PMCID: PMC2942870.
158. Zhang XH, Tee LY, Wang XG, Huang QS, Yang SH. Off-target Effects in CRISPR/Cas9-mediated Genome Engineering. Mol Ther Nucleic Acids. 2015;4:e264. doi: 10.1038/mtna.2015.37. PubMed PMID: 26575098; PMCID: PMC4877446.
159. Davis KM, Pattanayak V, Thompson DB, Zuris JA, Liu DR. Small molecule-triggered Cas9 protein with improved genome-editing specificity. Nat Chem Biol. 2015;11(5):316-8. doi: 10.1038/nchembio.1793. PubMed PMID: 25848930; PMCID: PMC4402137.
160. Ramakrishna S, Kwaku Dad AB, Beloor J, Gopalappa R, Lee SK, Kim H. Gene disruption by cell-penetrating peptide-mediated delivery of Cas9 protein and guide RNA. Genome Res. 2014;24(6):1020-7. doi: 10.1101/gr.171264.113. PubMed PMID: 24696462; PMCID: PMC4032848.
161. Kim S, Kim D, Cho SW, Kim J, Kim JS. Highly efficient RNA-guided genome editing in human cells via delivery of purified Cas9 ribonucleoproteins. Genome Res. 2014;24(6):1012-9. doi: 10.1101/gr.171322.113. PubMed PMID: 24696461; PMCID: PMC4032847.
162. Gabriel R, von Kalle C, Schmidt M. Mapping the precision of genome editing. Nat Biotechnol. 2015;33(2):150-2. doi: 10.1038/nbt.3142. PubMed PMID: 25658281.
163. Sung YH, Kim JM, Kim HT, Lee J, Jeon J, Jin Y, Choi JH, Ban YH, Ha SJ, Kim CH, Lee HW, Kim JS. Highly efficient gene knockout in mice and zebrafish with RNA-guided endonucleases. Genome Res. 2014;24(1):125-31. doi: 10.1101/gr.163394.113. PubMed PMID: 24253447; PMCID: PMC3875853.
164. Pasca AM, Sloan SA, Clarke LE, Tian Y, Makinson CD, Huber N, Kim CH, Park JY, O'Rourke NA, Nguyen KD, Smith SJ, Huguenard JR, Geschwind DH, Barres BA, Pasca SP. Functional cortical neurons and astrocytes from human pluripotent stem cells in 3D culture. Nat Methods. 2015;12(7):671-8. doi: 10.1038/nmeth.3415. PubMed PMID: 26005811; PMCID: PMC4489980.
165. Cho SW, Kim S, Kim Y, Kweon J, Kim HS, Bae S, Kim JS. Analysis of off-target effects of CRISPR/Cas-derived RNA-guided endonucleases and nickases. Genome Res. 2014;24(1):132-41. doi: 10.1101/gr.162339.113. PubMed PMID: 24253446; PMCID: PMC3875854.
166. Fu Y, Sander JD, Reyon D, Cascio VM, Joung JK. Improving CRISPR-Cas nuclease specificity using truncated guide RNAs. Nat Biotechnol. 2014;32(3):279-84. doi: 10.1038/nbt.2808. PubMed PMID: 24463574; PMCID: PMC3988262.
167. Pattanayak V, Lin S, Guilinger JP, Ma E, Doudna JA, Liu DR. High-throughput profiling of off-target DNA cleavage reveals RNA-programmed Cas9 nuclease specificity. Nat Biotechnol. 2013;31(9):839-43. doi: 10.1038/nbt.2673. PubMed PMID: 23934178; PMCID: PMC3782611.
168. Ran FA, Hsu PD, Lin CY, Gootenberg JS, Konermann S, Trevino AE, Scott DA, Inoue A, Matoba S, Zhang Y, Zhang F. Double nicking by RNA-guided CRISPR

Cas9 for enhanced genome editing specificity. Cell. 2013;154(6):1380-9. doi: 10.1016/j.cell.2013.08.021. PubMed PMID: 23992846; PMCID: PMC3856256.
169. Vierbuchen T, Ostermeier A, Pang ZP, Kokubu Y, Sudhof TC, Wernig M. Direct conversion of fibroblasts to functional neurons by defined factors. Nature. 2010;463(7284):1035-41. doi: 10.1038/nature08797. PubMed PMID: 20107439; PMCID: PMC2829121.
170. Yang N, Chanda S, Marro S, Ng YH, Janas JA, Haag D, Ang CE, Tang Y, Flores Q, Mall M, Wapinski O, Li M, Ahlenius H, Rubenstein JL, Chang HY, Buylla AA, Sudhof TC, Wernig M. Generation of pure GABAergic neurons by transcription factor programming. Nat Methods. 2017;14(6):621-8. doi: 10.1038/nmeth.4291. PubMed PMID: 28504679; PMCID: PMC5567689.
171. Tobe BT, Brandel MG, Nye JS, Snyder EY. Implications and limitations of cellular reprogramming for psychiatric drug development. Exp Mol Med. 2013;45:e59. doi: 10.1038/emm.2013.124. PubMed PMID: 24232258; PMCID: PMC3849573.
172. Brennand KJ, Marchetto MC, Benvenisty N, Brustle O, Ebert A, Izpisua Belmonte JC, Kaykas A, Lancaster MA, Livesey FJ, McConnell MJ, McKay RD, Morrow EM, Muotri AR, Panchision DM, Rubin LL, Sawa A, Soldner F, Song H, Studer L, Temple S, Vaccarino FM, Wu J, Vanderhaeghen P, Gage FH, Jaenisch R. Creating Patient-Specific Neural Cells for the In Vitro Study of Brain Disorders. Stem Cell Reports. 2015;5(6):933-45. doi: 10.1016/j.stemcr.2015.10.011. PubMed PMID: 26610635; PMCID: PMC4881284.
173. Fyfe LW, Cleary DR, Macey TA, Morgan MM, Ingram SL. Tolerance to the antinociceptive effect of morphine in the absence of short-term presynaptic desensitization in rat periaqueductal gray neurons. J Pharmacol Exp Ther. 2010;335(3):674-80. doi: 10.1124/jpet.110.172643. PubMed PMID: 20739455; PMCID: PMC2993552.
174. Pennock RL, Hentges ST. Differential expression and sensitivity of presynaptic and postsynaptic opioid receptors regulating hypothalamic proopiomelanocortin neurons. J Neurosci. 2011;31(1):281-8. doi: 10.1523/JNEUROSCI.4654-10.2011. PubMed PMID: 21209213; PMCID: PMC3061472.
175. Dong C, Filipeanu CM, Duvernay MT, Wu G. Regulation of G protein-coupled receptor export trafficking. Biochim Biophys Acta. 2007;1768(4):853-70. doi: 10.1016/j.bbamem.2006.09.008. PubMed PMID: 17074298; PMCID: PMC1885203.
176. Chaturvedi K, Shahrestanifar M, Howells RD. mu Opioid receptor: role for the amino terminus as a determinant of ligand binding affinity. Brain Res Mol Brain Res. 2000;76(1):64-72. PubMed PMID: 10719216.
177. Kranich H, Bartkowski S, Denton MJ, Krey S, Dickinson P, Duvigneau C, Gal A. Autosomal dominant 'sector' retinitis pigmentosa due to a point mutation predicting an Asn-15-Ser substitution of rhodopsin. Human molecular genetics. 1993;2(6):813-4. PubMed PMID: 8353500.
178. Standfuss J, Xie G, Edwards PC, Burghammer M, Oprian DD, Schertler GF. Crystal structure of a thermally stable rhodopsin mutant. Journal of molecular biology. 2007;372(5):1179-88. doi: 10.1016/j.jmb.2007.03.007. PubMed PMID: 17825322; PMCID: 2258155.
179. Huang W, Manglik A, Venkatakrishnan AJ, Laeremans T, Feinberg EN, Sanborn AL, Kato HE, Livingston KE, Thorsen TS, Kling RC, Granier S, Gmeiner P, Husbands SM, Traynor JR, Weis WI, Steyaert J, Dror RO, Kobilka BK. Structural insights into micro-opioid receptor activation. Nature. 2015;524(7565):315-21. doi: 10.1038/nature14886. PubMed PMID: 26245379; PMCID: PMC4639397.

180. Gupta A, Rozenfeld R, Gomes I, Raehal KM, Decaillot FM, Bohn LM, Devi LA. Post-activation-mediated changes in opioid receptors detected by N-terminal antibodies. J Biol Chem. 2008;283(16):10735-44. doi: 10.1074/jbc.M709454200. PubMed PMID: 18256033; PMCID: PMC2447646.
181. Salom D, Lodowski DT, Stenkamp RE, Le Trong I, Golczak M, Jastrzebska B, Harris T, Ballesteros JA, Palczewski K. Crystal structure of a photoactivated deprotonated intermediate of rhodopsin. Proc Natl Acad Sci U S A. 2006;103(44):16123-8. doi: 10.1073/pnas.0608022103. PubMed PMID: 17060607; PMCID: PMC1637547.
182. Stafford K, Gomes AB, Shen J, Yoburn BC. mu-Opioid receptor downregulation contributes to opioid tolerance in vivo. Pharmacol Biochem Behav. 2001;69(1-2):233-7. PubMed PMID: 11420091.
183. Christie MJ. Cellular neuroadaptations to chronic opioids: tolerance, withdrawal and addiction. Br J Pharmacol. 2008;154(2):384-96. doi: 10.1038/bjp.2008.100. PubMed PMID: 18414400; PMCID: PMC2442443.
184. Wang YJ, Huang P, Ung A, Blendy JA, Liu-Chen LY. Reduced expression of the mu opioid receptor in some, but not all, brain regions in mice with OPRM1 A112G. Neuroscience. 2012;205:178-84. doi: 10.1016/j.neuroscience.2011.12.033. PubMed PMID: 22240251; PMCID: PMC3772531.
185. Lanctot PM, Leclerc PC, Escher E, Guillemette G, Leduc R. Role of N-glycan-dependent quality control in the cell-surface expression of the AT1 receptor. Biochem Biophys Res Commun. 2006;340(2):395-402. doi: 10.1016/j.bbrc.2005.12.016. PubMed PMID: 16364240.
186. Ray K, Clapp P, Goldsmith PK, Spiegel AM. Identification of the sites of N-linked glycosylation on the human calcium receptor and assessment of their role in cell surface expression and signal transduction. J Biol Chem. 1998;273(51):34558-67. PubMed PMID: 9852126.
187. Compton SJ, Sandhu S, Wijesuriya SJ, Hollenberg MD. Glycosylation of human proteinase-activated receptor-2 (hPAR2): role in cell surface expression and signalling. Biochem J. 2002;368(Pt 2):495-505. doi: 10.1042/BJ20020706. PubMed PMID: 12171601; PMCID: PMC1222997.
188. Hawtin SR, Davies AR, Matthews G, Wheatley M. Identification of the glycosylation sites utilized on the V1a vasopressin receptor and assessment of their role in receptor signalling and expression. Biochem J. 2001;357(Pt 1):73-81. PubMed PMID: 11415438; PMCID: PMC1221930.
189. Li JG, Chen C, Liu-Chen LY. N-Glycosylation of the human kappa opioid receptor enhances its stability but slows its trafficking along the biosynthesis pathway. Biochemistry. 2007;46(38):10960-70. doi: 10.1021/bi700443j. PubMed PMID: 17711303.
190. Selley DE, Nestler EJ, Breivogel CS, Childers SR. Opioid receptor-coupled G-proteins in rat locus coeruleus membranes: decrease in activity after chronic morphine treatment. Brain Res. 1997;746(1-2):10-8. PubMed PMID: 9037478.
191. Sim LJ, Selley DE, Dworkin SI, Childers SR. Effects of chronic morphine administration on mu opioid receptor-stimulated [35S]GTPgammaS autoradiography in rat brain. J Neurosci. 1996;16(8):2684-92. PubMed PMID: 8786444.
192. Elliott J, Guo L, Traynor JR. Tolerance to mu-opioid agonists in human neuroblastoma SH-SY5Y cells as determined by changes in guanosine-5'-O-(3-[35S]-thio)triphosphate binding. Br J Pharmacol. 1997;121(7):1422-8. doi: 10.1038/sj.bjp.0701253. PubMed PMID: 9257923; PMCID: PMC1564818.

193. North RA, Vitek LV. The effect of chronic morphine treatment of excitatory junction potentials in the mouse vas deferens. Br J Pharmacol. 1980;68(3):399-405. PubMed PMID: 7052335; PMCID: PMC2044193.
194. Williams JT, Christie MJ, Manzoni O. Cellular and synaptic adaptations mediating opioid dependence. Physiol Rev. 2001;81(1):299-343. PubMed PMID: 11152760.
195. Jandial R, Levy ML. Cellular alchemy: induced pluripotent stem cells retain epigenetic memory. World Neurosurg. 2011;75(1):5-6. doi: 10.1016/j.wneu.2011.01.013. PubMed PMID: 21492641.
196. Mayshar Y, Ben-David U, Lavon N, Biancotti JC, Yakir B, Clark AT, Plath K, Lowry WE, Benvenisty N. Identification and classification of chromosomal aberrations in human induced pluripotent stem cells. Cell Stem Cell. 2010;7(4):521-31. doi: 10.1016/j.stem.2010.07.017. PubMed PMID: 20887957.
197. Taapken SM, Nisler BS, Newton MA, Sampsell-Barron TL, Leonhard KA, McIntire EM, Montgomery KD. Karotypic abnormalities in human induced pluripotent stem cells and embryonic stem cells. Nat Biotechnol. 2011;29(4):313-4. doi: 10.1038/nbt.1835. PubMed PMID: 21478842.
198. Chinchalongporn V, Koppensteiner P, Pre D, Thangnipon W, Bilo L, Arancio O. Connectivity and circuitry in a dish versus in a brain. Alzheimers Res Ther. 2015;7(1):44. doi: 10.1186/s13195-015-0129-y. PubMed PMID: 26045718; PMCID: PMC4456047.
199. Vera E, Studer L. When rejuvenation is a problem: challenges of modeling late-onset neurodegenerative disease. Development. 2015;142(18):3085-9. doi: 10.1242/dev.120667. PubMed PMID: 26395137.
200. Studer L, Vera E, Cornacchia D. Programming and Reprogramming Cellular Age in the Era of Induced Pluripotency. Cell Stem Cell. 2015;16(6):591-600. doi: 10.1016/j.stem.2015.05.004. PubMed PMID: 26046759; PMCID: PMC4508309.
201. Ho SM, Hartley BJ, Tcw J, Beaumont M, Stafford K, Slesinger PA, Brennand KJ. Rapid Ngn2-induction of excitatory neurons from hiPSC-derived neural progenitor cells. Methods. 2016;101:113-24. doi: 10.1016/j.ymeth.2015.11.019. PubMed PMID: 26626326; PMCID: PMC4860098.
202. Kriks S, Shim JW, Piao J, Ganat YM, Wakeman DR, Xie Z, Carrillo-Reid L, Auyeung G, Antonacci C, Buch A, Yang L, Beal MF, Surmeier DJ, Kordower JH, Tabar V, Studer L. Dopamine neurons derived from human ES cells efficiently engraft in animal models of Parkinson's disease. Nature. 2011;480(7378):547-51. doi: 10.1038/nature10648. PubMed PMID: 22056989; PMCID: PMC3245796.
203. Wang XF, Cynader MS. Effects of astrocytes on neuronal attachment and survival shown in a serum-free co-culture system. Brain Res Brain Res Protoc. 1999;4(2):209-16. PubMed PMID: 10446416.
204. Lancaster MA, Renner M, Martin CA, Wenzel D, Bicknell LS, Hurles ME, Homfray T, Penninger JM, Jackson AP, Knoblich JA. Cerebral organoids model human brain development and microcephaly. Nature. 2013;501(7467):373-9. doi: 10.1038/nature12517. PubMed PMID: 23995685; PMCID: PMC3817409.
205. Haberstock-Debic H, Wein M, Barrot M, Colago EE, Rahman Z, Neve RL, Pickel VM, Nestler EJ, von Zastrow M, Svingos AL. Morphine acutely regulates opioid receptor trafficking selectively in dendrites of nucleus accumbens neurons. J Neurosci. 2003;23(10):4324-32. PubMed PMID: 12764121.
206. Crist RC, Berrettini WH. Pharmacogenetics of OPRM1. Pharmacology, biochemistry, and behavior. 2013. doi: 10.1016/j.pbb.2013.10.018. PubMed PMID: 24201053.
207. Nikolov MA, Beltcheva O, Galabova A, Ljubenova A, Jankova E, Gergov G, Russev AA, Lynskey MT, Nelson EC, Nesheva E, Krasteva D, Lazarov P, Mitev

VI, Kremensky IM, Kaneva RP, Todorov AA. No evidence of association between 118A>G OPRM1 polymorphism and heroin dependence in a large Bulgarian case-control sample. Drug and alcohol dependence. 2011;117(1):62-5. doi: 10.1016/j.drugalcdep.2010.12.026. PubMed PMID: 21277709; PMCID: 3128690.

208. Bergen AW, Kokoszka J, Peterson R, Long JC, Virkkunen M, Linnoila M, Goldman D. Mu opioid receptor gene variants: lack of association with alcohol dependence. Mol Psychiatry. 1997;2(6):490-4. PubMed PMID: 9399694.
209. Zhang Y, Picetti R, Butelman ER, Ho A, Blendy JA, Kreek MJ. Mouse Model of the OPRM1 (A118G) Polymorphism: Differential Heroin Self-Administration Behavior Compared with Wild-Type Mice. Neuropsychopharmacology. 2014. doi: 10.1038/npp.2014.286. PubMed PMID: 25336208.
210. Ducat E, Ray B, Bart G, Umemura Y, Varon J, Ho A, Kreek MJ. Mu-opioid receptor A118G polymorphism in healthy volunteers affects hypothalamic-pituitary-adrenal axis adrenocorticotropic hormone stress response to metyrapone. Addiction biology. 2013;18(2):325-31. doi: 10.1111/j.1369-1600.2011.00313.x. PubMed PMID: 21507151; PMCID: 3789604.
211. Ray R, Ruparel K, Newberg A, Wileyto EP, Loughead JW, Divgi C, Blendy JA, Logan J, Zubieta JK, Lerman C. Human Mu Opioid Receptor (OPRM1 A118G) polymorphism is associated with brain mu-opioid receptor binding potential in smokers. Proc Natl Acad Sci U S A. 2011;108(22):9268-73. doi: 10.1073/pnas.1018699108. PubMed PMID: 21576462; PMCID: 3107291.
212. Noble EP, Zhang X, Ritchie T, Lawford BR, Grosser SC, Young RM, Sparkes RS. D2 dopamine receptor and GABA(A) receptor beta3 subunit genes and alcoholism. Psychiatry Res. 1998;81(2):133-47. PubMed PMID: 9858031.
213. Institute for Health Metrics and Evaluation. 2013 [cited 2014 1 Jun 2014]. Available from: http://www.healthmetricsandevaluation.org/gbd/visualizations/gbd-cause-patterns.
214. Mansvelder HD, McGehee DS. Cellular and synaptic mechanisms of nicotine addiction. J Neurobiol. 2002;53(4):606-17. doi: 10.1002/neu.10148. PubMed PMID: 12436424.
215. Pidoplichko VI, DeBiasi M, Williams JT, Dani JA. Nicotine activates and desensitizes midbrain dopamine neurons. Nature. 1997;390(6658):401-4. doi: 10.1038/37120. PubMed PMID: 9389479.
216. Mansvelder HD, Keath JR, McGehee DS. Synaptic mechanisms underlie nicotine-induced excitability of brain reward areas. Neuron. 2002;33(6):905-19. PubMed PMID: 11906697.
217. Mansvelder HD, McGehee DS. Long-term potentiation of excitatory inputs to brain reward areas by nicotine. Neuron. 2000;27(2):349-57. PubMed PMID: 10985354.
218. Saccone NL, Wang JC, Breslau N, Johnson EO, Hatsukami D, Saccone SF, Grucza RA, Sun L, Duan W, Budde J, Culverhouse RC, Fox L, Hinrichs AL, Steinbach JH, Wu M, Rice JP, Goate AM, Bierut LJ. The CHRNA5-CHRNA3-CHRNB4 nicotinic receptor subunit gene cluster affects risk for nicotine dependence in African-Americans and in European-Americans. Cancer Res. 2009;69(17):6848-56. doi: 10.1158/0008-5472.CAN-09-0786. PubMed PMID: 19706762; PMCID: 2874321.
219. Chatterjee S, Santos N, Holgate J, Haass-Koffler CL, Hopf FW, Kharazia V, Lester H, Bonci A, Bartlett SE. The alpha5 subunit regulates the expression and function of alpha4*-containing neuronal nicotinic acetylcholine receptors in the

ventral-tegmental area. PLoS One. 2013;8(7):e68300. doi: 10.1371/journal.pone.0068300. PubMed PMID: 23869214; PMCID: 3712017.
220. Changeux JP. Nicotine addiction and nicotinic receptors: lessons from genetically modified mice. Nat Rev Neurosci. 2010;11(6):389-401. doi: 10.1038/nrn2849. PubMed PMID: 20485364.
221. Morel C, Fattore L, Pons S, Hay YA, Marti F, Lambolez B, De Biasi M, Lathrop M, Fratta W, Maskos U, Faure P. Nicotine consumption is regulated by a human polymorphism in dopamine neurons. Mol Psychiatry. 2013. Epub 2013/12/04. doi: 10.1038/mp.2013.158. PubMed PMID: 24296975.
222. Tapia L, Kuryatov A, Lindstrom J. Ca2+ permeability of the (alpha4)3(beta2)2 stoichiometry greatly exceeds that of (alpha4)2(beta2)3 human acetylcholine receptors. Mol Pharmacol. 2007;71(3):769-76. doi: 10.1124/mol.106.030445. PubMed PMID: 17132685.
223. Kuryatov A, Berrettini W, Lindstrom J. Acetylcholine receptor (AChR) alpha5 subunit variant associated with risk for nicotine dependence and lung cancer reduces (alpha4beta2)alpha5 AChR function. Mol Pharmacol. 2011;79(1):119-25. Epub 2010/10/01. doi: 10.1124/mol.110.066357. PubMed PMID: 20881005; PMCID: 3014277.
224. Seok J, Warren HS, Cuenca AG, Mindrinos MN, Baker HV, Xu W, Richards DR, McDonald-Smith GP, Gao H, Hennessy L, Finnerty CC, Lopez CM, Honari S, Moore EE, Minei JP, Cuschieri J, Bankey PE, Johnson JL, Sperry J, Nathens AB, Billiar TR, West MA, Jeschke MG, Klein MB, Gamelli RL, Gibran NS, Brownstein BH, Miller-Graziano C, Calvano SE, Mason PH, Cobb JP, Rahme LG, Lowry SF, Maier RV, Moldawer LL, Herndon DN, Davis RW, Xiao W, Tompkins RG, Inflammation, Host Response to Injury LSCRP. Genomic responses in mouse models poorly mimic human inflammatory diseases. Proc Natl Acad Sci U S A. 2013;110(9):3507-12. doi: 10.1073/pnas.1222878110. PubMed PMID: 23401516; PMCID: 3587220.
225. Carpenter RS, Kigerl KA, Marbourg JM, Gaudet AD, Huey D, Niewiesk S, Popovich PG. Traumatic spinal cord injury in mice with human immune systems. Exp Neurol. 2015;271:432-44. doi: 10.1016/j.expneurol.2015.07.011. PubMed PMID: 26193167; PMCID: PMC4586484.
226. Muotri AR. The Human Model: Changing Focus on Autism Research. Biol Psychiatry. 2016;79(8):642-9. doi: 10.1016/j.biopsych.2015.03.012. PubMed PMID: 25861701; PMCID: PMC4573784.
227. Costantini TW, Dang X, Coimbra R, Eliceiri BP, Baird A. CHRFAM7A, a human-specific and partially duplicated alpha7-nicotinic acetylcholine receptor gene with the potential to specify a human-specific inflammatory response to injury. J Leukoc Biol. 2015;97(2):247-57. doi: 10.1189/jlb.4RU0814-381R. PubMed PMID: 25473097; PMCID: PMC4304420.
228. Abeliovich A, Doege CA. Reprogramming therapeutics: iPS cell prospects for neurodegenerative disease. Neuron. 2009;61(3):337-9. Epub 2009/02/17. doi: 10.1016/j.neuron.2009.01.024. PubMed PMID: 19217371.
229. Wen Z, Nguyen HN, Guo Z, Lalli MA, Wang X, Su Y, Kim NS, Yoon KJ, Shin J, Zhang C, Makri G, Nauen D, Yu H, Guzman E, Chiang CH, Yoritomo N, Kaibuchi K, Zou J, Christian KM, Cheng L, Ross CA, Margolis RL, Chen G, Kosik KS, Song H, Ming GL. Synaptic dysregulation in a human iPS cell model of mental disorders. Nature. 2014;515(7527):414-8. doi: 10.1038/nature13716. PubMed PMID: 25132547.
230. Bavamian S, Mellios N, Lalonde J, Fass DM, Wang J, Sheridan SD, Madison JM, Zhou F, Rueckert EH, Barker D, Perlis RH, Sur M, Haggarty SJ. Dysregulation of

miR-34a links neuronal development to genetic risk factors for bipolar disorder. Mol Psychiatry. 2015;20(5):573-84. doi: 10.1038/mp.2014.176. PubMed PMID: 25623948; PMCID: PMC4414679.

231. Mertens J, Wang QW, Kim Y, Yu DX, Pham S, Yang B, Zheng Y, Diffenderfer KE, Zhang J, Soltani S, Eames T, Schafer ST, Boyer L, Marchetto MC, Nurnberger JI, Calabrese JR, Odegaard KJ, McCarthy MJ, Zandi PP, Alda M, Nievergelt CM, Pharmacogenomics of Bipolar Disorder S, Mi S, Brennand KJ, Kelsoe JR, Gage FH, Yao J. Differential responses to lithium in hyperexcitable neurons from patients with bipolar disorder. Nature. 2015;527(7576):95-9. doi: 10.1038/nature15526. PubMed PMID: 26524527; PMCID: PMC4742055.
232. Panchision DM. Concise Review: Progress and Challenges in Using Human Stem Cells for Biological and Therapeutics Discovery: Neuropsychiatric Disorders. Stem Cells. 2016;34(3):523-36. doi: 10.1002/stem.2295. PubMed PMID: 26840228; PMCID: PMC4803616.
233. Moore JC, Sheldon MH, Hart RP. Biobanking in the Era of the Stem Cell: A Technical and Operational Guide. Ding W, editor: Morgan & Claypool Life Sciences; 2012. 78 p.
234. Seki T, Yuasa S, Oda M, Egashira T, Yae K, Kusumoto D, Nakata H, Tohyama S, Hashimoto H, Kodaira M, Okada Y, Seimiya H, Fusaki N, Hasegawa M, Fukuda K. Generation of induced pluripotent stem cells from human terminally differentiated circulating T cells. Cell Stem Cell. 2010;7(1):11-4. Epub 2010/07/14. doi: 10.1016/j.stem.2010.06.003. PubMed PMID: 20621043.
235. Trapnell C, Roberts A, Goff L, Pertea G, Kim D, Kelley DR, Pimentel H, Salzberg SL, Rinn JL, Pachter L. Differential gene and transcript expression analysis of RNA-seq experiments with TopHat and Cufflinks. Nature protocols. 2012;7(3):562-78. Epub 2012/03/03. doi: 10.1038/nprot.2012.016. PubMed PMID: 22383036; PMCID: 3334321.
236. Dudoit S, Gentleman RC, Quackenbush J. Open source software for the analysis of microarray data. BioTechniques. 2003;Suppl:45. PubMed PMID: 2759.
237. Sauvageau M, Goff LA, Lodato S, Bonev B, Groff AF, Gerhardinger C, Sanchez-Gomez DB, Hacisuleyman E, Li E, Spence M, Liapis SC, Mallard W, Morse M, Swerdel MR, D'Ecclessis MF, Moore JC, Lai V, Gong G, Yancopoulos GD, Frendewey D, Kellis M, Hart RP, Valenzuela DM, Arlotta P, Rinn JL. Multiple knockout mouse models reveal lincRNAs are required for life and brain development. Elife. 2013;2(0):e01749. doi: 10.7554/eLife.01749. PubMed PMID: 24381249; PMCID: 3874104.
238. Miller JD, Ganat YM, Kishinevsky S, Bowman RL, Liu B, Tu EY, Mandal PK, Vera E, Shim JW, Kriks S, Taldone T, Fusaki N, Tomishima MJ, Krainc D, Milner TA, Rossi DJ, Studer L. Human iPSC-based modeling of late-onset disease via progerin-induced aging. Cell Stem Cell. 2013;13(6):691-705. doi: 10.1016/j.stem.2013.11.006. PubMed PMID: 24315443.
239. Maximov A, Pang ZP, Tervo DG, Sudhof TC. Monitoring synaptic transmission in primary neuronal cultures using local extracellular stimulation. J Neurosci Methods. 2007;161(1):75-87. doi: 10.1016/j.jneumeth.2006.10.009. PubMed PMID: 17118459.
240. Pang ZP, Yang N, Vierbuchen T, Ostermeier A, Fuentes DR, Yang TQ, Citri A, Sebastiano V, Marro S, Sudhof TC, Wernig M. Induction of human neuronal cells by defined transcription factors. Nature. 2011. Epub 2011/05/28. doi: 10.1038/nature10202. PubMed PMID: 21617644.

241. Heatherton TF, Kozlowski LT, Frecker RC, Fagerstrom KO. The Fagerstrom Test for Nicotine Dependence: a revision of the Fagerstrom Tolerance Questionnaire. British journal of addiction. 1991;86(9):1119-27. PubMed PMID: 1932883.
242. Muller FJ, Schuldt BM, Williams R, Mason D, Altun G, Papapetrou EP, Danner S, Goldmann JE, Herbst A, Schmidt NO, Aldenhoff JB, Laurent LC, Loring JF. A bioinformatic assay for pluripotency in human cells. Nature methods. 2011. Epub 2011/03/08. doi: 10.1038/nmeth.1580. PubMed PMID: 21378979.
243. Fowler CD, Kenny PJ. Nicotine aversion: Neurobiological mechanisms and relevance to tobacco dependence vulnerability. Neuropharmacology. 2014;76 Pt B:533-44. Epub 2013/09/24. doi: 10.1016/j.neuropharm.2013.09.008. PubMed PMID: 24055497; PMCID: 3858456.
244. Sun W. Dopamine neurons in the ventral tegmental area: drug-induced synaptic plasticity and its role in relapse to drug-seeking behavior. Current drug abuse reviews. 2011;4(4):270-85. PubMed PMID: 21834753.
245. Broussard JI. Co-transmission of dopamine and glutamate. J Gen Physiol. 2012;139(1):93-6. doi: 10.1085/jgp.201110659. PubMed PMID: 22200950; PMCID: PMC3250102.
246. Stuber GD, Hnasko TS, Britt JP, Edwards RH, Bonci A. Dopaminergic terminals in the nucleus accumbens but not the dorsal striatum corelease glutamate. J Neurosci. 2010;30(24):8229-33. doi: 10.1523/JNEUROSCI.1754-10.2010. PubMed PMID: 20554874; PMCID: PMC2918390.
247. Smith RM, Alachkar H, Papp AC, Wang D, Mash DC, Wang JC, Bierut LJ, Sadee W. Nicotinic alpha5 receptor subunit mRNA expression is associated with distant 5' upstream polymorphisms. European journal of human genetics : EJHG. 2011;19(1):76-83. Epub 2010/08/12. doi: 10.1038/ejhg.2010.120. PubMed PMID: 20700147; PMCID: 2995013.
248. Huang da W, Sherman BT, Lempicki RA. Systematic and integrative analysis of large gene lists using DAVID bioinformatics resources. Nature protocols. 2009;4(1):44-57. Epub 2009/01/10. doi: 10.1038/nprot.2008.211. PubMed PMID: 19131956.
249. Huang da W, Sherman BT, Lempicki RA. Bioinformatics enrichment tools: paths toward the comprehensive functional analysis of large gene lists. Nucleic Acids Res. 2009;37(1):1-13. Epub 2008/11/27. doi: 10.1093/nar/gkn923. PubMed PMID: 19033363; PMCID: 2615629.
250. !!! INVALID CITATION !!! (30, 214).
251. George AA, Lucero LM, Damaj MI, Lukas RJ, Chen X, Whiteaker P. Function of human alpha3beta4alpha5 nicotinic acetylcholine receptors is reduced by the alpha5(D398N) variant. J Biol Chem. 2012;287(30):25151-62. Epub 2012/06/06. doi: 10.1074/jbc.M112.379339. PubMed PMID: 22665477; PMCID: 3408138.
252. De Filippis L, Halikere A, McGowan H, Moore JC, Tischfield JA, Hart RP, Pang ZP. Ethanol-mediated activation of the NLRP3 inflammasome in iPS cells and iPS cells-derived neural progenitor cells. Mol Brain. 2016;9(1):51. doi: 10.1186/s13041-016-0221-7. PubMed PMID: 27160314; PMCID: PMC4862119.
253. Lin L, Swerdel MR, Lazaropoulos MP, Hoffman GS, Toro-Ramos AJ, Wright J, Lederman H, Chen J, Moore JC, Hart RP. Spontaneous ATM Gene Reversion in A-T iPSC to Produce an Isogenic Cell Line. Stem Cell Reports. 2015;5(6):1097-108. Epub 11/19/2015. doi: 10.1016/j.stemcr.2015.10.010. PubMed PMID: 26677768.
254. Marchetto MC, Gage FH. Modeling brain disease in a dish: really? Cell stem cell. 2012;10(6):642-5. Epub 2012/06/19. doi: 10.1016/j.stem.2012.05.008. PubMed PMID: 22704498.

255. Dolmetsch R, Geschwind DH. The human brain in a dish: the promise of iPSC-derived neurons. Cell. 2011;145(6):831-4. Epub 2011/06/15. doi: 10.1016/j.cell.2011.05.034. PubMed PMID: 21663789.
256. Lee G, Studer L. Induced pluripotent stem cell technology for the study of human disease. Nature methods. 2010;7(1):25-7. Epub 2009/12/30. doi: 10.1038/nmeth.f.283. PubMed PMID: 20038952.
257. Beevers JE, Caffrey TM, Wade-Martins R. Induced pluripotent stem cell (iPSC)-derived dopaminergic models of Parkinson's disease. Biochemical Society transactions. 2013;41(6):1503-8. doi: 10.1042/BST20130194. PubMed PMID: 24256244.
258. Jiang Y, Cowley SA, Siler U, Melguizo D, Tilgner K, Browne C, Dewilton A, Przyborski S, Saretzki G, James WS, Seger RA, Reichenbach J, Lako M, Armstrong L. Derivation and functional analysis of patient-specific induced pluripotent stem cells as an in vitro model of chronic granulomatous disease. Stem Cells. 2012;30(4):599-611. doi: 10.1002/stem.1053. PubMed PMID: 22311747; PMCID: 3593166.
259. Stamatakis AM, Jennings JH, Ung RL, Blair GA, Weinberg RJ, Neve RL, Boyce F, Mattis J, Ramakrishnan C, Deisseroth K, Stuber GD. A unique population of ventral tegmental area neurons inhibits the lateral habenula to promote reward. Neuron. 2013;80(4):1039-53. doi: 10.1016/j.neuron.2013.08.023. PubMed PMID: 24267654; PMCID: 3873746.
260. Tritsch NX, Ding JB, Sabatini BL. Dopaminergic neurons inhibit striatal output through non-canonical release of GABA. Nature. 2012;490(7419):262-6. doi: 10.1038/nature11466. PubMed PMID: 23034651; PMCID: 3944587.
261. Rose JE, Mukhin AG, Lokitz SJ, Turkington TG, Herskovic J, Behm FM, Garg S, Garg PK. Kinetics of brain nicotine accumulation in dependent and nondependent smokers assessed with PET and cigarettes containing 11C-nicotine. Proc Natl Acad Sci U S A. 2010;107(11):5190-5. doi: 10.1073/pnas.0909184107. PubMed PMID: 20212132; PMCID: PMC2841893.

Appendix

Increased nicotine response in iPS Cell-derived human neurons carrying the CHRNA5 N398 allele

The following study which I have co-authored has been published in *Scientific Reports* and included in this dissertation. *Scientific Reports* is an open access journal that applies a Creative Commons license allowing re-use of this published work.

Oni E*, **Halikere A***, Li G, Toro-Ramos AJ, Swerdel MR, Verpeut JL, Moore JC, Bello NT, Bierut LJ, Goate A, Tischfield JA, Pang ZP, Hart RP. Increased nicotine response in iPSC-derived human neurons carrying the CHRNA5 N398 allele. *Scientific Reports*. 2016 Oct 4;6:34341. PMID: 27698409. ***These authors contributed equally to this work.**

Introduction

Drug abuse and addiction are a major burden to society with the total cost of substance abuse in the U.S. exceeding $600 billion annually (NIDA). Smoking is the largest preventable cause of death in the U.S., leading to more than 465,000 deaths in 2010 (213). Since addiction and comorbid behaviors are a consequence of brain function, the understanding of the neural basis underlying addiction becomes crucial to determine the etiology and the pathophysiology of addiction. However, little is known about the specific neuronal, synaptic and cell biological mechanisms underlying addiction behaviors, impacting the variable treatment outcomes for substance abuse disorders.

Nicotine, considered to be the primary contributor to tobacco addiction, stimulates the nicotinic acetylcholine receptor (nAChR) of different neuronal subtypes in the brain including the midbrain dopaminergic (DA) (214, 215) as well as forebrain glutamatergic neurons (216, 217). Genome wide association studies (GWAS) have identified several genetic variants associated with increased risk of addiction, including single nucleotide polymorphism (SNP) variants within the *CHRNA5-CHRNA3-CHRNB4*

gene cluster of the 15q25 region, encoding the α5, α3, and β4 subunits of nAChR (33, 218). Of these variants, the SNP rs16969668 encodes an amino acid substitution at position 398 from aspartate (D) to asparagine (N), referred to as the D398 (major) or N398 (minor) alleles, of *CHRNA5*. Given that variation in α5 expression alters nAChR expression and function (219), nonsynonymous variants within α5 are likely to affect neurophysiological functions, which potentially contribute to addictive behaviors (33). However, how such nAChR gene variants in humans affect receptor activity along with neuronal function and lead to addiction behaviors is not known.

Studies using animal models provide some clue on how nAChR may contribute to addiction behavior. The α5 knockout mouse models exhibit increased nicotine consumption compared to controls, suggesting a role for the α5 subunit in modulating reward behavior (36, 220). The N398 α5 subunit, when selectively expressed in VTA (ventral tegmental area) DA neurons of CHRNA5$^{-/-}$ mice, produced a partial loss of function and increased nicotine self-administration (221). Mechanistic studies using similar systems concluded that the functional change in N398 is likely due to intracellular modulation of the receptor (37). Meanwhile, heterologous expression of the human N398 α5 variant in Xenopus oocytes revealed it might affect the expression of the other nAChR subunits (222), reduce Ca^{2+} permeability and increase short-term desensitization to nicotine (223).

While carefully controlled animal models have been quite successful in understanding the global mediating pathways of motivational and reward behaviors, attempts to study more complex human diseases in animal models may correlate poorly, given the evolutionary distance between humans and rodents, as has been demonstrated in inflammation models (224), spinal cord injury (225), and neurodevelopmental disorders (226). The mouse-human evolutionary divergence is further illustrated through the report of a human-specific nicotinic acetylcholine receptor

(CHRFAM7A) that is thought to play a role in inflammatory response (227). Given the complexity of the human neuronal function compared to that of rodents, it is critical to understand the role of nAChR gene variants in modulating neuronal function in a human-specific context. To overcome the lack of living human neurons to study the role of human nAChR genetic variants, recent advances in stem cell biology, especially the development of subject-specific induced pluripotent stem cells (iPSCs) now allows the use of human neurons derived from phenotypically variant subjects to model human neuropsychiatric disorders at a cell biological and mechanistic level, which was not previously possible (228-232).

Here we have drawn upon the collection of cryopreserved lymphocytes stored in the Collaborative Genetic Study of Nicotine Dependence (COGEND) repository to construct multiple induced pluripotent stem cell (iPSC) subject lines with and without the α5 N398 variant using non-integrating Sendai viral vectors (233, 234). We successfully derived two subtypes of neurons from these iPSCs: 1) midbrain DA neurons using a dual-SMAD inhibition protocol (202); as well as 2) pure excitatory forebrain glutamatergic neurons generated using induced neuronal (iN) technology (116). We found that DA neurons exhibit mature neuronal characteristics such as spontaneous repetitive action potentials (APs) and synaptic activities; expressing pan-neuronal markers, midbrain DA neuronal markers, and nAChR mRNAs. Gene ontology (GO) and pathway analysis of RNAseq data as well as functional characterization using electrophysiology revealed functional and nicotine response differences between N398 and D398 neuron cultures. Interestingly, our results indicate that the DA neurons also co-release glutamate. The N398 DA neurons exhibit a more profound response to nicotine stimulation and this response is likely caused by presynaptic input from glutamatergic neurons in the culture. Moreover, nicotine exhibited a transiently increased but desensitizing effect on synaptic transmission in excitatory iN cells. These results provide important insights on how

nAChR5 gene variants may affect neuronal activity and offer a proof-of-principle for utilizing human neurons derived from somatic cells to study the contribution of gene variants to addiction behavior.

Materials and Methods

Human induced pluripotent stem cell culture and neural induction

Preparation of iPSC from human primary lymphocytes using Sendai viral vectors (CytoTune™, Life Technologies) has been described (233). All biomaterials were de-identified repository specimens and therefore are exempt from human subjects regulations. Midbrain-like DA neurons were generated using a dual SMAD inhibition protocol (202). Excitatory neurons were induced through a modified protocol(116) where during day 5 of the protocol iNs were gently dissociated with accutase (StemCell Technologies), and (7.0×10^4) were co-cultured with mouse glia (3.5×10^4 cells) (169). Electrophysiological analyses were performed following at least 30 days of differentiation and maturation.

Real-time RT-PCR (qPCR)

Total cellular RNA was prepared using TRIzol reagent (Invitrogen). Human-selective TaqMan™ probes were purchased from Life Technologies and PCR conditions followed the manufacturer's recommendations. A sample of 17-week post-conception human fetal VTA RNA (a generous gift from Drs. Yuka Imamura Kawasawa and Nenad Sestan, Yale University) was used to normalize expression levels to obtain relative quantity (RQ) values. Statistical analysis was performed using R software; ANOVA was used to compare control and affected group means.

RNA sequencing (RNAseq)

Preparation of cDNA libraries (TruSeq Kit, Illumina) and sequencing (HiSeq 2500, Illumina) were performed by RUCDR Infinite Biologics® (Piscataway, NJ). Data were aligned with human genome using TopHat (235) and analyzed with Cuffdiff and R/BioConductor using the cummeRbund package (235, 236). Sequencing data can be found in NIH repositories (SRA accession number SRP040275; GEO accession number GSE56398). H1 hESC-derived NSC data for days 0 and 5 are part of GEO series GSE56785 (237). Datasets for DA neuron cultures were from the following SRA accession numbers: SRR1030497, SRR1030496, SRR1030493, and SRR1030492 (238).

Electrophysiology

Electrophysiology was performed as described previously (239, 240). Specific procedures are provided in the Supplemental Methods. Electrophysiological data are presented as mean ± SEM. All statistical comparisons were made using Student's t-test or with general linear mixed model packages in R/BioConductor.

Immunofluorescence

DA neurons were fixed for 15 min in 4% paraformaldehyde (Electron Microscopy Sciences) in PBS at room temperature and then incubated in blocking buffer (1X PBS, 1% Goat serum, 4% BSA) for 1 hr. Cells were permeabilized in 0.2% Triton X-100 in PBS for 10 minutes and incubated overnight with primary antibodies. Primary antibodies are listed in the Supplemental Methods. The Click-iT EdU Alexa Fluor® 488 Imaging Kit was used to assess the mitotic state of TH^+ neurons. Confocal and spinning disk epifluorescence confocal imaging analysis was performed using a Zeiss LSM700 or Olympus Axiovert 100M confocal microscope (Carl Zeiss, Olympus). Cells were counted

using Zeiss confocal microscope software (Zeiss). Ten images from one coverslip from two independent experiments were used for counting.

Nicotine exposure

Cultures were whole cell patch clamped as described previously. Nicotine was perfused in extracellular medium in increasing amounts 0.1 μM to 6 μM in 3 minute intervals. EPSC frequencies were counted using the pClampfit software (Molecular dynamics). Frequencies were normalized to the first 30 seconds of wash buffer and dosage frequencies were averaged over 30 second intervals within first minute. Amplitudes within each 10 second interval were also averaged in the same time frame.

Experimental Results

iPSCs of multiple subjects carrying CHRNA5 D398/N398 gene variants

Nicotine dependent subjects were selected from the COGEND collection (33, 34) using the results of the Fagerström test of nicotine dependence(241) and the homozygous presence of the minor allele (AA) of rs16969968 as well as the presence of homozygous major alleles for other SNPs known to affect addiction behaviors and/or nAChR function: rs880395 (GG), rs8192475 (GG), rs12914008 (GG), and rs56218866 (TT) (**Figure 33**). Non-nicotine dependent control subjects who smoked came from the same collection, and were homozygous for the major allele of rs16969968 (GG) but matched at the other SNPs. One male and two females were selected for each group. Primary lymphocytes were processed for reprogramming as described previously (233). Pluripotency was confirmed by immunocytochemistry (ICC) for Oct4 and TRA-1-60 (**Figure 35A-B**), by embryoid body formation followed by detection of three germ layers by immunocytochemistry (not shown), and by gene expression studies, including the PluriTest algorithm (242) (**Figure 34**). All tests were positive for pluripotency.

Cell Line	Gender	Status	rs880395	rs16969968	rs1799971	rs8192475	rs12914008	rs56218866	Group
70	Male	Affected	GG	AA	AA	GG	GG	TT	N398
67	Female	Affected	GG	AA	AA	GG	GG	TT	N398
31	Female	Affected	GG	AA	AA	GG	GG	TT	N398
37	Female	Control	GG	GG	AA	GG	GG	TT	D398
73	Female	Control	GG	GG	AA	GG	GG	TT	D398
41	Male	Control	GG	GG	AA	GG	GG	TT	D398

Figure 33: Human subjects used in the study.
All SNP genotypes were confirmed by PCR in iPSC DNA.

Subject	Stage	Group	Pluripotency raw	Pluripotency logit-p	Novelty	Novelty logit-p	RMSD
H1	ESC	hESC	20.863	1	1.53	0.034	0.462
03	CPL	CPL	-105.33	0	3.04	1	1.162
03	T-cell	T-cell	-93.18	0	2.862	1	0.996
03	iPSC	TiPSC	28.398	1	1.649	0.104	0.413
03	iPSC	TiPSC	32.179	1	1.657	0.113	0.424
70 (P26)	iPSC	TiPSC	28.115	1	1.519	0.03	0.399
70 (P13)	iPSC	TiPSC	28.238	1	1.507	0.027	0.433
41	iPSC	TiPSC	38.518	1	1.491	0.023	0.423

Figure 34: PluriTest Algorithm Values.
As comparison, H1 hESC sample is used as a control for pluripotency and crude cryopreserved lymphocytes (CPL) as well as enriched CD4+ T-cells serve as controls for differentiated cells. Samples from iPSC cell line 03, not used in this study, are included to match the source CPL and T-cell samples. Two different passages of line 70 and one from 41 are included to demonstrate pluripotency of iPSC lines used in this study. According to Müller et al. (2012), pluripotency can be identified with the pluripotency score greater than 20 and a novelty score less than 1.67. All iPSC pass these thresholds. TiPSC: T-cell-derived iPSC.

CHRNA5 N398 DA neurons exhibit greater induced activity

To study the functional consequences of the N398 genetic variant of CHRNA5, we used each of the six subject-derived iPSC lines to generate human DA neuron cultures resembling midbrain VTA DA neurons, which are critical mediators of the mesolimbic DAergic system, a pathway whose performance is altered in addiction (243, 244). iPSC were differentiated using the dual SMAD inhibition protocol (202). Expression of DA-specific and mature neuronal markers was confirmed by

immunocytochemical (ICC) staining of the rate-limiting enzyme tyrosine hydroxylase (TH), the early neuronal marker TuJ1 (βIII tubulin, not shown), and the more mature neuronal marker MAP2 (**Figure 35C-D**). More than 75% of MAP2-labeled cells coexpressed TH (D398 75.0% ± 0.092, n=3; N398 78.4% ± 0.027, n=3). Cells positive for TH were also associated with punctate staining for the vesicular DA transporter (DAT; **Figure 35E-F**). To confirm that TH^+ cells were postmitotic, cultures were incubated with EdU for 24 hours to label cells in S phase. Only a small fraction of TH^+ cells stained positive for EdU (Figure 35**G-H**; 3.0 ± 0.007% for D398; 2.02 ± 0.008% for N398, n=3), indicating that nearly all cells were postmitotic.

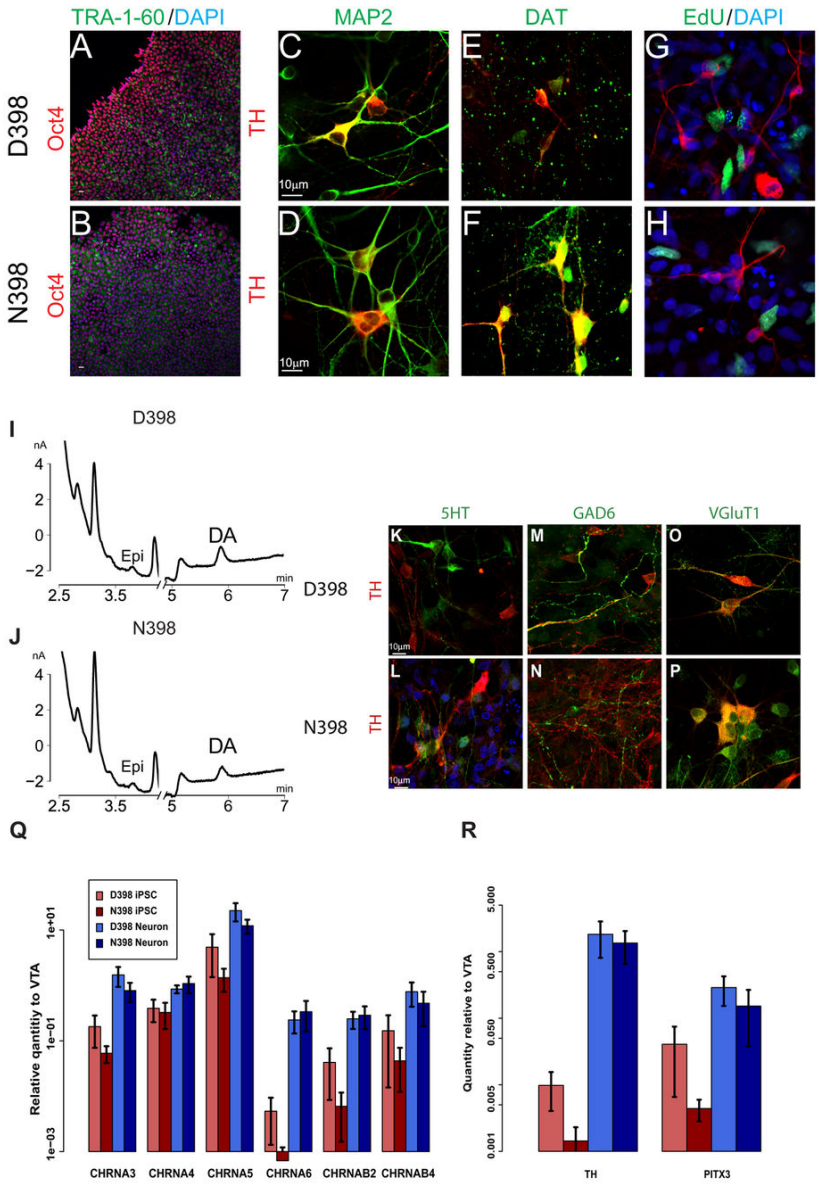

Figure 35: Functionally mature midbrain-like DA neurons present in both D398 and N398 DA cultures.

Representative iPSC cultures from **(A)** D398 and **(B)** N398 groups stained positively for pluripotency markers TRA-1-60 (green) and Oct4 (red). The majority of cells in iPSC-derived DA cultures expressed both MAP2+ (green) cells and TH (red) in both D398 **(C)** and N398 **(D)** groups. **(E,F)** Punctate staining indicates the presence of DAT (green), likely localized to synapses and surrounding TH+ cells. (G,H) Few TH+ were labeled with a pulse of EdU (green), indicating that most cells were postmitotic. **(I,J)** HPLC traces showing release of DA into culture medium with 1 mM nicotine. **(K–P)** Identification of alternative neuronal subtypes in mDA cultures. Cultures were stained with TH (red) and either **(K,L)** 5HT, **(M,N)** GAD6, or **(O,P)** VGluT1 (green). **(Q)** qPCR analysis of nAChR subunit-encoding mRNAs a3,a4,a5,a6, b2, b4, of D398 (red) or N398 (blue), for either iPSC (lighter) or DA (darker) cultures. mRNA levels are normalized to GAPDH and human fetal VTA RNA. Cultures were also assayed by qPCR for mRNAs encoding **(R)** TH and the midbrain marker PITX3. For all qPCR assays, DA neurons were different from iPSC cultures (ANOVA, $p<0.05$) but there was no difference between N398 and D398.

To determine whether the cultures were capable of releasing DA in response to stimulation, we replaced culture medium with buffer containing 1 mM nicotine for 30 minutes, and analyzed the DA content in the medium using HPLC. A distinct peak consistent with DA retention time was observed (**Figure 36**). All results are consistent with the presence of midbrain-like DA neurons, but the cultures also contained a small minority of serotonergic (5-HT positive) and inhibitory (GAD6 positive) neurons (**Figure 37**). Results also identified cells that were both TH^+ and $VGlut^+$ (**Figure 37**), consistent with the notion that some DA neurons also co-release glutamate (245, 246). Moreover, DA cultures express mRNAs encoding nAChR subunits α3, α4, α5, α6, β2, and β4 at levels similar to those found in developing midbrain VTA, using a sample of human fetal VTA mRNA as a reference (**Figure 35Q**). To further confirm the lineage of our culture, we observed mRNA expression for TH and the classic midbrain marker, PITX3 (**Figure 35R**). All nAChR subunit and marker mRNAs increased significantly upon differentiation from iPSC to midbrain-like DA neuron cultures (ANOVA, $p<0.05$) even though there was some variability between iPSC lines derived from different subjects, as depicted by the large error bars shown in **Figure 35Q**. However there was no significant difference in expression between CHRNA5 variant groups. Therefore, the rs16969968 SNP in CHRNA5 does not affect the generation of the DA cellular phenotype through the dual SMAD inhibition protocol.

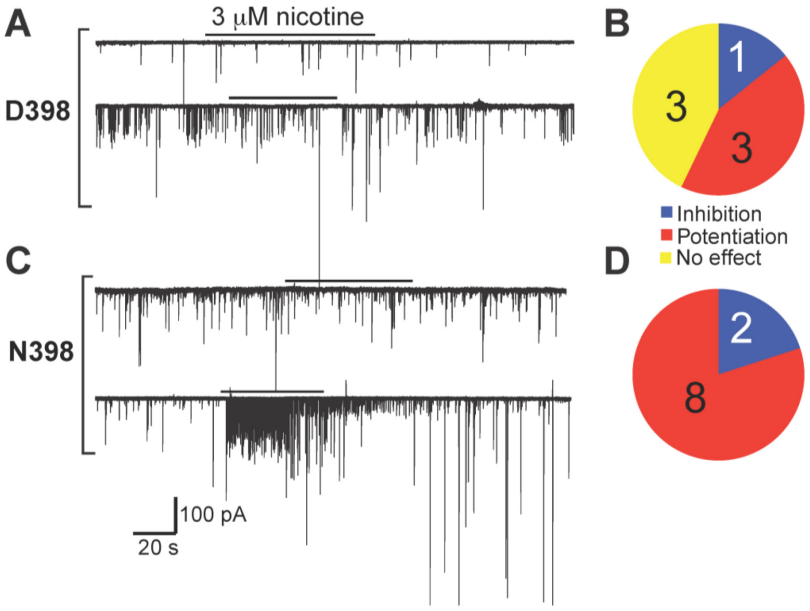

Figure 36: N398 and D398 iN Response to Nicotine.
N398 DA neurons exhibit increased potentiation following nicotine exposure **(A)** Representative traces of PSCs observed after 3 μM nicotine exposure to D398 DA neurons. **(B)** Pie graph showing the number of cells showing different responses to nicotine application in D398 neurons. “Potentiation, inhibition and no effect” reflect the frequencies of PSCs during the applications of nicotine, when compared to before the application of nicotine, were higher, lower or no change, respectively. **(C)** Representative traces and quantification of EPSCs observed after 3 μM nicotine exposure to N398 DA neurons. **(D)** Pie graph showing the number of cells with different responses to nicotine application in N398 neurons.

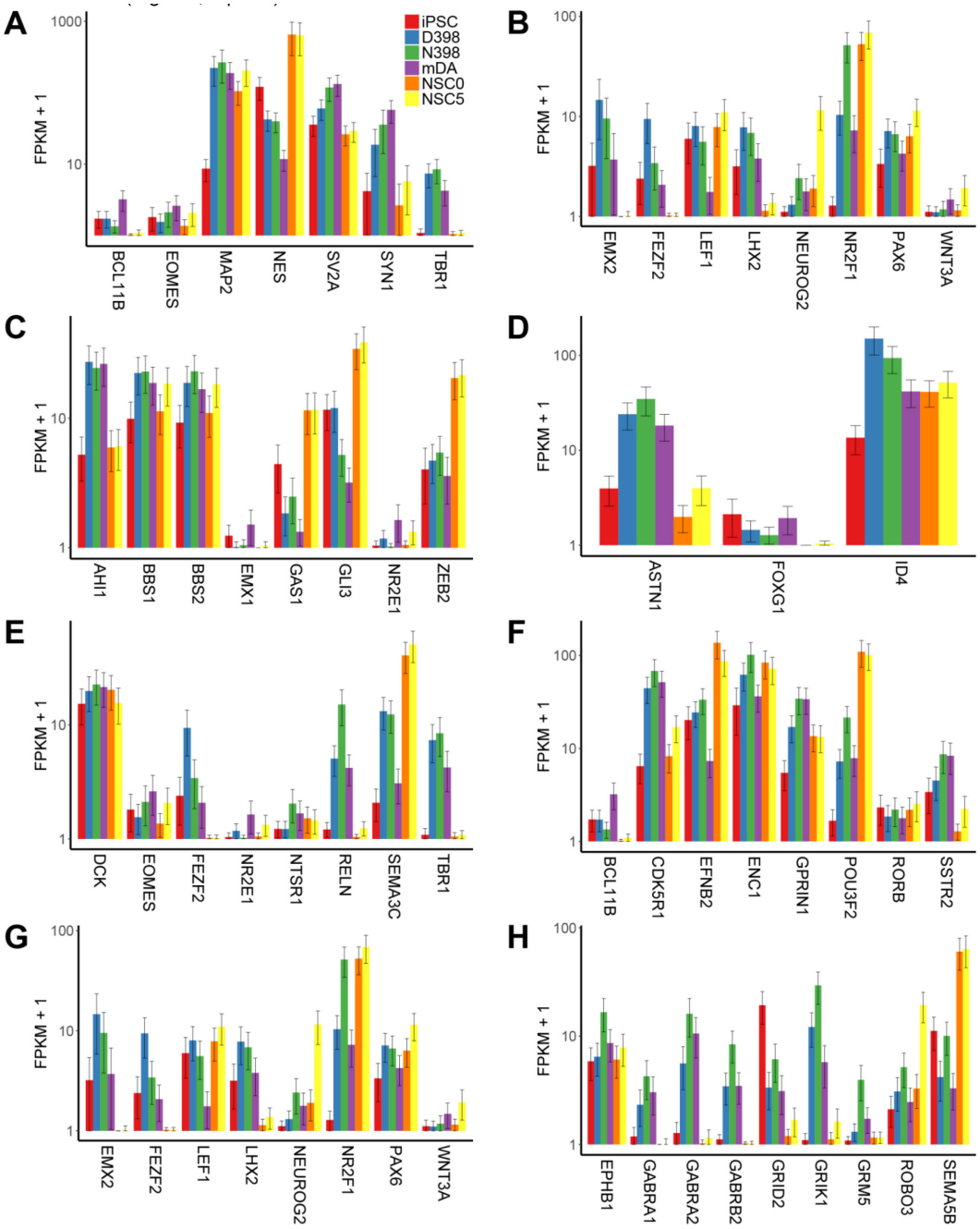

Figure 37: Example RNA Levels, in FPKM, for Several Representative Groups of Genes. FPKM levels are depicted on a $\log_{10}$ scale. **(A)** Cortex markers. **(B)** and **(C)** Dorsal telencephalon. **(D)** Cortex proliferative markers. **(E)-(G)** Cortical migration layer markers. **(H)** Selected markers from the KEGG pathway enrichment list.

We next assessed the functional parameters of derived human DA neurons from subjects with D398 or N398 variants. Using whole cell patch clamp recordings, we found that both the D398 and N398 DA cultures produced robust and repetitive spontaneous action potentials (APs) (**Figure 38A-B**) and had similar membrane properties, including membrane capacitance, resting membrane potentials, and input resistance (**Figure 38C-E**) While the spontaneous APs in DA neurons of both genotypes have statistically similar frequencies ($p=0.258$), the N398 neurons tend to fire more APs (**Figure 38F**). Next, we tested the intrinsic excitability of these DA neurons by inducing APs using different amplitudes of current injections; however, neurons of both genotypes exhibited similar neuronal excitability as indicated by a similar frequency of induced APs (**Figure 38G-H**). These data suggest that the N398 variant in CHRNA5 does not impair neuronal excitability, nor does it produce any major changes in the passive membrane properties of D398 and N398 human neurons (**Figure 38I**) However, while DA neurons with different CHRNA5 gene variants have similar intrinsic excitabilities, the N398 variants also have a slightly higher frequency of spontaneous APs (**Figure 38F**), which could be due to differences in synaptic network activity. Since the DA neuronal cultures also form synapses as revealed by synapsin puncta (**Figure 38J-L**), we turned to measurements of postsynaptic activity.

In order to test whether the N398 variant alters synapse function, we measured spontaneous postsynaptic currents (sPSCs, **Figure 38L**). Both N398 and D398 neurons exhibited robust sPSCs, which is indicative of mature synapse formation and synaptic transmission among these neurons. Interestingly, consistent with the slightly greater spontaneous AP firing frequency in N398 DA neurons, the N398 DA neurons also exhibited greater spontaneous synaptic activity when compared to the D398 neurons (**Figure 38L-M**), indicated by the increased frequency and the amplitudes of the sPSCs

in N398 neurons when compared to the D398 DA neurons. Therefore, neurons in the N398 cultures have a higher excitability due to more synaptic activity.

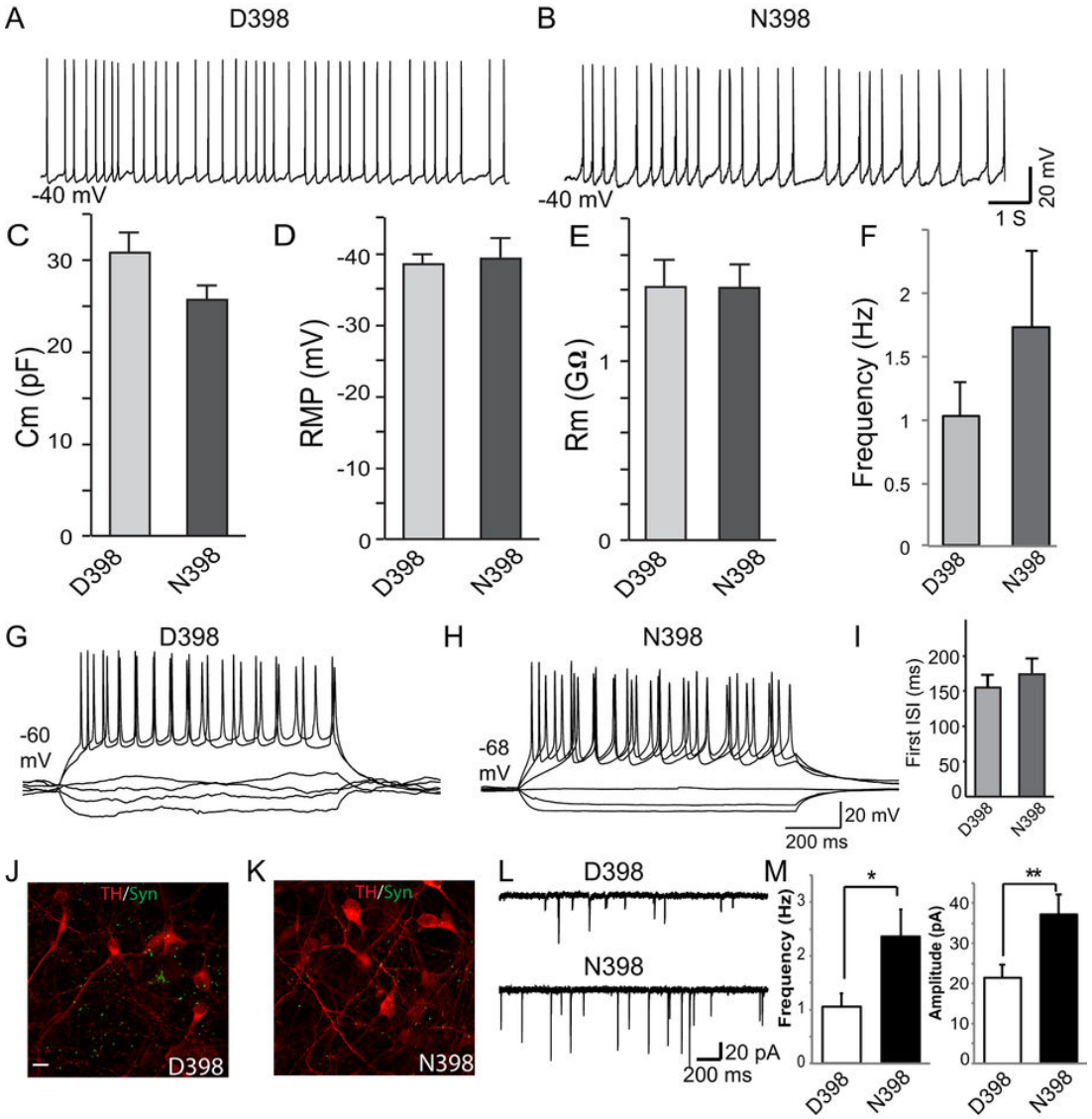

Figure 38: Spontaneous Postsynaptic Activity is Increased in N398 DA Cultures

(**A**,**B**) Spontaneous action potentials of D398 and N398 DA neurons. (**C**) Membrane capacitance, (**D**) Resting membrane potentials (RMP), (**E**) Input resistance of cell membrane (Rm), and (**F**) Spontaneous firing frequency of D398 and N398 DA neurons. (**G**,**H**) Repetitive action potentials from depolarizing current injections in D398 and N398 DA neurons. (**I**) Interstimulus intervals of induced action potentials of D398 and N398 DA neurons. (**J**,**K**) ICC of TH (Red) and Synapsin (Green) for D398 and N398 DA neurons. (**L**) Spontaneous postsynaptic currents of D398 and N398 DA neurons. (**M**) Frequency and amplitudes of postsynaptic current responses from D398 and N398 DA neurons.

Gene expression patterns predict functional differences between D398 and N398 DA neurons

In order to probe the gene expression network changes that may contribute to the functional differences we observed between D398 and N398 human neurons (**Figure 38**), we conducted gene expression profiling by RNAseq, using replicate cultures from single donors from each variant group (**Figure 39**). We included in our analysis RNAseq data from control DA cultures published by the Studer lab (mDA) (238), iPSC cultures, and hESC-derived neural stem cells (NSC) at two stages of differentiation (producing glutamatergic neurons, day 0 [NSC0] and day 5 [NSC5]) (237). Clustering analysis shows that D398 and N398 cultures are more similar to DA neuron cultures than to cortical glutamatergic NSC (**Figure 39A**). We find similar expression levels of several mRNAs known to be associated with DA neurons in midbrain-like DA, D398, and N398 cultures (**Figure 39B**). CORIN, FOXA1, LMX1A, NR4A2, and PITX3 mRNAs are all prominent and similar to levels found in previously-published mDA cultures. EN1 levels are lower, but well above the limit of detection, and were also observed in cultures of excitatory neuron precursors (NSC0 and NSC5). All results support the relationship shown in **Figure 39A**, that the N398 and D398 cultures are most similar to the previously-published mDA cultures. We conclude that gene expression patterns are consistent with the presence of midbrain-like DA neurons in our cultures.

The vast majority of mRNAs detected in these cultures was expressed at similar levels in either D398 or N398 DA neurons. The set of nAChR subunit mRNAs (**Figure 39C**, green dots), as previously detected by qPCR, was primarily within the 2-fold difference range (depicted by the vertical dashed lines), except for CHRNA5, which was relatively increased in D398 (8.7-fold higher, 0.02% FDR). qPCR assay (**Figure 35Q**) indicated a similar difference although it was not statistically significant. Subjects were

chosen for a homozygous major allele in rs880395 to exclude the potential effect on CHRNA5 mRNA levels observed previously (247). Other groups of genes indicative of neuronal identity or maturity, including the gene ontology group members specific for dopaminergic differentiation (**Figure 39C**, blue dots) were unaffected by the variation.

Focusing on differences between D398 and N398 cultures, 1,194 genes were significantly different (≤1% FDR and at least 2-fold different, dashed lines; black dots in (**Figure 39C**). Taking the 349 genes that were relatively lower in N398, only two KEGG pathways were found to be enriched at relatively low confidence levels (blue bars in **Figure 39B**), as determined by DAVID software (248, 249). However, the 845 genes relatively increased in N398 were significantly enriched in Neuroactive ligand-receptor interaction, Ca^{2+} signaling pathway, and Axon guidance KEGG pathways (red bars in **Figure 39D**). A selected sample of genes in this group is plotted in **Figure 37H**. Enrichment of GO functional groups similarly highlights neuron activity-specific biological processes (**Figure 41**). This predicts that N398 DA neuron cultures are likely to exhibit functional differences in response to ligand, potentially through changes calcium influx. This also suggests that the N398 variant may contribute to the excitatory response of neurons during nicotine exposure.

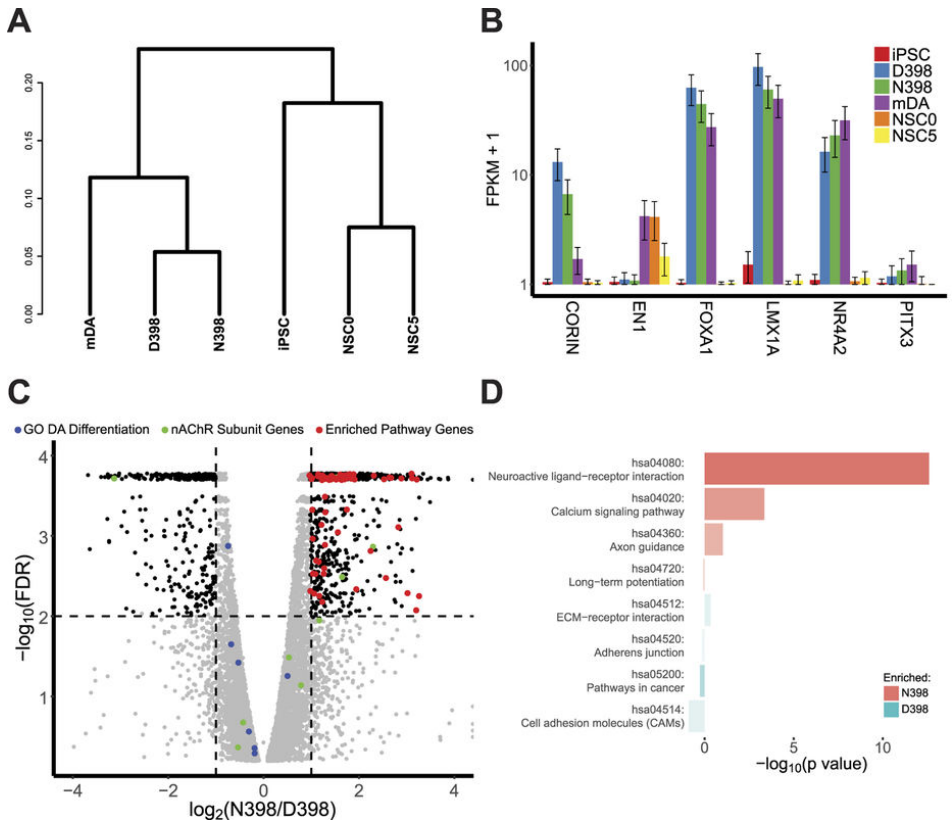

Figure 39: Gene Expression Differences in iPSC Derived DA Neurons Exhibit Patterns of Differential Response.

(A) Hierarchical clustering indicates that D398 and N398 DA cultures were more similar to mDA cultures than to iPSC or iPSC-derived NSC (NSC0), or NSC differentiating into glutamatergic neurons (5 days of differentiation, NSC5). The dendrogram shows relative distances (based on the Jenson-Shannon divergence metric) for the top 500 genes varying by group. **(B)** Expression patterns for genes characteristic of midbrain DA neurons. The mean FPKM is plotted ± the 95% confidence interval, n = 3/group. **(C)** RNAseq volcano plot. The horizontal axis shows the $\log_2$ fold-change, comparing N398 to D398. The vertical axis shows the false discovery rate (FDR) as the $-\log_{10}$ of the value. Points are plotted as individual genes not significantly different (grey dots) or significantly different (black dots) at 1% FDR (horizontal dashed line) and at least 2-fold different (vertical dashed lines). Colored dots indicate the nAChR receptor neuronal markers (green), GO dopamine differentiation genes (blue) and differentially-regulated genes belonging to the significantly-enriched pathways relatively increased in N398 (red). **(D)** Pathway (KEGG) analysis identifies three functional groups as enriched in the list of genes increased in N398. Bar colors indicate enrichment in N398 (red) or D398 (blue). The bar length indicates the FDR, and the color intensity (alpha) indicates the number of genes enriched.

Glutamatergic N398 neurons exhibit increased activity following nicotine.

Results from the dual-SMAD-derived DA cultures suggest that human DA neurons may co-release glutamate (**Figure 35O-P**Figure 37) and the release of glutamate was likely differentially affected by the N398 or D398 nAChR variants (**Figure 38L-M**). Gene expression patterns predict a difference in neurotransmitter response pathways, particularly for glutamate signaling. We considered whether the difference in response between N398 and D398 variant nAChRs could be observed in cultures of purely excitatory neurons, which have been puromycin-selected to increase the uniformity of the cultures. To test this, we differentiated N398 and D398 iPSC into forebrain excitatory neurons using iN protocols (116) (**Figure 40A**) and studied the impact of nicotine on synaptic transmission. Forebrain excitatory glutamatergic neurons are modulated by nAChRs (214); thus we hypothesize that the N398 variant would have a greater functional impact on excitatory neurons. We examined the effects of nicotine on spontaneous excitatory PSCs (sEPSCs) in both D398 and N398 human excitatory neurons. The frequencies of sEPSCs in both N398 and D398 neurons are stable before the application of nicotine (**Figure 40B-D**). However, within 30 s of 0.1 μM nicotine exposure, frequencies of sEPSCs were significantly increased in the N398 subjects compared to the D398 controls (**Figure 40C**). Interestingly, following the dramatic increase of the sEPSCs in N398 neurons, the facilitatory effects appeared to decrease over time in the continued presence of nicotine, likely due to the desensitization of the receptor, which mimics the desensitization reported with ectopic expression studies in Xenopus oocytes (223). Similarly, the amplitude of response trended higher during the initial 30 s but then fell below D398 shortly thereafter (**Figure 40D**). The difference in response at 0.1 μM nicotine was not limited to a single outlier cell or to cells prepared from a single subject (**Figure 40**). The distribution of responses was variable but

showed clearly that multiple cells from multiple subjects exhibited increased EPSC frequencies and amplitudes.

Since the greatest effect of nicotine on EPSCs occurred immediately after introducing nicotine, we analyzed responses from each cell during the initial 10 s exposures to sequential additions of 0.1 to 6 μM nicotine (**Figure 40G-H**). The apparent desensitization in N398 was maintained during addition of higher doses of nicotine to the same patched cells. The amplitudes increased notably in D398 at higher doses (3 and 6 μM) while the N398 neurons exhibited minimal changes in frequency or amplitude of response. The combined effect of nicotine dose and CHRNA5 genotype on EPSC frequency was significant overall at $p=0.00046$ using a Tukey post-hoc test of an ANOVA linear mixed-effects model with repeated measures (n=115/group, with a minimum of 25 cells in at least 3 different cultures from each of 3 different subjects per group). These results show that N398 neurons have higher initial responsiveness to nicotine but with enhanced desensitization. These data are largely in line with the notion that was reported previously using heterologous expression system (223). Therefore, the enhanced excitatory response and subsequent desensitization at concentrations of nicotine on par with that of heavy smokers carrying the N398 minor allele gene variant might contribute to their addictive behavior.

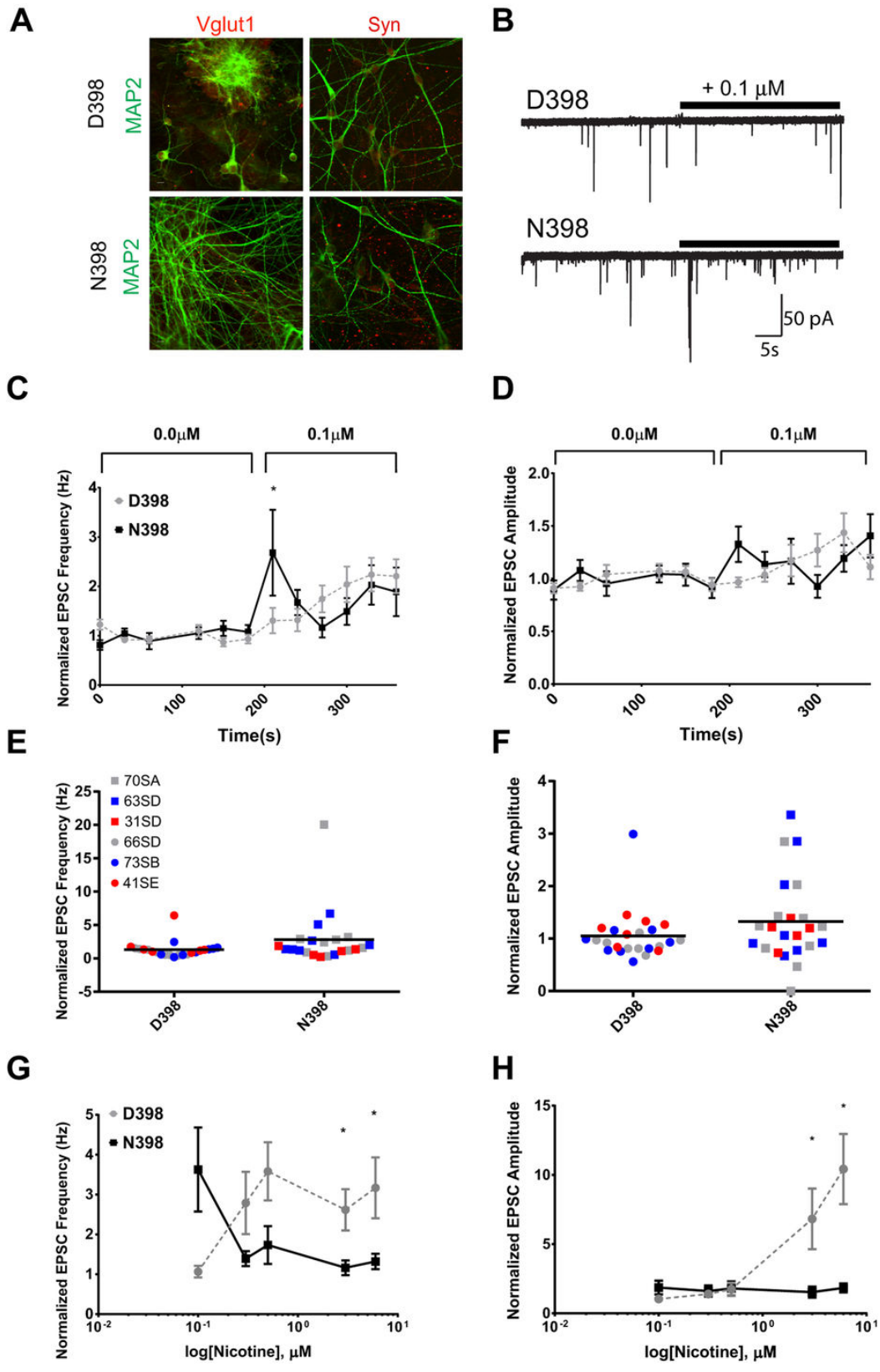

Figure 40: Excitatory N398 Neurons Exhibit Increased Response to Nicotine Followed by Desensitization.

Figure 40 continued. (A) Glutamatergic iN cultures are positive for MAP2 (green), vesicular glutamate transporter 1 (VGluT1, left, red), and synapsin (Syn, right, red) as detected by ICC. **(B)** Example traces from a patched neuron to show changes in response upon introduction of 0.1 μM nicotine (indicated by bar). Patched neurons exhibited increased frequency **(C)** and amplitude **(D)** during initial exposure to 0.1 μM nicotine. By 60 s after nicotine addition, frequency trended lower in N398 cells, although not significantly. Plotting the initial response to 0.1 μM nicotine for individual cells, it is clear that the changes in frequency **(E)** or amplitude **(F)** in N398 was not due to a single cell or subject. D398 samples are plotted as circles and N398 as squares. Color denotes cells from individual subjects (see key and Supplemental Table 1). However, subsequent additions of increasing doses of nicotine had reduced initial frequency **(G)** and amplitude **(H)** in N398 compared with D398 cells. N398 was different in frequency response from D398 as assessed by a Tukey post-hoc test of a general linear mixed-effects model with repeated measures ($p = 0.00046$, $n = 115$ cells per genotype; 5 cells per culture; 5–7 cultures per individual cell line).

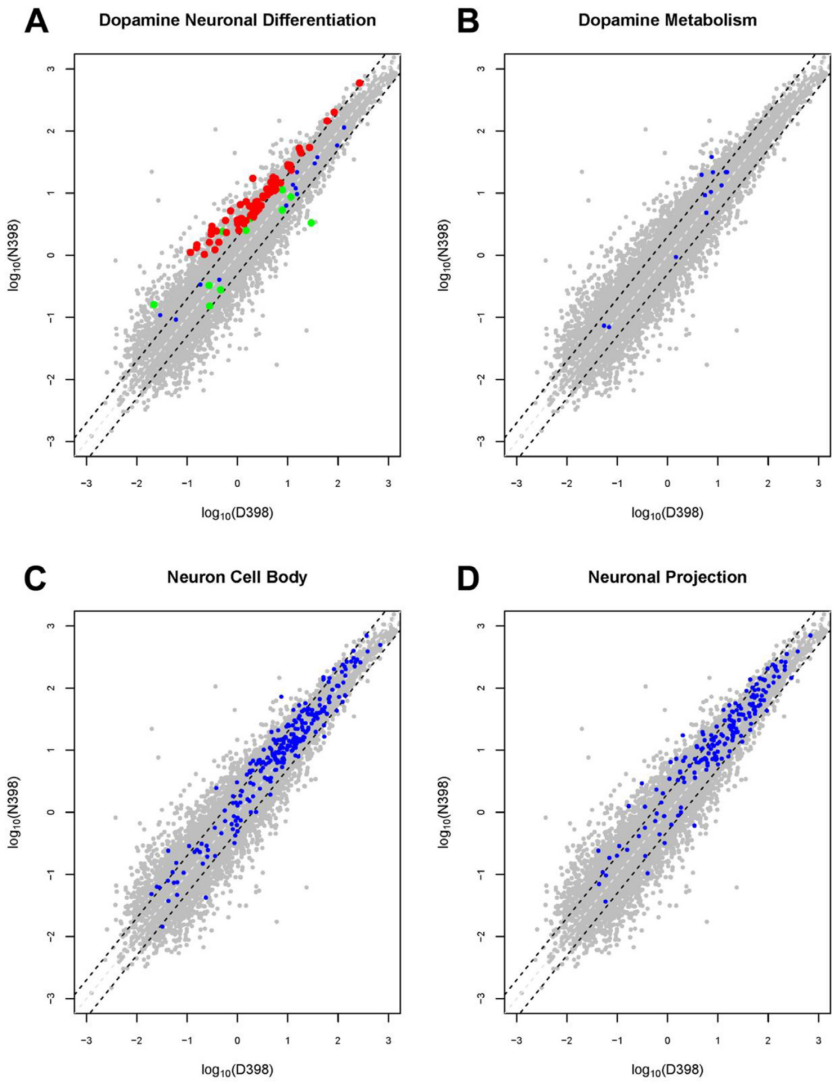

Figure 41: Scatterplot Expression Patterns of Gene Ontology Groups Associated with Midbrain DA Neuronal Differentiation, using RNAseq FPKM.

In panel A, dot colors match those shown in the volcano plot in Fig. 3C. For panels B-D, blue dots denote genes within the entitled biological process group.

Discussion

Our results indicate that the N398 variant of *CHRNA5* is associated with greater excitability and desensitization in response to nicotine, at least in excitatory cells but also affecting DA cells postsynaptically. The presence of rs16969968 minor allele in *CHRNA5* increases risk of nicotine addiction (250). Experiments using heterologous expression of *CHRNA5* suggest that the N398 variant alters Ca^{2+} permeability and mediates nicotine consumption (36, 220, 221, 223, 251). While these findings reveal potential effects on reward circuitry, as we began this study, we hypothesized that subtle effects of the α5 subunit genetic variants on nAChR would be detectable at the cellular level, especially at the synaptic level.

To address this hypothesis, we obtained repository blood samples collected as part of a large genetics study (COGEND) previously used for genome-wide association studies (33, 34). iPSC were prepared from cryopreserved, de-identified repository lymphocyte specimens. This strategy is particularly appealing because it allows access to large numbers of genetically diverse samples large studies with cryopreserved specimens each having a clear clinical diagnostic history. We have developed reliable and reproducible methods to convert cryopreserved primary T-cells isolated from the RUCDR Infinite Biologics™ cell repository to iPSC (233), and we successfully used this approach to study effects of alcohol on NSCs (252) and mutations found in Ataxia telangiectasia (253). We selected donors carrying homozygous rs16966968 major or minor allele, encoding the D398 or N398 variant, respectively, of the nAChR α5 subunit. Samples also contained homozygous major alleles for several related SNPs (Supplemental Table 1), particularly rs880395, since it has been reported to have secondary effects on CHRNA5 mRNA levels (247). The goal was to represent isolated genotypes in order to test the difference between the major and minor allele of

rs16969968. It has been suggested that cell lines from multiple patients and controls as well as multiple subclones from each patient should be analyzed to provide a convincing cellular or functional phenotype. However, the resulting high workload is a major obstacle to the identification of disease-associated phenotypes (254-256). The most convincing solution to this problem is the creation of isogenic pairs of cells differing only in a single locus, usually by genetic engineering techniques (257, 258). Indeed, our previous RNAseq analyses demonstrate broad variability among subject iPSCs, even among members of the same family, and a vastly reduced variability when comparing isogenic samples (253). However, editing to create an isogenic rs16969968 iPSC is time consuming and technically challenging. Nevertheless, our results derived from different subjects and different subtypes of human neuronal population are consistent and possibly more relevant overall to human populations. Therefore, we believe that by testing a reasonable number of subject-specific iPSC lines we capture sufficient variability while searching for reproducible phenotypes based on the non-synonymous SNP.

To begin to test *CHRNA5* variant function, midbrain-like DA neuronal cultures were chosen to mimic the DA neurons of the VTA, thought to be an important member of the reward/addiction circuit (243, 244). The presence of the N398 variant does not interfere with the generation of mature DA neurons, as determined by the expression of neuronal markers (**Figure 35**), or of the basic membrane properties, and the capacity for generating action potentials is not different between the two *CHRNA5* variants (**Figure 38**). Expression of nAChR mRNAs was similarly expressed in both variants. While mRNA levels cannot predict cellular protein levels or assembly into functional receptors, and a complete set of nAChR subunit-selective antibodies is not available, cultures expressed robust levels of mRNAs encoding *CHRNA3, 4, 5,* and *6*, *CHRNB2* and *4* as

would be expected for central nAChRs (**Figure 35Q**). We used fetal human VTA RNA as a reference, so we can conclude that the relative quantities of these mRNAs in cultures were within 2-3-fold of that found in developing midbrain DA neurons. However, it appears that N398 neurons are receiving more synaptic inputs, as revealed by an increased PSC amplitude and frequency in N398 compared with D398 (**Figure 38M**), consistent with a possible increase in excitability of N398 neurons, or reduced input from inhibitory neurons, as suggested by the relative higher frequency of spontaneous action potentials. This correlates with results from others suggesting that while the α5 subunit does not contribute to nicotine binding with nAChRs, the loss or alteration of α5 contributes to a shift in nicotine response, specifically in VTA DA neurons (221). We ascribed the increased network activity to interactions among the mixtures of neuronal subtypes in the culture. The dual-SMAD inhibition method was used to generate cultures of relatively high purity DA neurons (≥75% of $MAP2^+$ cells co-expressed TH) with a smaller number of other neuron subtypes (**Figure 35M-R; Figure 37**).

To investigate intracellular regulatory processes, we interrogated global gene expression by RNAseq. Results identified mRNAs differentially expressed between D398 and N398 (**Figure 39** and Supplemental Table 3). The most informative and significant functional enrichment was for KEGG pathways specific for neuroactive ligand receptor interaction, calcium signaling, and axon guidance (red bars in **Figure 39**). Whether the altered expression of these genes is an effect of the N398 variant or whether it is only a correlation due to differences in neuronal function, the RNAseq results demonstrate identifiable differences between cultures based on *CHRNA5* genotype and they predict that N398 cells will have altered response to stimuli. Because some of the differentially regulated genes were components of the glutamatergic pathway, and because we detected as much as 20% excitatory glutamatergic neurons in

the mDA cultures (**Figure 37**), we reasoned that the increased excitability in mDA cultures may be due to nAChR activity in the DA neurons or to pre-synaptic input from other cells in culture—possibly an excitatory input. It is also possible that some TH^+ cells co-release glutamate. Recent reports identify GABA release by DA neurons (259, 260). To test this prediction we differentiated iPSC into glutamatergic neurons.

Results using excitatory iN cell cultures and nicotine exposure confirm the prediction that N398 cells exhibit a more robust network activity response to nicotine specifically in excitatory neurons. This enhanced activity was confirmed by assessing the frequencies of PSCs in response to increasing nicotine exposure (**Figure 40**). Results show an increased frequency of PSC in N398 iN cells at the lowest dose tested (0.1 μM), followed by results at higher doses that were consistent with desensitization of the receptor, as was observed in a Xenopus injection model (223). Desensitization was only found in that model with α2β4-containing nAChRs (223) and, while other subunit mRNAs were present in our cultures, α2 and β4 mRNAs are prominent. Levels of the α5 subunit mRNA were somewhat lower in N398 mDA neurons (**Figure 35Q**), which was confirmed and extended by the RNAseq study (Supplemental Table 3), so it remains possible that reduced neuronal expression of α5 may contribute to the observed nicotine sensitivity. This would agree with results from CHRNA5 knockout mouse models as well, where reduced α5 subunit caused substantial behavioral effects (36, 220). Observations of the increased neuronal activity triggered by nicotine, supported by the increased basal frequency of PSCs and the predicted pathway changes revealed by RNAseq, leads us to conclude that the N398 variant produces neurons with increased responsiveness to nicotine followed by desensitization to subsequent exposure. This difference in response occurs at nicotine concentrations typical of heavy smokers (0.025-0.5μM), potentially contributing to the increased risk of nicotine addiction (261).

Since the stem cell-derived neuronal cultures are likely to be most similar to neurons present in early stages of human development, and not those in adults responding to repeated nicotine stimulation such as in addiction, we do not suggest that the altered activity found in N398 explains addiction behaviors. Instead, we believe that our results predict that naïve neurons in human brains of individuals with the N398 variant would exhibit enhanced response from initial nicotine exposure, perhaps contributing to development of addiction, followed by a lack of response, leading to an unsatisfied craving for additional stimulus. This stem cell-based approach serves as a proof-of-principle to study how addiction risk-associated gene variants may affect human neuronal functions. Continuing these studies is likely to lead to a better understanding of the impact of gene variants on human behavior and may identify strategies for intervention in addiction.